DOT/FAA/AR-06/9

Office of Aviation Research
and Development
Washington, DC 20591

Statistical Testing of Aircraft Materials for Transport Airplane Rotor Burst Fragment Shielding

May 2006

Final Report

U.S. Department of Transportation
Federal Aviation Administration

NOTICE

Technical Report Documentation Page

1. Report No.	2. Government Accession No.	3. Recipient's Catalog No.
DOT/FAA/AR-06/9		

4. Title and Subtitle	5. Report Date
STATISTICAL TESTING OF AIRCRAFT MATERIALS FOR TRANSPORT AIRPLANE ROTOR BURST FRAGMENT SHIELDING	May 2006
	6. Performing Organization Code
7. Author(s)	8. Performing Organization Report No.
Sean Kelley and George Johnson	
9. Performing Organization Name and Address	10. Work Unit No. (TRAIS)
University of California, Berkeley Berkeley, CA 94720	
	11. Contract or Grant No.
12. Sponsoring Agency Name and Address	13. Type of Report and Period Covered
U.S. Department of Transportation Federal Aviation Administration Office of Aviation Research and Development Washington, DC 20591	Final Report 1/2003-6/2004
	14. Sponsoring Agency Code
	ANM-100

15. Supplementary Notes

The Federal Aviation Administration Airport and Aircraft Safety R&D Division Technical Monitor was Donald Altobelli.

16. Abstract

Fragment barrier systems are being examined and developed for commercial airplanes to prevent accidents as a result of an engine rotor burst failure. To use this system, it is necessary to understand how the existing aircraft materials behave under ballistic impact. The material response of 0.063, 0.125, and 0.25-in-thick 2024 aluminum, 0.25-in-thick Makrolon® polycarbonate, and sandwich composite panels were investigated under ballistic impact. Failure modes were evaluated and ballistic limits obtained for each set of targets. The testing was done in the UC Berkeley Ballistics Laboratory using a gas gun, and a powder gun setup with a 1/2-inch diameter chrome steel spherical projectile. This report documents the testing and analysis of the UC Berkeley ballistic testing. The testing yielded excellent results on aluminum but more data is needed for titanium, composites, and polycarbonate materials.

17. Key Words	18. Distribution Statement
Ballistic, Gas gun, Powder gun, Ballistic limit, Petaling, Plugging, Shear plugging, Dishing, Delamination	This document is available to the public through the National Technical Information Service (NTIS) Springfield, Virginia 22161.

19. Security Classif. (of this report)	20. Security Classif. (of this page)	21. No. of Pages	22. Price
Unclassified	Unclassified	112	

Form DOT F1700.7 (8-72) Reproduction of completed page authorize

TABLE OF CONTENTS

LIST OF FIGURES

LIST OF TABLES

LIST OF ACRONYMS

AC	Advisory Circular
FAA	Federal Aviation Administration
FEM	Finite element method
IA	Interagency Agreement
LLNL	Lawrence Livermore National Laboratory
SHCS	Socket head cap screws
UCB	University of California Berkeley

EXECUTIVE SUMMARY

Fuselage fragment barrier systems are being examined and developed for commercial airplanes to provide protection from an engine rotor burst failure. Part of this development was to understand how the existing aircraft materials behave under ballistic impact, and then to model those results to aid the aircraft industry in designing these barriers, and the evaluation of existing aircraft structures for fragments from rotor burst events. In September 2002, the Federal Aviation Administration (FAA) issued a grant under the Airworthiness Assurance Center of Excellence to the University of California at Berkeley (UCB), who teamed with The Boeing Company and Lawrence Livermore National Laboratory (LLNL) to acquire additional data on aluminum and titanium and preliminary data on composites and polycarbonate. This data was then used to improve material models in the LSDYNA computer codes. This work yielded excellent test data on aluminum but more data is needed on titanium, composites, and polycarbonate.

This report contains Sean Kelley's UCB master's thesis that entails detailed results and analysis of metal's testing conducted at UCB under the supervision of Professor T. I. Zohdi and Professor G. Johnson.

This report details how several existing aircraft materials behave under ballistic impact. The material response of 0.063- and 0.125-inch-thick aluminum 2024-T3 sheets, 0.25-inch-thick aluminum 2024-T351 plates, 0.25-inch Makrolon® polycarbonate, and 0.25-inch sandwich composite panels were investigated under ballistic impact, evaluating failure modes and obtaining the ballistic limits for each set of targets. The testing was done in the UCB Ballistics Laboratory using a gas gun and a powder gun setup with a 1/2-inch-diameter chrome steel spherical projectile. The ballistic tests showed that the aluminum plates failed by dishing and petaling, with slight plugging for the thinnest targets. As the aluminum target thickness increased, the amount of dishing and petaling decreased, and the failure mode tended towards pure plugging. The 0.25-inch-thick polycarbonate targets failed by denting and viscoelastic petaling. The main type of failure for the composite panels was petaling and delamination, with petal fracture occurring in the ±45° directions from the point of impact, forming four petals in a pyramid shape. The ballistic tests also showed that the amount of energy absorbed by a target beyond the ballistic limit is nearly constant. Additional work is required to develop a detailed model for the residual velocity and ballistic limit of a target based on the assumption of a constant absorbed kinetic energy.

1. INTRODUCTION.

There have been several instances in the past where a rotor disk of a main propulsion engine on a commercial aircraft experienced fatigue failure, ruptured the engine containment structure, and showered the fuselage section of the aircraft with engine fragments. Although the loss of one engine on a multiengine aircraft is not necessarily enough to cause a disastrous failure, the engine fragments resulting from this type of failure can wreak havoc on the fuselage. The fragments may penetrate the fuselage and damage critical control systems, such as hydraulic and fuel lines, compromising the ability of the pilot to control the aircraft.

One such accident occurred in 1989 to a McDonnell Douglas DC-10 commercial aircraft. While cruising at 37,000 feet, the aircraft suffered a catastrophic engine failure. As described above, one of the engine's fan rotor disks failed and resulted in the loss of all three of the aircraft's redundant hydraulic flight control systems, making the aircraft nearly uncontrollable. This loss of control resulted in a crash landing and the fatality of nearly half of the 285 passengers and 11 crew members [1].

As a result of these types of accidents, material property data and analytical modeling capabilities are being developed to improve the design capability of lightweight fragment barrier shielding to protect critical aircraft systems. Part of the development of these fragment barrier systems is to understand the ballistic performance of the existing materials in the fuselage and to be able to model this behavior using finite element modeling (FEM)-based computations.

The work presented in this report examined the ballistic performance of materials used by the aircraft industry through experiments that were run to provide ballistic threshold data for each material. An error analysis and statistical analysis were also performed on the results to present the level of accuracy that could be expected. This data provided insight into failure characteristics of the materials, as well as providing information that is essential to improving computer-based models.

Experiments were performed on targets of 0.063-and 0.125-inch 2024-T3 aluminum, 0.25-inch-thick 2024-T351 aluminum, 0.25-inch-thick polycarbonate, and 0.25-inch-thick sandwich composites. The objective was to provide a ballistic curve for each material and thickness as well as an approximate ballistic limit (v_{50}), using controlled geometries, impact conditions, and materials. The postimpact targets were also examined to assess observed failure characteristics of each material and thickness. The goal was to provide experimental results useful for the design of a suitable fragment barrier system to prevent further accidents caused by rotor burst failure.

1.1 BACKGROUND.

In 1997, the Federal Aviation Administration (FAA) signed an Interagency Agreement (IA) with Lawrence Livermore National Laboratory (LLNL) to have them use their DYNA-3D model to improve the material codes for aircraft and engine metallic materials experiencing impact from uncontained engine fragments. This work was in support of the Aviation Rulemaking Advisory Committee Powerplant Installation and Harmonization Working Group efforts to update FAA Advisory Circular (AC) 20-128. Since inception, LLNL has produced several FAA reports documenting their progress [2, 3, and 4]. The main goal of this effort was to update the aluminum and titanium material constants so the industry could use them in an updated AC 20-128 that accounted for multiple small fragments.

The work done at LLNL showed that the then current Johnson-Cook material constants available for DYNA3D simulations were not accurate for uncontained engine fragments. In addition, thick plates (thicker than 0.25 inch) may require different material constants than thinner plates. In April 2002, the FAA (with The Boeing company) had a review at LLNL to discuss the final deliverables of the IA. Though the test data looked very promising, funding for this program was insufficient to validate new material models. A final report was issued recommending additional work in this area [2].

In September 2002, an Airworthiness Assurance Center of Excellence (AACE) grant was issued to University of California at Berkeley (UCB) who teamed with Boeing and LLNL to continue the work on metals and acquire preliminary data on composites and polycarbonate. This report presents UCB's portion of the testing and analysis done from January 2003 to June 2004.

1.2 EXPERIMENTAL OBJECTIVES.

The main objective of the experiments presented in this report was to provide information on the ballistic characteristics of several different materials and several different thicknesses of material. The materials tested were the following: 2024-T3 aluminum sheet at 0.063 and 0.125 inch thick, 2024-T351 aluminum plate at 0.25 inch thick; 0.25-inch-thick Polycarbonate (Makrolon®), and 0.25-inch-thick sandwich graphite composite sheets with a Nomex® honeycomb core. For each of the materials tested, a ballistic curve presenting initial velocity of the projectile against the residual or postimpact velocity of the projectile was developed. From this curve, an approximate ballistic limit, or the speed at which the projectile first penetrated the material, was obtained for each material. The material absorbed energy, or more accurately, projectile kinetic energy loss was also plotted against the initial kinetic energy of the projectile. These curves gave information on the energy-absorbing capabilities of the different materials.

2. EXPERIMENTAL SYSTEM AND PROCEDURE.

The experiments were performed using two separate setups, a low-velocity setup consisting of a nitrogen gas gun and a high-velocity set up consisting of a powder gun. Each setup also made use of a blast shield, initial velocity measurement system, target holder, target mount, residual velocity measurement system, catcher box, and a high-speed camera setup. The test apparatus are described in detail in the following sections.

2.1 PNEUMATIC GUN SETUP.

2.1.1 Nitrogen Gas Gun.

The high-pressure pneumatic ballistic gun and associated controls were used for all tests in which the speed required was less than the maximum speed the gun could produce. The gun employed industrial-grade compressed nitrogen gas to a maximum pressure of 1500 psi. This pressure gives a maximum velocity of about 900 ft/s for the 1/2-inch-diameter steel spheres used.

For tests requiring a higher velocity, a powder gun was used. The pneumatic gun setup is shown in figures 1 and 2, and is shown schematically in figure 3.

FIGURE 1. ANGLED VIEW OF THE GAS GUN SETUP USED FOR MOST OF THE TESTS

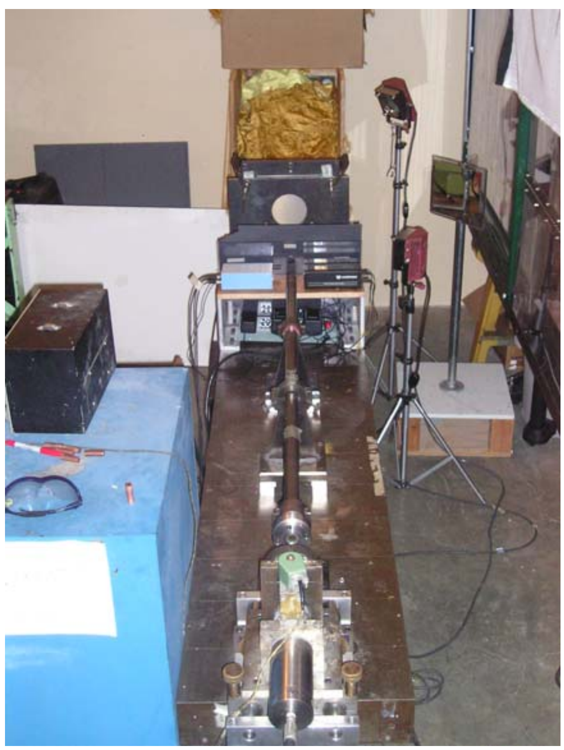

FIGURE 2. STRAIGHT ON VIEW OF THE GAS GUN SETUP

Pneumatic Gun Setup

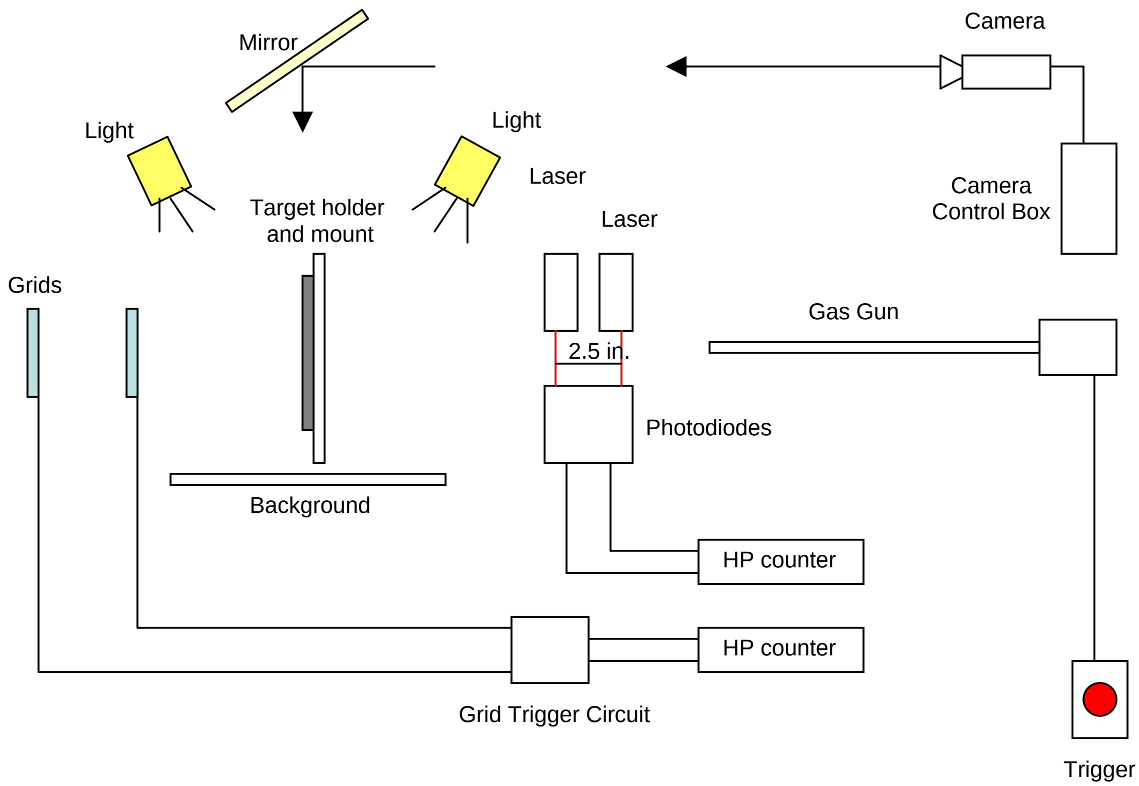

FIGURE 3. SCHEMATIC OF EXPERIMENTAL ARRANGEMENT USING THE GAS GUN

The pneumatic gun has a 1/2-inch nominal diameter barrel that is approximately 52 inches long. However, after 39 inches, there are slits in the barrel that relieve the pressure behind the projectile. The pressure of the gas used for each test is controlled by the regulator on the nitrogen tank. The regulator can be set for any pressure from about 25 to 1500 psi. An electronic control box is then used that opens a solenoid valve releasing the gas at the desired pressure from the tank to the breech pressure chamber. Another solenoid valve between the breech and the gun barrel is controlled by a trigger outside the laboratory. This trigger releases the gas from the breech pressure chamber into the barrel of the gun, accelerating the projectile through the barrel. A diagram of the gas flow can be seen in figure 4.

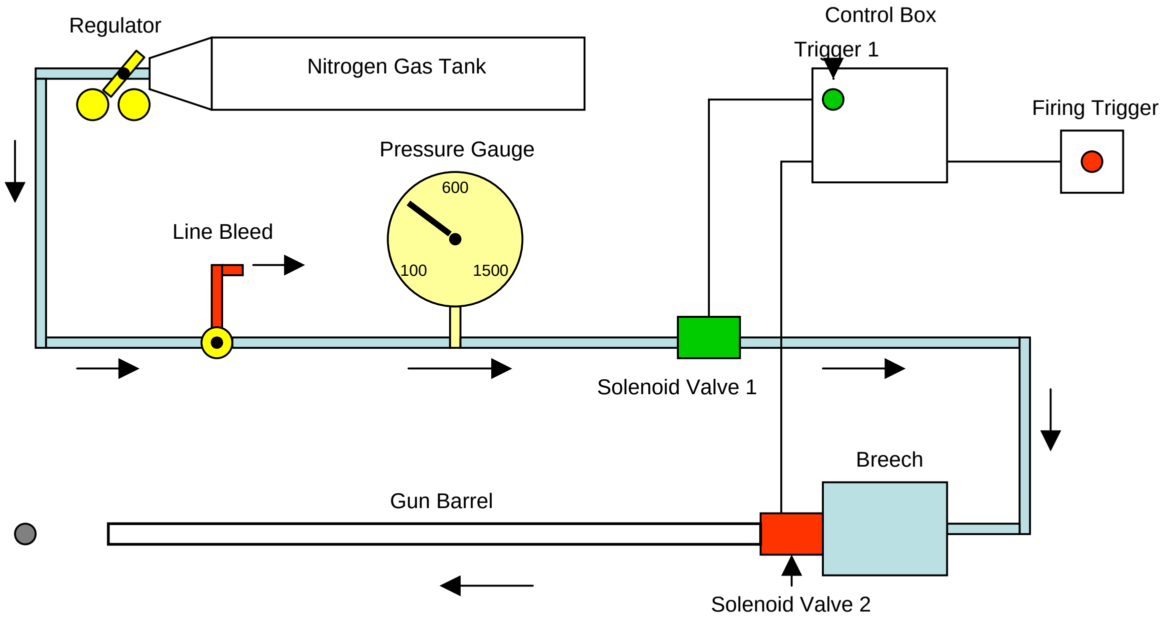

FIGURE 4. FLOW OF NITROGEN GAS THROUGH THE PNEUMATIC CONTROLS

2.1.2 Initial Velocity Measurement System.

The initial velocity of the projectile was found using a laser/photodiode setup (shown in figure 5) that was constructed specifically for this test program. Two Uniphase, helium-neon, gas laser beams were focused through the path of the projectile at two Sharp IS489 high-sensitivity light detectors, 2.5 inches apart. Upon firing, the projectile broke the path of each laser beam causing its respective photodiode circuit to produce a voltage drop (fall time ~.1 µs) that was detected by a Hewlett Packard 53131A Universal Counter. The counter measured the time between the two voltage drops, and the time was used to calculate the velocity of the projectile. The wiring diagram for the photodiode circuit constructed for this program is shown in appendix D.

FIGURE 5. INITIAL VELOCITY MEASUREMENT SYSTEM
(The photodiodes and their accompanying circuit are within the gray box.)

2.1.3 Target Holder.

The targets were all held by two square, 1/2-inch-thick steel frames, 10 inches square on the inside, 14 inches square on the outside. The target was placed in the middle of the two frame plates, and the plates were then tightened together using eight 3/8-16- by 2-1/2-inch socket head cap screws (SHCS) alloy steel bolts. The target holder used for all the testing in this program is shown in figure 6.

FIGURE 6. A 0.25-INCH ALUMINUM PLATE WITHIN THE TARGET HOLDER

2.1.4 Target Mount.

The target holder was held in the line of the projectile by a large steel angle manufactured specifically for this purpose. The mount was made so that the target holder could be moved, and the target could be impacted at nearly all of its 10-inch square area. The target mount, shown in figure 7, was securely fastened to the steel table to prevent any motion upon impact. The target holder was attached to the mount by four C-clamps, one at each corner.

FIGURE 7. TARGET HOLDER WITH THE TARGET MOUNT ATTACHED

2.1.5 Residual Velocity Measurement System.

Two methods were used to measure the residual or postimpact velocity of the projectile. The first method used paper grids. The paper grids consist of two sets of interdigitated, conducting silver ink lines, as shown in figure 8. Each set of lines had a large lead where an alligator clip was attached. The alligator clips were attached to an HP 53131A universal counter and to a circuit that produced a small voltage output. As the projectile (which was also a conductive material) hit the grids, it completed the circuit, sending a positive voltage gain to the counter. To measure the residual velocity, two grids were held 7.25 inches apart directly behind the target. The counter recorded the time between the two successive signals that were sent as the projectile passed through the two grids, which was used to calculate the residual velocity.

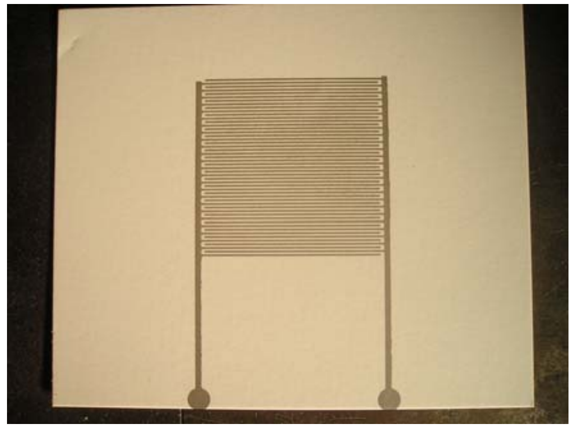

FIGURE 8. GRID HOLDER WITH GRIDS ATTACHED BY CLIPS ON THE TOP CORNERS, ALLIGATOR CLIPS ATTACHED TO THE LEADS (LEFT), AND A GRID BY ITSELF (RIGHT)

2.1.6 High-Speed Camera.

A Photron Fastcam high-speed camera controller with a Kodak Motion Corder Analyzer, Series SR camera was also set up to measure the residual velocity of the projectile (see figure 9). The camera was used as a backup to the grid system and also identified when a plug preceded the projectile to the grids creating an experimental error. Using a recording speed of 10,000 frames per second, the projectile's flight path could be recorded just before and after impact. At 10,000 frames per second, the maximum shutter speed was 1/20,000 second. This required a great deal of light. This illumination was provided by two high-intensity, 650-watt lamps that would be turned on only during filming. The camera was set up approximately 9 feet away, perpendicular to the projectile's flight path. Using a wide angle lens, this distance allowed a field of view of around 10 inches wide and 2 inches high at 10,000 frames per second. The camera was set up such that the field of view consisted of 2 inches before impact and about 8 inches after impact. With this field of view, at least three frames of postimpact projectile flight were recorded at the highest residual velocity recorded (~1300 ft/s on the powder gun). The recorded files were analyzed to obtain a residual velocity of the projectile. For each series of shots, a scale was placed in the field of view in line with the projectile's flight path to determine how many pixels per inch the camera was recording. The camera controller also allowed the user to scroll through the pixels in the x and y directions to record the projectile's position within the field of view. By stepping through frames and recording the position of the projectile, the residual velocity was obtained by simple calculation.

FIGURE 9. KODAK CAMERA (LEFT) AND THE PHOTRON FASTCAM CAMERA CONTROLLER (RIGHT)

The high-speed camera recordings also provided valuable information about target and projectile behavior. The files were examined in great detail to obtain any information on failure characteristics of the target and how the projectile behaved upon, during, and after impact. Evidence of shattering and plugging of the target, finite strain bending, melting, and projectile deviation were all observed by analyzing the recordings. The recordings for each test were viewed and then saved as .avi files.

2.1.7 Catcher Box.

The catcher box, shown in figure 10, was designed to catch or stop the projectile after each test without damaging anything within the lab and to prevent ricochet of the projectile. The catcher box was simply a large wooden box filled with old Zylon® sheets with a large 1/2-inch-thick steel plate secured to the back. After each test, the projectile was found in the catcher box and examined for permanent deformation. The catcher box also often caught plugs that exited most of the aluminum targets. If a plug was present, it would be retrieved after each test, examined, and weighed.

FIGURE 10. CATCHER BOX AT THE END OF THE GAS GUN

2.2 POWDER GUN SETUP.

2.2.1 Powder Gun.

In the event that the pneumatic gun could not achieve the necessary velocity for a given set of tests, the powder gun was used. The powder gun could achieve speeds upwards of 2000 ft/s using 1/2-inch steel spheres. The powder gun consisted of a 63-inch-long SAE 5130 steel smooth bore barrel with an inner diameter of 1/2 inch. The powder gun was configured to use .50 caliber shells. These shells were filled with IMR 3031 smokeless powder. The amount of powder was determined by the desired speed of the projectile. The shells were loaded into the breech, which used an interlocking mechanism, and the gun was fired electronically from outside the laboratory. A pin within the breech was designed to ignite the primer of the shell when the trigger was fired. A view of the powder gun setup is shown in figure 11, and a diagram of the set up is shown in figure 12.

FIGURE 11. STRAIGHT ON VIEW OF THE POWDER GUN SETUP

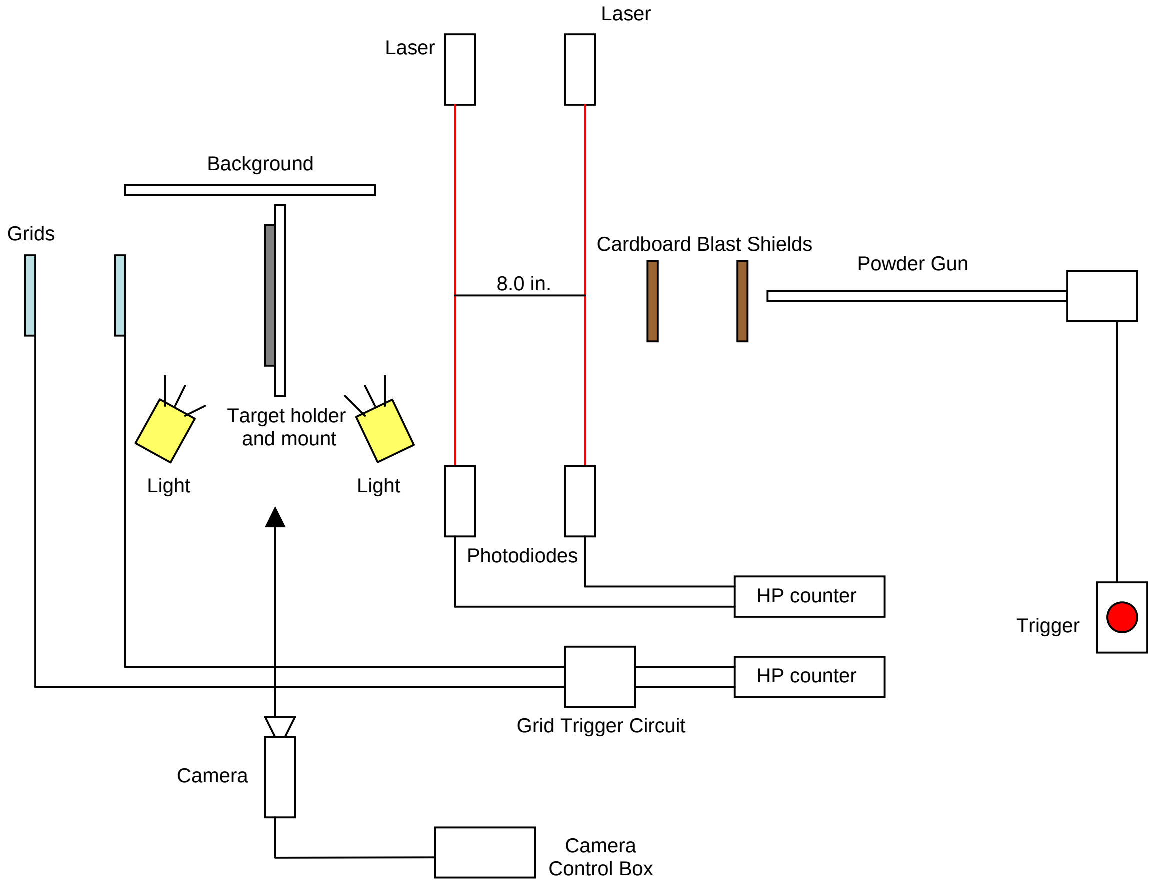

FIGURE 12. SCHEMATIC OF EXPERIMENTAL ARRANGEMENT USING THE POWDER GUN

2.2.2 Initial Velocity Measurement System.

The initial velocity measurement system on the powder gun, shown in figure 13, was nearly identical to the system that was on the pneumatic gun. It also used a laser/photodiode setup. The lasers were also helium-neon gas lasers, but the light detectors were custom-designed photodiodes that produced a positive voltage pulse (rise time ~2 μs) as the path of the laser was broken by the projectile. In this setup, the lasers were placed 8 inches apart. As in the other setup, an HP 53131A Universal Counter was used to detect the time between voltage pulses. This time was used to calculate the velocity.

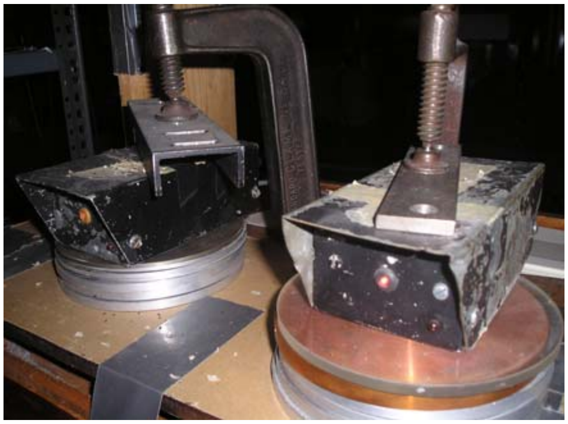

(a)

(b)

FIGURE 13. (a) PHOTODIODE BOXES AND (b) A VIEW OF THE LASER/PHOTODIODE SETUP WITH THE LASERS ON THE LEFT AND THE PHOTODIODES ON THE RIGHT

2.2.3 Target Holder.

The target holder that was used was the same as described in section 2.1 for the pneumatic gun setup.

2.2.4 Target Mount.

The cast iron target mount serves the same purpose as the target mount described in section 2.1.4. It was used to hold the target holder in line of the projectile by four C-clamps. The mount was securely attached to the powder gun table and held the target approximately 54 inches from the muzzle of the powder gun. The target mount is shown in figure 14.

FIGURE 14. TARGET HOLDER ATTACHED TO THE TARGET MOUNT USED IN THE POWDER GUN SETUP

2.2.5 Cardboard Blast Shields.

One problem that was found while testing with the 1/2-inch steel sphere projectile on the powder gun, was that there was a small amount of space between the projectile and the gun barrel. This resulted in unignited powder pellets escaping past the projectile in the barrel and often triggering the lasers ahead of the projectile. To solve this problem, a series of two cardboard sheets were used directly in front of the muzzle as a blast shield, allowing the projectile to pass easily but stopping the powder pellets before they reached the lasers. The cardboard sheets were approximately 3 and 10.25 inches from the muzzle. The cardboard blast shields are shown in figure 15.

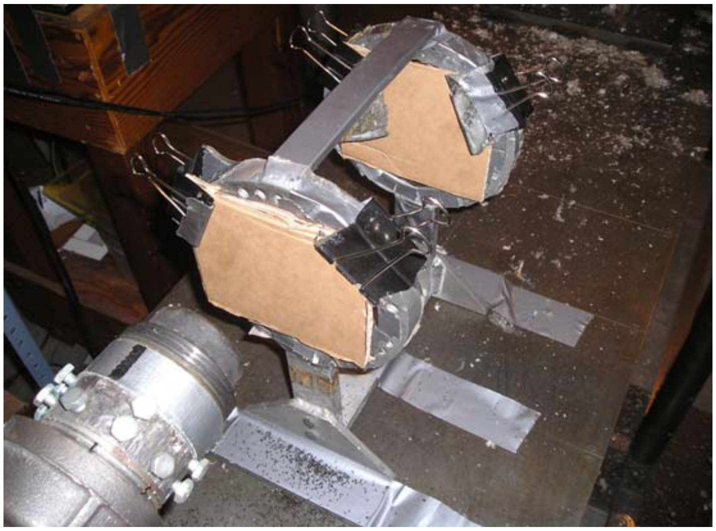

FIGURE 15. CARDBOARD SHEETS USED AS A BLAST SHIELD IN FRONT OF THE MUZZLE OF THE POWDER GUN

2.2.6 Residual Velocity Measurement System.

The residual velocity measurement system on the powder gun is identical to that used and described in the pneumatic gun setup as described in section 2.1.5.

2.2.7 High-Speed Camera.

The camera setup is identical to that used and described in section 2.1.6 for the gas gun setup.

2.2.8 Catcher Box.

Although the catcher box used for the powder gun, shown in figure 16, is slightly larger than that used for the pneumatic gun, it worked exactly the same way.

FIGURE 16. CATCHER BOX AT THE END OF THE POWDER GUN

2.3 TEST PROCEDURE.

2.3.1 Pneumatic Gun Tests.

The following test procedure was followed for each of the pneumatic gun tests:

1. All the targets used in the tests were precut to a 12- by 12-inch square. These targets were placed within the target holder and eight 3/8-16- by 2-1/2-inch SHCS alloy steel bolts were placed within the target holder, four at the corners and four at the midpoints. The bolts were tightened using a torque wrench to approximately 10 ft/lb. The composite sheets were more carefully tightened due to the low compressive strength of the hexagonal sandwich core, only hand tightening the bolts.

2. The target holder was placed on the target mount, and the center of the target was carefully lined up with the path of the projectile, ensuring that the projectile would hit the center of the sheet in each test to avoid possible differences in boundary effects. Care was also taken to ensure that the target plane was nearly perpendicular to the path of the projectile to avoid oblique impacts. The target holder was then clamped at each of its four corners using C-clamps.

3. The initial and residual velocity measurement systems were prepared and tested. Two paper grids were placed in line with the path of the projectile approximately 6 inches from the target. The grids were tested several times to ensure proper function. If errors occurred during the testing process, the grids were replaced. The laser/photodiode system was also tested several times to guarantee a successful measurement during the test.

4. The pressure was set in the system to the desired value using the regulator valve on the end of the nitrogen tank. The value of the pressure depended on the desired velocity for the given test, which was obtained by a calibration curve developed for the 1/2-inch steel sphere projectile relating pressure to velocity, as shown in figure 17.

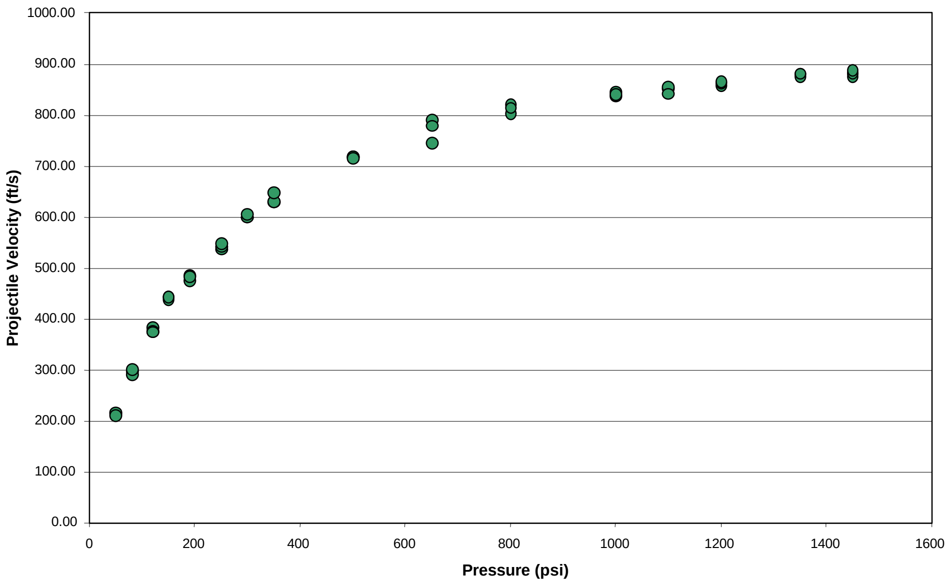

FIGURE 17. CALIBRATION CURVE FOR 1/2-INCH STEEL PROJECTILES ON THE GAS GUN, RELATING PRESSURE TO INITIAL PROJECTILE VELOCITY

5. The breech of the gun was slid back on its two support rails, and the projectile was placed just in front of pressure chamber in the barrel. The breech was brought forward and reattached to the barrel. This process is shown in figure 18.

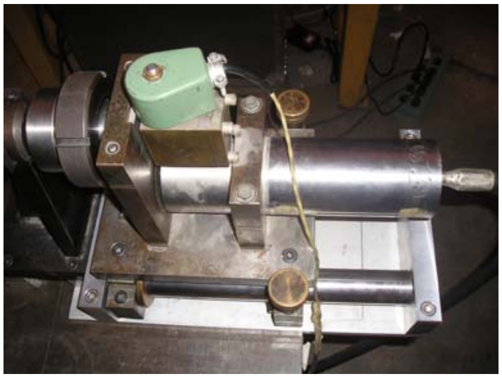
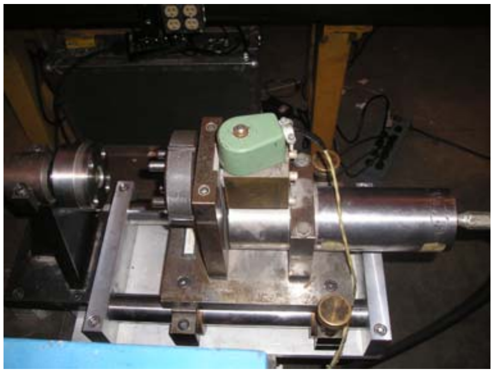

FIGURE 18. PRESSURE CHAMBER AND BREECH ATTACHED TO THE BARREL (LEFT) AND SLID BACK FROM THE BARREL ON ITS SUPPORT RAILS (RIGHT)

6. The high-speed camera was prepared to record the shot. The camera was adjusted to 10,000 frames per second, and the high-intensity lamps were turned on. The camera was lined up correctly to record the shot by observing the video output of the camera and adjusted accordingly.

7. The pressure was released into the pressure chamber of the breech, and the firing trigger was connected to the electronic control box. The counters were reset and prepared to take measurements, at which point everything was prepared to perform the test.

8. The room was evacuated and the camera control box brought outside the laboratory. Using the camera control box, the recording was started. The trigger was fired, and the recording was stopped.

9. After the test was performed, all the measurements were recorded, the recording of the test was analyzed and saved, the projectile (and plug if used) were recovered, and the target was taken down and inspected for failure characteristics. The target (and target plug if it resulted) was then labeled and stored for future reference.

<u>2.3.2 Powder Gun Procedure</u>.

The following test procedure was followed for each of the power gun tests.

1. All the targets used in the tests were precut to a 12- by 12-inch square. These targets were placed within the target holder and eight 3/8-16- by 2-1/2-inch SHCS alloy steel bolts were placed within the target holder, four at the corners and four at the midpoints. The bolts were tightened using a torque wrench to approximately 10 ft/lb. The composite sheets were more carefully tightened due to the low compressive strength of the hexagonal sandwich core, only hand tightening the bolts.

2. The target holder was placed on the target mount, and the center of the target was carefully lined up with the path of the projectile, ensuring that the projectile would hit the center of the sheet in each test to avoid possible differences in boundary effects. Care was also taken to ensure that the target plane was nearly perpendicular to the path of the projectile to avoid oblique impacts. The target holder was then clamped at each of its four corners using C-clamps.

3. The initial and residual velocity measurement systems were prepared and tested. Two paper grids were placed in line with the path of the projectile approximately 6 inches from the target. The grids were tested several times to ensure proper function. If errors occurred during the testing process, the grids were replaced. The laser/photodiode system was also tested several times to guarantee a successful measurement during the test.

4. The barrel of the gun was cleared of debris from the previous test, and the cardboard blast shields were set up.

5. A shell was then prepared for the test. A specific amount of powder pertaining to a desired velocity was weighed on a small balance scale and poured into the bottom of the shell. The amount of powder used was based on the velocities obtained in previous tests for a given powder amount, not a calibration curve. A quarter of a standard tissue was then placed into the shell and tamped down several times to ensure an even packing of the powder. The projectile was then placed into the shell, as shown in figure 19.

6. The high-speed camera was prepared to record the shot. The camera was adjusted to 10,000 frames per second, and the high-intensity lamps were turned on. The camera was lined up correctly to record the shot by observing the video output of the camera and adjusted accordingly.

7. The shell was then loaded into the breech of the powder gun, as shown in figure 20, and the breech was closed. The triggering mechanism was attached to the back of the breech and the counters were reset and prepared for taking measurements. At this point, everything was prepared to perform the test.

8. The room was evacuated and the camera control box brought outside the laboratory. Using the camera control box, the recording was started. The trigger was fired, and the recording was stopped.

9. After the test was performed, all the measurements were recorded, the recording of the test was analyzed and saved, the projectile (and plug if used) were recovered, and the target was taken down and inspected for failure characteristics. The target (and target plug if it resulted) was then labeled and stored for future reference.

FIGURE 19. A LOADED SHELL

FIGURE 20. SHELL BEING LOADED INTO THE BREECH OF THE POWDER GUN

3. RESULTS AND DISCUSSION.

3.1 PROJECTILES.

The projectiles used in all the tests were 1/2-inch-diameter AISI 52100 chrome steel spheres purchased from Bearing Engineering in Emeryville, CA. These projectiles were chosen to avoid yaw and rotation problems that had arisen when using cylindrical projectiles. This allowed a consistent point of impact, greatly increasing the repeatability of the tests. It is also important to note that the projectiles suffered no permanent deformation in any of the tests performed. The hardness of the spheres was 60-64 Rockwell "C." Some material properties for the projectiles are provided in table 1.

TABLE 1. MATERIAL PROPERTIES OF THE PROJECTILES

Ultimate Tensile Strength	Yield Strength	Density	Mass
325,000 psi	295,000 psi	0.283 lbs/in^3	0.29 oz.
2.2 GPa	2.0 GPa	7.833 g/cc	8.3 g

It should also be noted that all test shots in this study were center shots on the targets.

3.2 2024 ALUMINUM.

3.2.1 Material Properties.

The 2024-T3 and T351 alloy aluminum target material was purchased and cut into 12- by 12-inch squares by Alco Iron and Metal in San Leandro, CA. Target plates, 0.063, 0.125, and 0.25 inch thick, were ballistically evaluated. The chemical composition of 2024-T3 and T351 are identical and are given in table 2. The 2024-T3 material was desired for all testing; however, it was available as sheet material only, but thicknesses of 0.25 inch and greater are only available in 2024-T351 material. There are some slight property differences between the two materials.

TABLE 2. CHEMICAL COMPOSITION OF 2024-T3 AND T351 ALUMINUM

Aluminum	Balance (%)
Copper	4.76
Magnesium	1.38
Manganese	0.65
Iron	0.22
Silicon	0.08
Zinc	0.07
Titanium	0.03
Chromium	0.01

Some of the material properties for 2024-T3 and T351 aluminum from Aerospace Specification Metals (ASM) are summarized in table 3.

TABLE 3. MATERIAL PROPERTIES

2024-T3 Aluminum Sheet				
Ultimate Tensile Strength	Yield Strength	Strain at Break	Shear Modulus	Density
70,000 psi	50,000 psi	18%	4,060,000 psi	0.1 lbs/in^3
Material Properties of the 2024-T351 Aluminum Plates				
Ultimate Tensile Strength	Yield Strength	Strain at Break	Shear Modulus	Density
68,000 psi	50,000 psi	19-20%	4,060,000 psi	0.1 lbs/in^3

To avoid ambiguity in the descriptions of the failure mechanisms of the targets, the following terms will be defined as in reference 5 and section 7. The distal face of the plate is the surface opposite the impact surface. Dishing is the flexural and stretching deformation of an annular region of the plate surrounding the projectile impact point, where the dished region is displaced normal to the surface of the plate. Denting is the localized indentation of the plate material under the common interface between the projectile and the plate, often accompanied by bulging. Bulging is the localized deformation or displacement of the distal face of the plate normal to its surface. Petaling is the formation of petals caused by radial cracking from the point of impact. Shear plugging is the shearing of the target plate around the point of impact causing the formation of a plug of target material. Shattering refers to the case when several fragments exit the target material upon impact. Perforation is the breaking through of the distal face of the plate by the projectile. The ballistic limit velocity, or v_{50}, is defined here as the velocity beyond which the projectile fully perforates a target and below which it will not [6].

3.2.2 Aluminum Targets, 0.063 Inch Thick.

The full ballistic curve for 0.063-inch-thick aluminum, plotting the residual projectile velocity against the initial projectile velocity, is shown in figure 21. The amount of energy absorbed by each target relative to the initial projectile velocity was also plotted and is shown in figure 22. In these graphs, error bars are present showing the amount of error possible for each data point. A detailed discussion of the error analysis explaining the sources of error for each point is contained in appendix A.

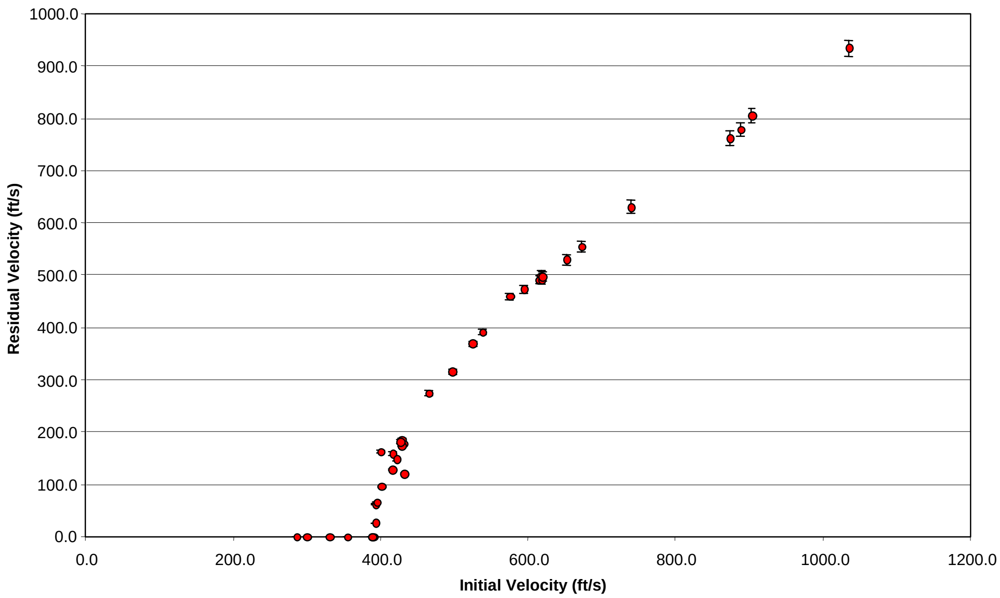

FIGURE 21. BALLISTIC CURVE FOR 0.063-INCH ALUMINUM

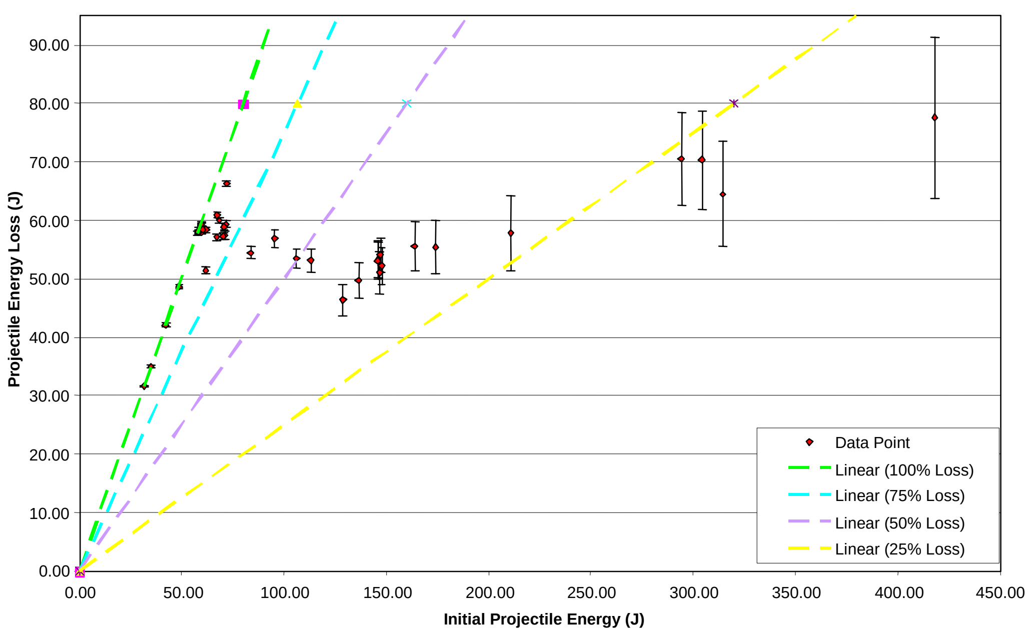

FIGURE 22. INITIAL KINETIC ENERGY OF THE PROJECTILE VS THE AMOUNT OF ENERGY ABSORBED BY THE 0.063-INCH ALUMINUM TARGETS

The ballistic limit for these targets was found to be approximately 391 ft/s. At speeds significantly below the ballistic limit ($v_i < 300$ ft/s), the plates suffered from local dishing around the point of impact, where the amount of dishing decreased with initial velocity. At these speeds, no plug exited the target.

As the initial velocity approached the ballistic limit (300 ft/s < v_i < v_{50}), the target dished and then underwent petaling, radial cracks propagating from the center of the impact site, as well as some shear plug formation, shearing of the target around the center of the impact site. Even though petaling and shear plugging took place, the projectile did not fully penetrate the material at these speeds. At initial projectile velocities above the ballistic limit (v_i > v_{50}), the target also dished and then failed by petaling and shear plug formation. At initial impact, the projectile pushed out a plug by shear forces around the center of impact. The plug size was dependent upon the speed of the projectile. The projectile then began to petal the target plate. The petals of aluminum were pushed in a radial direction by the projectile until it slipped through the central hole. Elastic recovery of the plate and the petals occurred immediately after the projectile had cleared the petals. Therefore, the hole formed in the target plate was smaller than the projectile. As the initial velocity increased beyond the ballistic limit, the size of the plugs exiting the target increased, as shown in table 4 and figure 23.

TABLE 4. PLUG DIAMETER AT DIFFERENT PROJECTILE VELOCITIES

Initial Projectile Velocity v_i (ft/s)	Plug Diameter (in.)
390	0.28
619	0.34
888	0.39

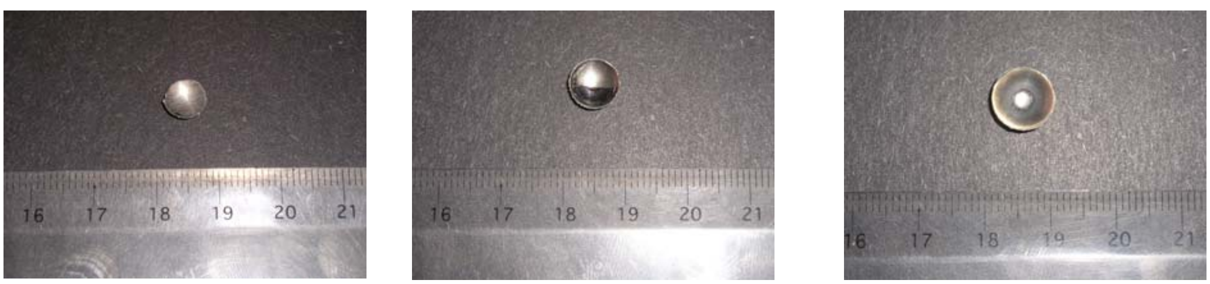

v_i = 390 ft/s v_i = 619 ft/s v_i = 888 ft/s

FIGURE 23. VIEWS OF PLUGS AT DIFFERENT INITIAL PROJECTILE VELOCITIES, SHOWING INCREASING SIZE WITH INCREASING VELOCITY

As a result of the larger plugs, the amount of deformation due to petaling decreased, as the projectile needed to push away less of the target material to slip through the central hole. However, the number of petals or the number of radial cracks propagating from the center of the impact site increased with the velocity of the projectile, as shown in table 5 and figure 24.

TABLE 5. NUMBER AND SIZE OF PETALS RELATIVE TO v_i

Initial Projectile Velocity v_i (ft/s)	Number of Petals	Normal Distance of Petal Deformation From Distal Face d* (in.)
390	4	0.28
619	5	0.20
888	6	0.16

*See appendix B for a diagram

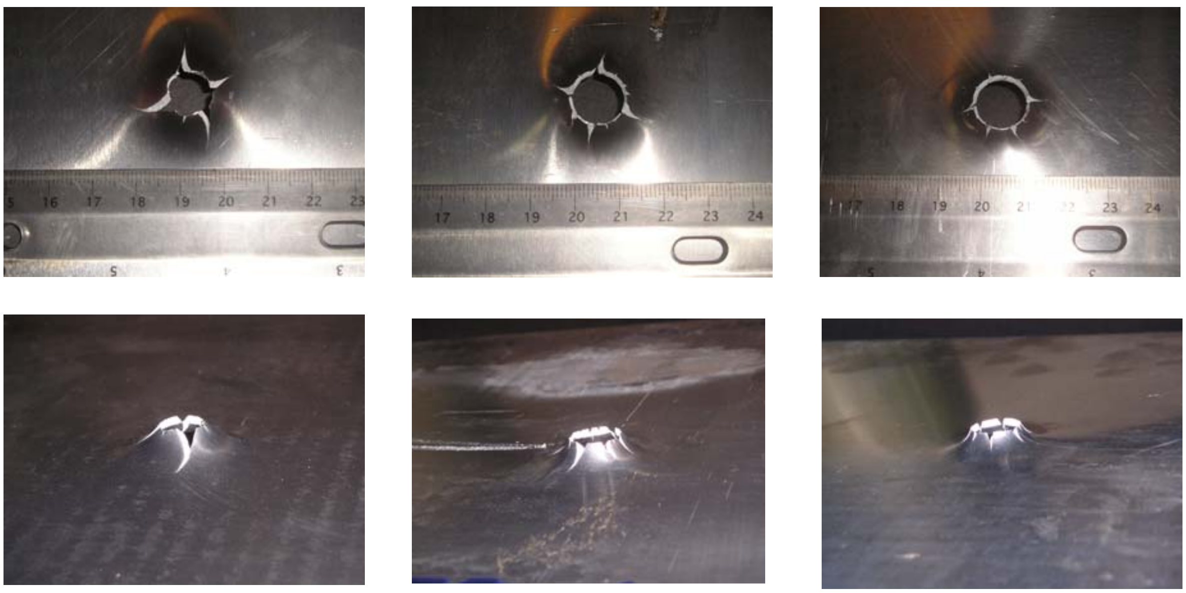

v_i = 390 ft/s v_i = 619 ft/s v_i = 888 ft/s

FIGURE 24. BACK AND ANGLED BACK VIEWS OF PLATES SHOT AT DIFFERENT INITIAL VELOCITIES, SHOWING THE INCREASE IN THE NUMBER OF PETALS AND DECREASE IN PETAL SIZE WITH INCREASING PROJECTILE VELOCITY

The consistency of the residual velocity for a given initial velocity was also examined for these targets by taking multiple shots at a given pressure. Because it was not possible to get identical initial projectile velocities for a given pressure, a true analysis could not be performed. Instead, this examination resulted in a cluster of shots around similar initial velocities, which were subjectively examined for consistency. For the 0.063-inch aluminum targets, two groups of clusters were obtained, as shown in figure 25.

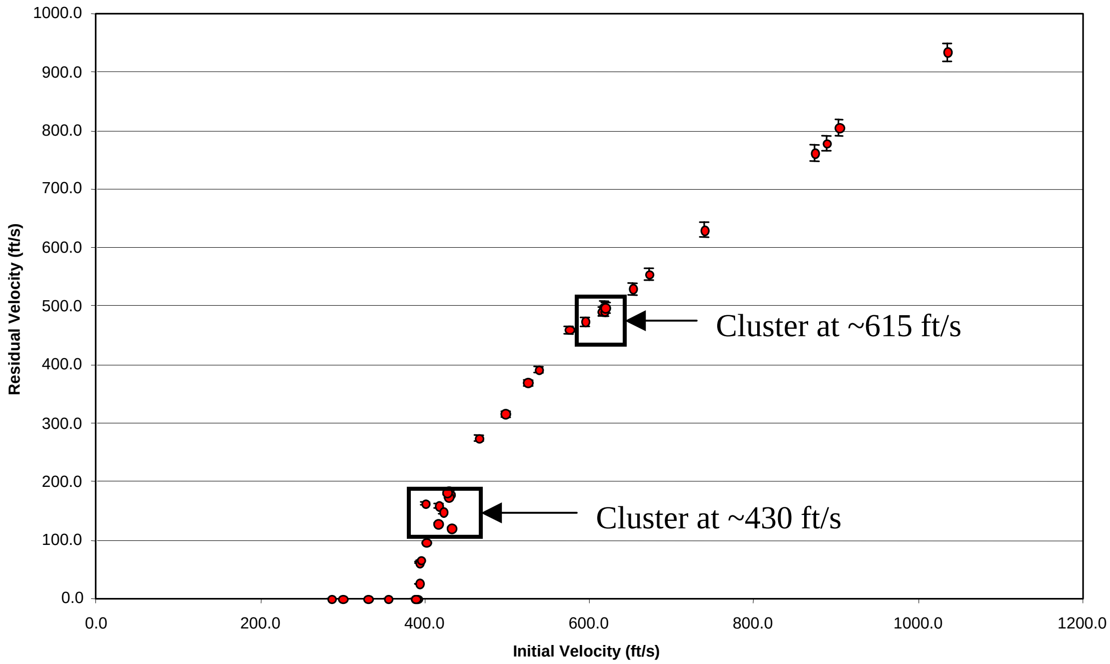

FIGURE 25. BALLISTIC CURVE FOR 0.063-INCH ALUMINUM SHOWING CONSISTENCY CLUSTERS

As seen in figure 25, the results for tests performed at approximately 430 ft/s were less consistent than the tests performed at approximately 615 ft/s. The results for the tests performed at the higher velocity form a very tight cluster with little variation. However, the results for the tests performed at the lower velocity are scattered. This scatter may be a result of measurement error (see appendix A), or more simply, a result of inherent scatter near the ballistic limit.

3.2.3 Aluminum Targets, 0.125 Inch Thick.

The full ballistic curve for 0.125-inch aluminum, plotting the residual projectile velocity against the initial projectile velocity, is shown in figure 26. The amount of energy absorbed by each target relative to the initial projectile velocity was also plotted and is shown in figure 27. The results for this thickness are the most consistent, which is probably a result of the consistent method of failure of the targets at all initial projectile velocities.

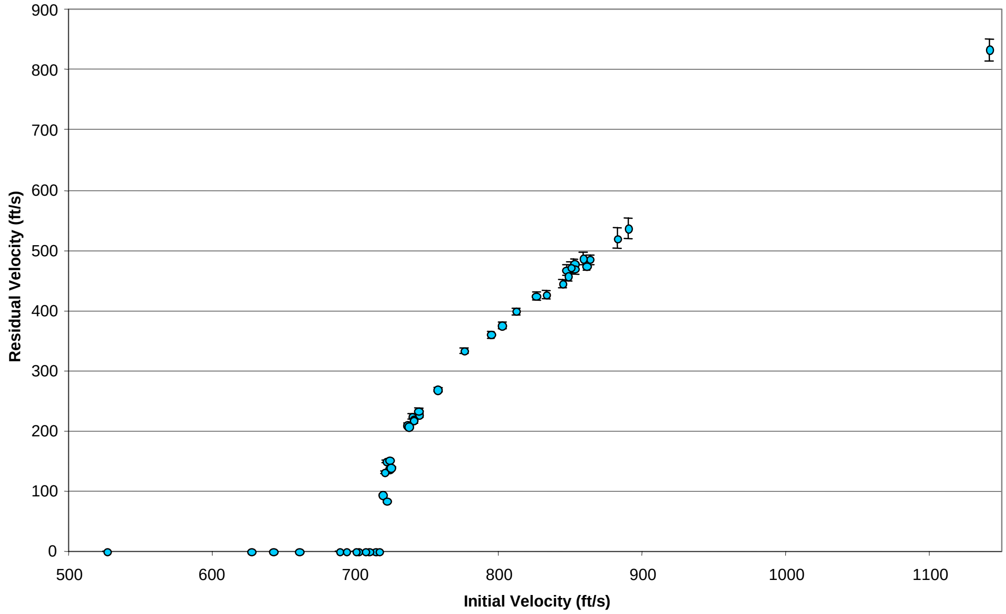

FIGURE 26. BALLISTIC CURVE FOR 0.125-INCH ALUMINUM

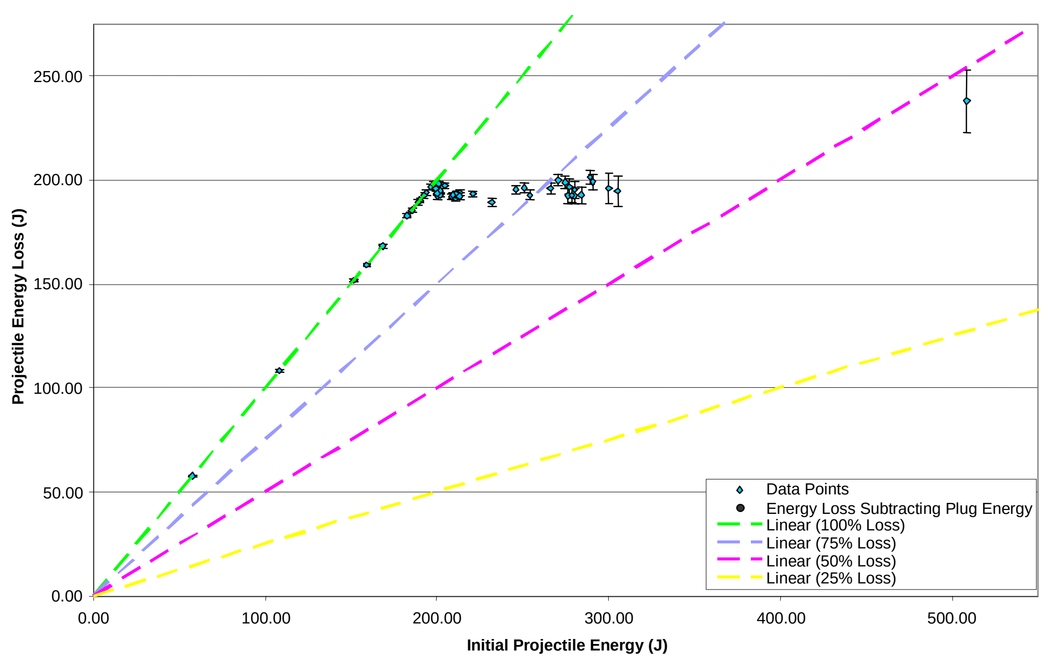

FIGURE 27. INITIAL KINETIC ENERGY OF THE PROJECTILE VS THE AMOUNT OF ENERGY ABSORBED BY THE 0.125-INCH ALUMINUM TARGETS

The ballistic limit for these targets was found to be approximately 717 ft/s. The response of these targets was intermediate between those of the thin and thick plates. For $v_i < v_{50}$, little dishing occurred compared to the 0.063-inch targets, but there was still noticeable deformation around the immediate site of impact, as shown in figure 28. As v_i approached v_{50}, petaling and shear plugging began to take place once again, but for this plate thickness, the deformation was dominated by shear plugging. Large plugs were formed despite the projectile not penetrating the target.

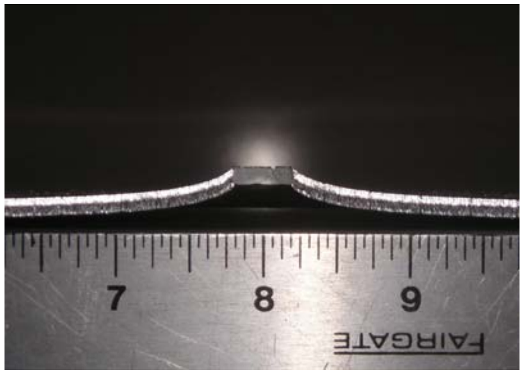

FIGURE 28. CROSS-SECTIONAL VIEW OF A 0.125-INCH TARGET TESTED AT AN INITIAL PROJECTILE VELOCITY OF 627 ft/s, BELOW THE BALLISTIC LIMIT, SHOWING DISHING DEFORMATION AROUND THE POINT OF IMPACT

For $v_i > v_{50}$, the failure method continued to be dominated by shear plugging, with slight petaling occurring. The size of the plugs and the petals only changed slightly with initial projectile velocity, remaining nearly constant after perforation, as shown in tables 6 and 7, and figures 29 and 30. The impact response for this thickness plate was the most predictable and consistent of all aluminum targets.

TABLE 6. PLUG PROPERTIES AT DIFFERENT PROJECTILE VELOCITIES

Initial Projectile Velocity, v_i (ft/s)	Plug Diameter (in.)
724	0.39
861	0.41
1142	0.41

v_i = 724 ft/s v_i = 861 ft/s v_i = 1142 ft/s

FIGURE 29. VIEWS OF PLUGS AT SEVERAL DIFFERENT INITIAL PROJECTILE VELOCITIES, SHOWING THE PLUGS REMAINED NEARLY CONSTANT SIZE WITH INCREASING PROJECTILE VELOCITY

TABLE 7. NUMBER AND SIZE OF PETALS RELATIVE TO v_i

Initial Projectile Velocity, v_i (ft/s)	Number of Petals	Normal Distance of Petal Deformation From Distal Face, d* (in.)
724	9	0.20
861	8	0.20
1142	9	0.20

* See appendix B for a diagram

v_i = 724 ft/s　　v_i = 861 ft/s　　v_i = 1142 ft/s

FIGURE 30. VIEWS OF PLATES SHOT AT DIFFERENT INITIAL VELOCITIES, SHOWING THE CONSISTENCY IN PETAL DEFORMATION WITH INCREASING PROJECTILE VELOCITY

The consistency of the residual velocity for a given initial velocity was also examined for the 0.125-inch aluminum targets by the same method described for the 0.063-inch targets. For this group of targets, two groups of clusters were obtained, as shown in figure 31.

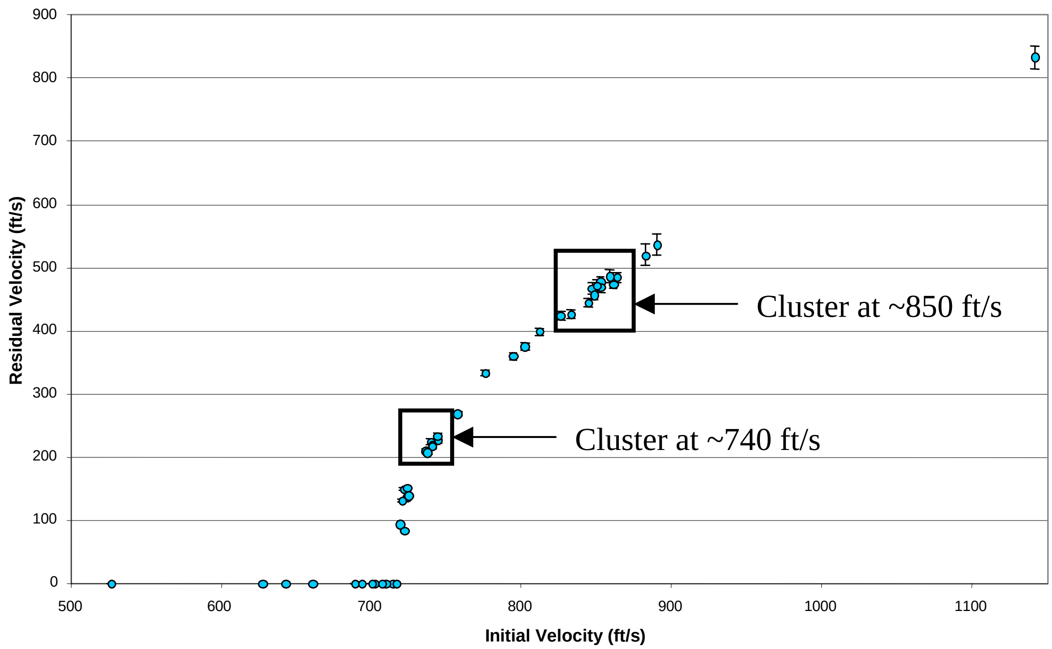

FIGURE 31. BALLISTIC CURVE FOR 0.125-INCH ALUMINUM, SHOWING CONSISTENCY CLUSTERS

As can be seen in figure 31, both clusters of data points for the 0.125-inch tests contain very little variation.

3.2.4 Aluminum Targets, 0.25 Inch Thick.

The full ballistic curve for 0.25-inch aluminum, plotting the residual projectile velocity against the initial projectile velocity, is shown below in figure 32. The amount of energy absorbed by each target relative to the initial projectile velocity was also plotted and is shown in figure 33. The results for this thickness plate are the most scattered. This is partly a result of the inconsistent nature of the failure mechanism, but also errors in the velocity measurements are magnified by the higher velocities. For a more thorough description, see the error analysis in appendix A.

The ballistic limit for these targets was found to be approximately 1327 ft/s. A rare picture of a target with the projectile lodged within the plate identifying the ballistic limit is shown in figure 34. For this thickness plate, little or no dishing occurred for all initial projectile velocities, leaving the plates with a nearly flat profile except for the impact site. For $v_i < v_{50}$, the target plate was dented by the projectile, leaving a projectile-shaped crater within the plate, as shown in figure 35. Similar to the 0.125-inch-thick plates, shear plugging started before the ballistic limit. For this thickness, shear plugging started nearly 300 ft/s below the ballistic limit at approximately 1030 ft/s. The impact response and deformation for velocities above shear plugging and below the ballistic limit were consistently similar, with only slight differences in the plug size and mass.

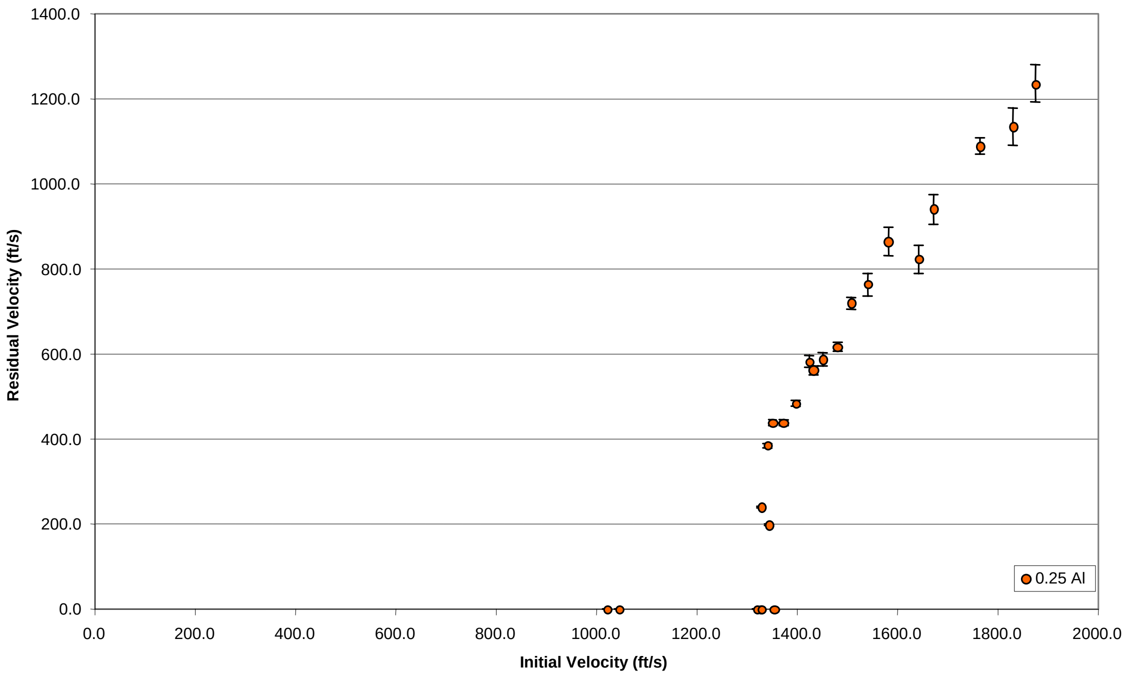

FIGURE 32. BALLISTIC CURVE FOR 0.25-INCH ALUMINUM

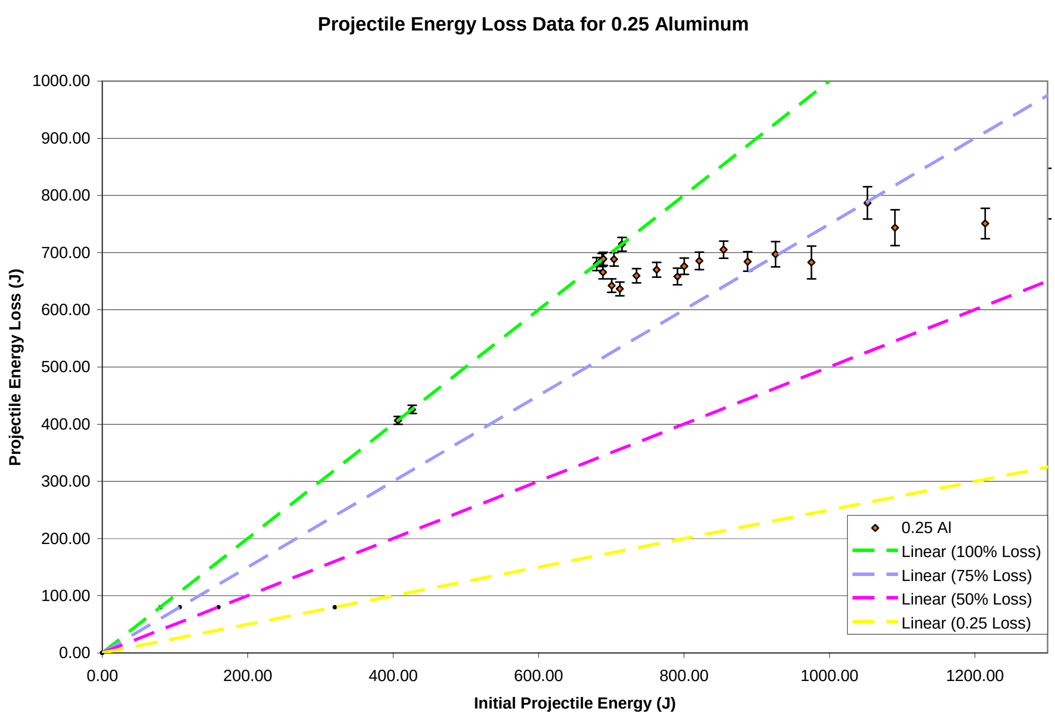

FIGURE 33. INITIAL KINETIC ENERGY OF THE PROJECTILE VS THE AMOUNT OF ENERGY ABSORBED BY THE 0.25-INCH ALUMINUM TARGETS

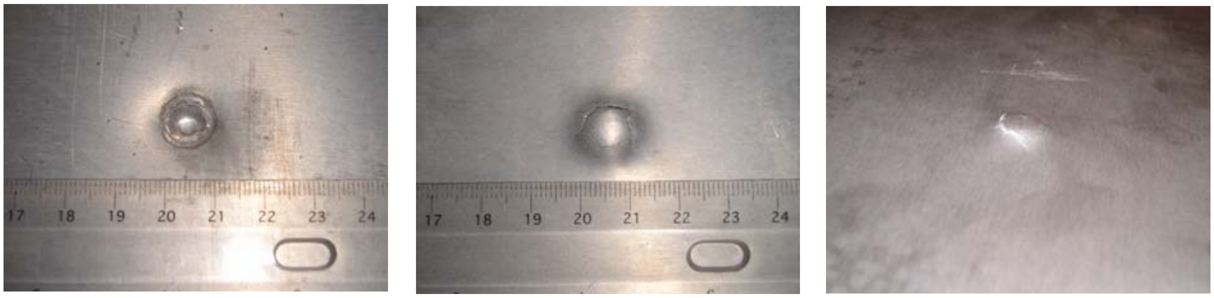

Front View | Back View | Angled Back View

FIGURE 34. PLATE WITH AN INITIAL PROJECTILE VELOCITY OF 1021 ft/s, BEFORE SHEAR PLUGGING
(Note the denting of the target as well as signs of shearing.)

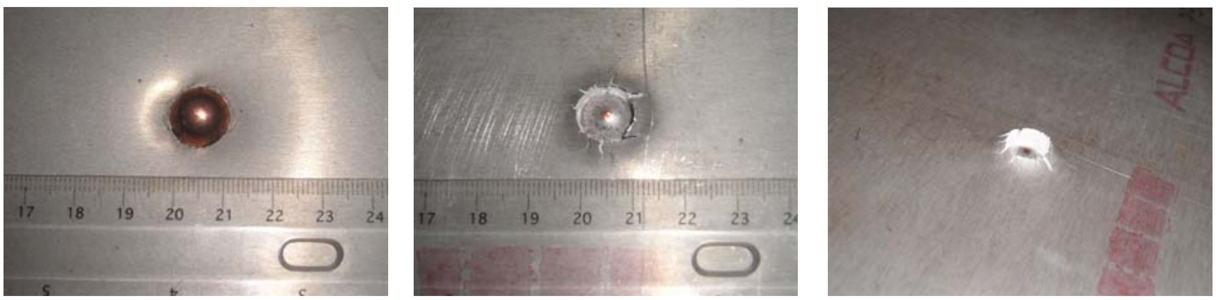

Front View | Back View | Angled Back View

FIGURE 35. PLATE WITH AN INITIAL PROJECTILE VELOCITY AT THE BALLISTIC LIMIT, 1327 ft/s
(Note the projectile neither rebounded nor perforated the target, but remained lodged within the plate.)

For $v_i > v_{50}$, the failure method of the plates continued to be dominated by shear plugging, but the shear plugging was accompanied with both shattering and melting of the target plate. For most of the tests above the ballistic limit, there was not a single plug exiting the material, as witnessed in the other thickness targets. For this thickness, shattering was seen. Several pieces of target material were seen exiting the material, and the projectile did not exit the material as clean as the other thicknesses, as shown in figure 36. The exit holes in the targets were jagged and inconsistent. At these projectile speeds, evidence of melting was observed in the test recordings and on the projectiles themselves. The projectiles were all found with a thin hemispherical film of aluminum around their points of impact, as shown in figure 37. In nearly all the recordings where the projectile fully perforated the target, a white flash was noticed upon impact, as shown in figure 38. These white flashes are indicative of high temperatures and possible phase transformations, which would point towards some target melting.

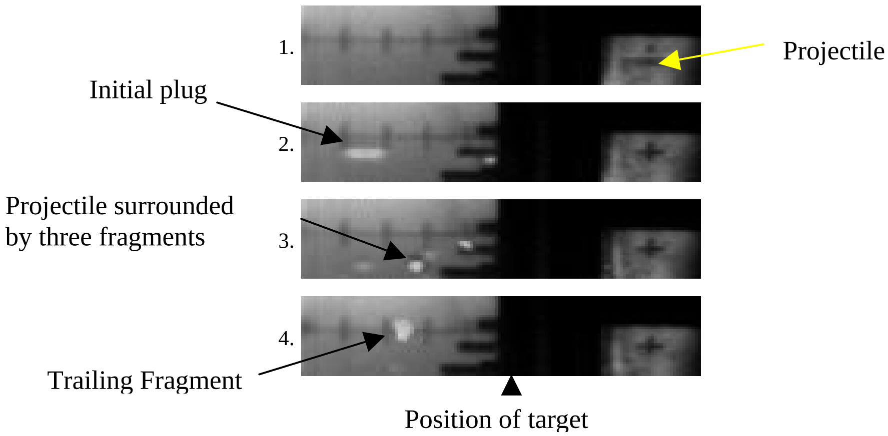

FIGURE 36. IMAGE SEQUENCE SHOWING SHATTERING OF THE TARGET PLATE

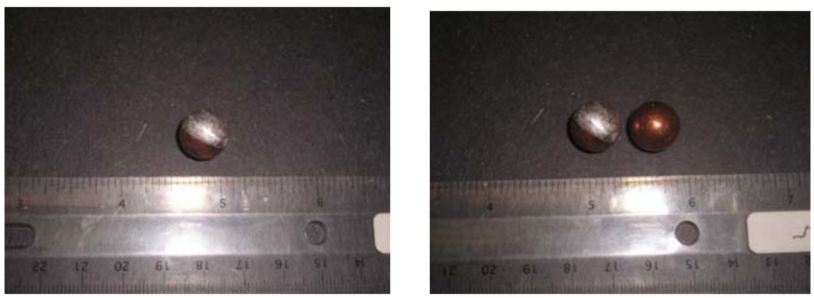

FIGURE 37. PROJECTILE WITH HEMISPHERICAL THIN FILM OF MELTED ALUMINUM FROM IMPACT (LEFT) COMPARED TO A NORMAL PROJECTILE (RIGHT)

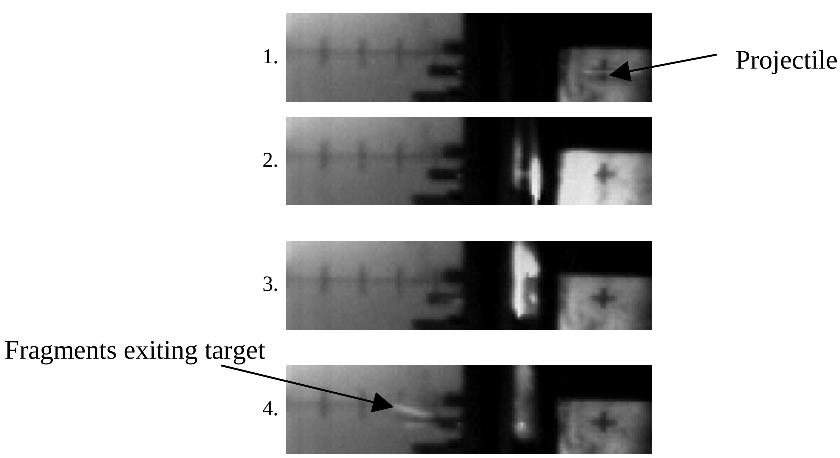

FIGURE 38. IMAGE SEQUENCE SHOWING THE FLASH OF WHITE LIGHT AT IMPACT

Figures 39 through 41 show several targets at varying velocities.

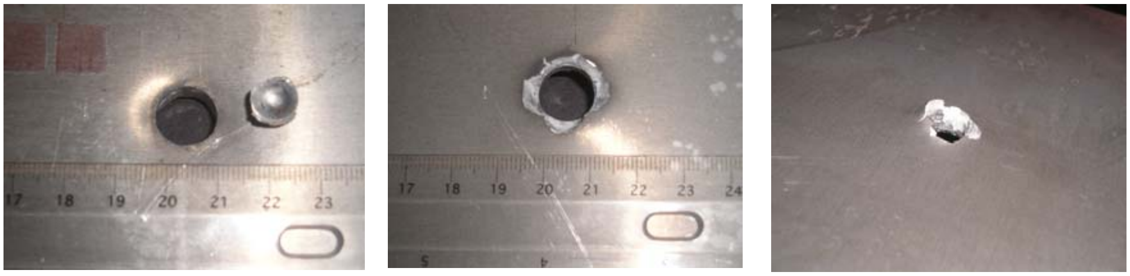

Front View With Plug Back View Angled Back View

FIGURE 39. PLATE WITH AN INITIAL PROJECTILE VELOCITY OF 1343 ft/s, JUST ABOVE BALLISTIC LIMIT
(Note jaggedness of exit hole, which is characteristic of the shattering that occurs at this thickness.)

Front View with Plug Back View Angled Back View

FIGURE 40. PLATE WITH AN INITIAL PROJECTILE VELOCITY OF 1581 ft/s

Front View With Plug Back View Angled Back View

FIGURE 41. PLATE WITH AN INITIAL PROJECTILE VELOCITY OF 1875 ft/s

3.2.5 Summary.

Ballistic experiments were conducted with 1/2-inch-diameter spherical projectiles normal incident at the approximate center of aluminum plates 0.063, 0.125, and 0.25 inch thick. The ballistic limit results for aluminum are summarized in figure 42. The nominal projectile velocity is plotted against plate thickness. The ballistic limit was found to be nearly a linear relationship with plate thickness for these three plate thicknesses.

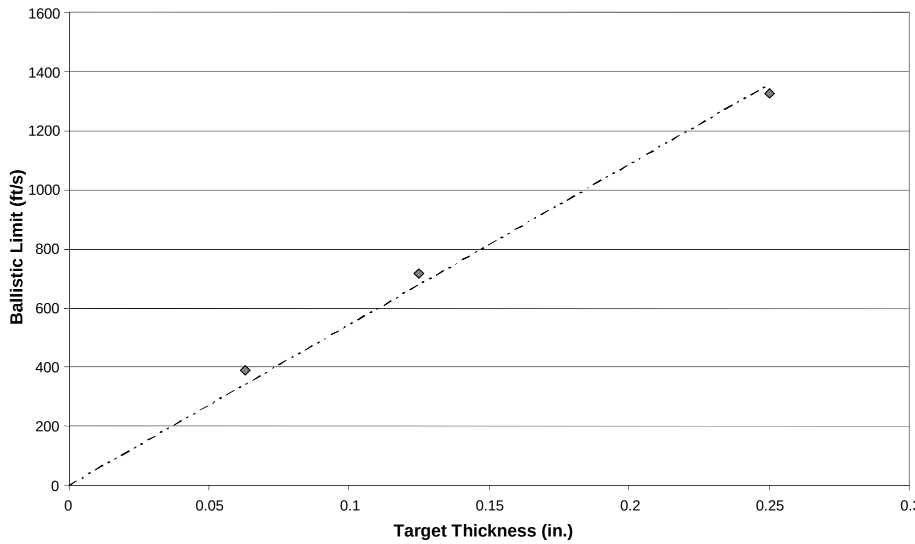

FIGURE 42. BALLISTIC LIMIT OF 2024-T351 Al RELATIVE TO THICKNESS

Six main types of plate failure behavior were identified during these experiments: dishing, petaling, shear plugging, denting, shattering, and melting. Petaling was the main mode of failure for the 0.063-inch plates, followed by dishing. However, as v_i increased, the main mode of failure became shear plugging. For the 0.125-inch plates, shear plugging was the main mode of failure, with slight petaling and dishing occurring. For the 0.25-inch plates, the main mode of failure remained shear plugging, with little to no petaling and dishing occurring. The shear plugging was also accompanied by shattering and melting of the target plates. For some more information on the ballistic behavior of aluminum see references 2, 3, and 7.

3.3 POLYCARBONATE.

3.3.1 Material Properties.

The 0.25-inch polycarbonate was purchased from Interstate Plastics in San Leandro, CA. The brand of the polycarbonate was Makrolon produced by Bayer Plastics. A 24- by 48-inch sheet was purchased, and then cut into 12- by 12-inch squares using a standard band saw in the UBC machine shop. This transparent polymer is unusual in that it exhibits very large yield and fracture strains. Some material properties for Makrolon polycarbonate are shown in table 8.

TABLE 8. MATERIAL PROPERTIES FOR MAKROLON POLYCARBONATE

Tensile Modulus	Yield Stress	Strain at Break	Density
348 ksi	9428 psi	110%	0.043 lbs/in^3

3.3.2 Test Results.

The full ballistic curve for 0.25-inch Makrolon polycarbonate, plotting the residual projectile velocity against the initial projectile velocity, is shown in figure 43. The data seems to undergo a jump around 1200 ft/s, from one curve to another. This could possibly be the result in a change in the failure mechanism which caused the material to absorb slightly more energy. However, no major change in failure mechanism was observed during the test. One possible explanation could be the onset of some material melting that began to occur around this velocity. As shown in the results of the 0.25-inch aluminum plates, the temperature upon impact can become very high with increasing velocities. The process of melting would absorb more energy, which may explain the negative jump in the ballistic curve. This phenomenon can also be seen in the absorbed energy plot shown in figure 44.

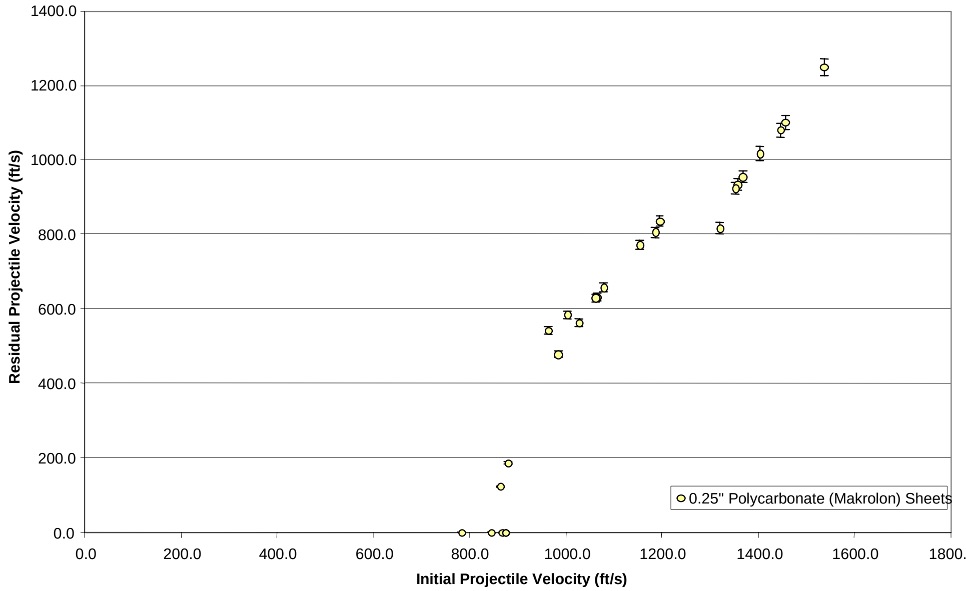

FIGURE 43. BALLISTIC CURVE FOR 0.25-INCH POLYCARBONATE

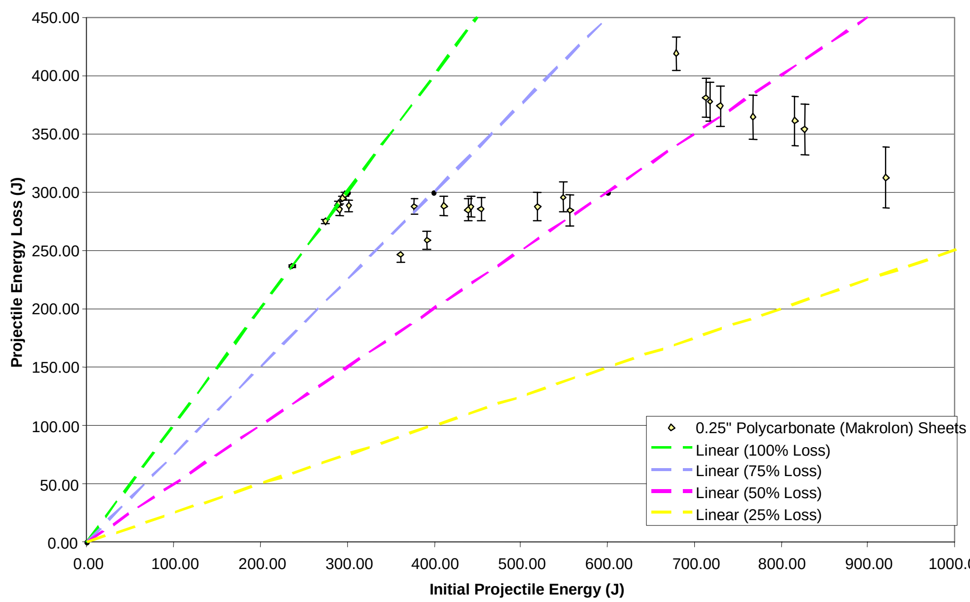

FIGURE 44. INITIAL KINETIC ENERGY OF THE PROJECTILE VS THE AMOUNT OF ENERGY ABSORBED BY THE 0.25-INCH POLYCARBONATE TARGETS

The ballistic limit for the 0.25-inch Makrolon polycarbonate targets was found to be approximately 861 ft/s. At projectile speeds below the ballistic limit, little to no dishing occurred, and all the deformation remained local to the immediate impact site. Although bending of the targets was noticeable upon impact, the sheets underwent complete elastic recovery everywhere except the immediate impact site. Denting occurred at the impact site, producing a depression that was slightly smaller than the projectile. The depression often had a pointed shape caused by radial elastic recovery. At the tip of the bulge, small-scale cracking was visible as the projectile approached the ballistic limit.

At projectile speeds above the ballistic limit, some dishing (bending) was seen just after penetration. The dishing was again mostly elastic, as the postimpact target was observed to have a nearly flat profile except for the immediate impact site. The failure mechanism was mainly petaling. The projectile dented the target and formed a bulge. At the tip of this bulge, fracture was initiated and propagated in the radial direction through the thickness of the material forming triangular petals. Upon perforation of the target by the projectile, the petals underwent extensive viscoelastic recovery closing the hole that the projectile passed through. However, the petals became entangled and remained bent out of the plane of the plate. The number of petals formed increased with the speed of the projectile, as seen in the aluminum plates, ranging from about four to eight petals. The petaling relieved the constraint in the central region of the plate, allowing elastic recovery of the target back to a flat profile outside the immediate impact site. See references 5, 8, and 9 for more information on the ballistic behavior of polycarbonate.

Figures 45-48 show the targets impacted at various velocities above and below the ballistic limit.

Front View

Back View

Angled Front View

Angled Back View

FIGURE 45. POLYCARBONATE TARGET WITH AN INITIAL VELOCITY OF 874 ft/s
(No projectile perforation.)

Front View

Back View

Angled Front View

Angled Back View

FIGURE 46. POLYCARBONATE TARGET WITH AN INITIAL VELOCITY OF 963 ft/s

Front View

Back View

Angled Front View

Angled Back View

FIGURE 47. POLYCARBONATE TARGET WITH AN INITIAL VELOCITY OF 1186 ft/s

Front View

Back View

Angled Front View

Angled Back View

FIGURE 48. POLYCARBONATE TARGET WITH AN INITIAL VELOCITY OF 1537 ft/s

3.4 COMPOSITES.

3.4.1 Material Properties.

The sandwich composite panels that were tested in this program were supplied by the FAA. The panels were a representative sample of composite structures found on an aircraft and were fabricated specifically for ballistic testing. The lay-up of the panels consisted of two orthotropic, symmetric laminates of ±45° and 0°/90° weaves with a Nomex honeycomb core, as shown in figure 49 [10]. The total thickness of the panels was 0.25 inch.

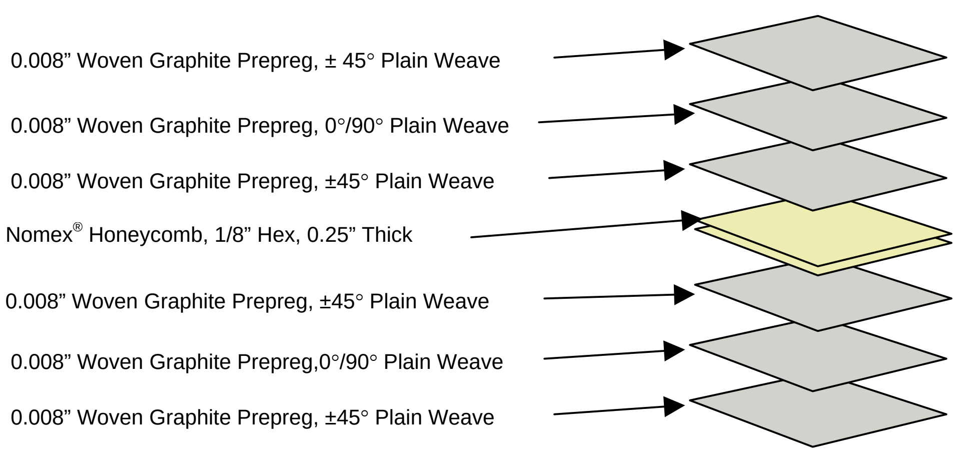

FIGURE 49. COMPOSITE PANEL LAY-UP

3.4.2 Test Results.

The full ballistic curve for the sandwich composite panels, plotting the residual projectile velocity against the initial projectile velocity, is shown in figure 50. The amount of energy absorbed by each target relative to the initial projectile velocity was also plotted and is shown in figure 51.

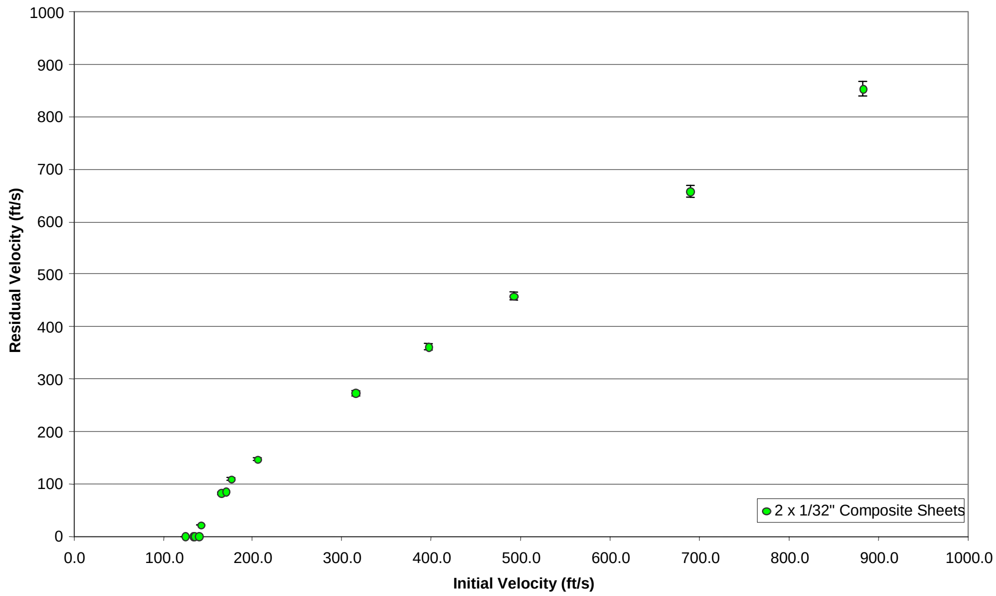

FIGURE 50. BALLISTIC CURVE FOR THE SANDWICH COMPOSITE PANELS

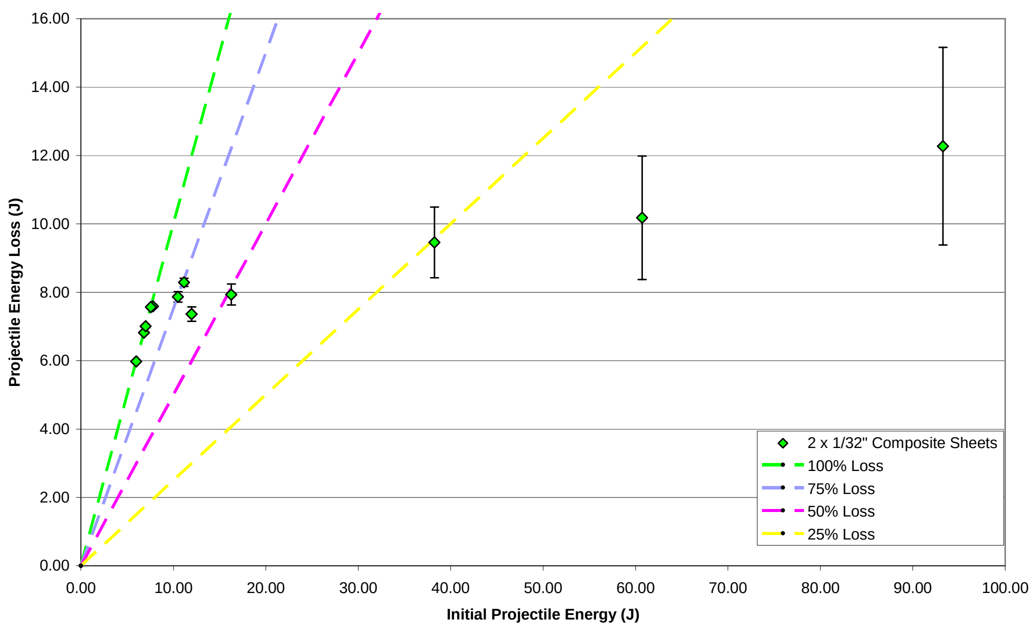

FIGURE 51. INITIAL KINETIC ENERGY OF THE PROJECTILE VS THE AMOUNT OF ENERGY ABSORBED BY THE SANDWICH COMPOSITE PANELS

The ballistic limit of the sandwich composite panels was found to be approximately 141 ft/s. The ballistic limit indicates the speed at which the projectile fully perforates the entire composite panel, not just one of the laminates. Unlike the aluminum and polycarbonate tests, the results of these tests were unique to this specific composite lay-up, which says little about global material behavior under ballistic impact. For all tested projectile velocities below the ballistic limit, the front laminate of the panel was fully perforated. A speed at which no perforation of the composite panel occurred could not be obtained due to low-speed limitations of the pneumatic gun. In each case, the projectile, perforated the front laminate leaving a hole slightly smaller than the projectile indicating some elastic recovery. The deformation in the front laminate was completely local to the impact site. Absolutely no dishing was present in the postimpact target. A consistent fracture pattern was observed in the rear laminate. In each case, a crack propagated from the point of impact along each of the outer ply's fiber direction, or the ±45° directions. This caused a pyramid-shaped deformation of four petals to form on the rear laminate. As the velocity approached the ballistic limit, the petal pyramid extended further out of the plane of the laminate.

At projectile speeds above the ballistic limit, the projectile pushed the petals outward until it was able to pass through the rear laminate. At lower projectile speeds, the petals recovered elastically after the projectile fully perforated the target. As the speed increased, the petals began to delaminate from the rear face and could be seen coming off the target in the high-speed films, as shown in figure 52. Eventually, as the speed became great enough, all the petals delaminated and left the rear laminate with a jagged hole that was slightly smaller than the projectile. At speeds much greater than the ballistic limit, the laminates were shattered by the incoming projectile, producing much less consistent failure patterns.

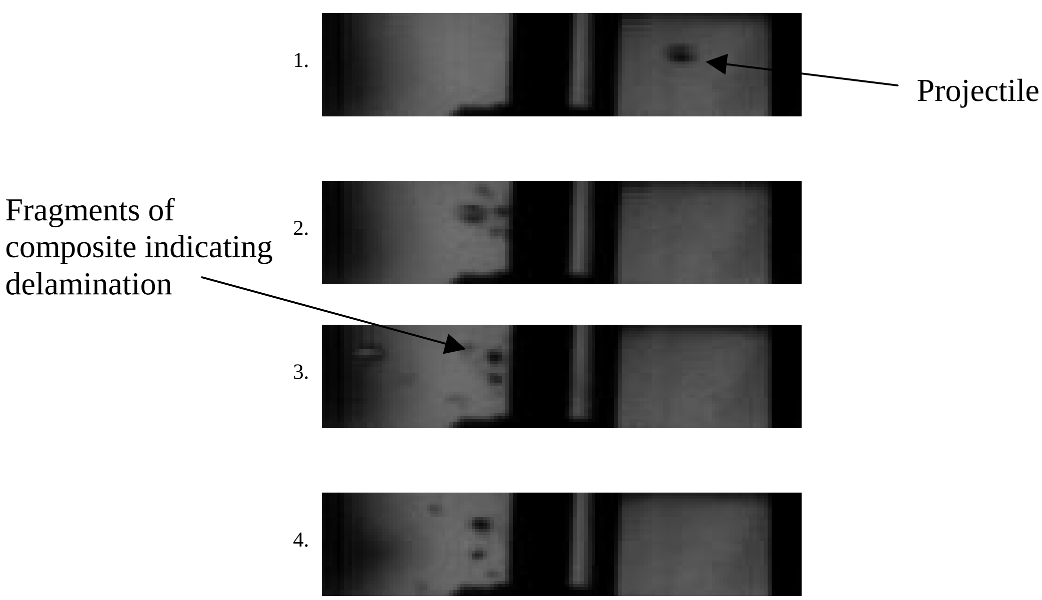

FIGURE 52. IMAGE SEQUENCE SHOWING DELAMINATION OF PETALS

The front laminate failed by a similar mechanism as the rear laminate; however, the honeycomb core added slightly more resistance to the petaling of the laminate, and the petals were also contained by the core preventing their full delamination. The honeycomb core did little to prevent the perforation of the composite panels. For more information on the impact response of composites, see references 11 through 13.

Figures 53 through 56 show the targets impacted at various velocities above and below the ballistic limit.

Front View   Back View

FIGURE 53. COMPOSITE PANEL TARGET WITH AN INITIAL VELOCITY OF 135 ft/s, BELOW THE BALLISTIC LIMIT
(Note the 45° fracture lines, forming a petal pyramid.)

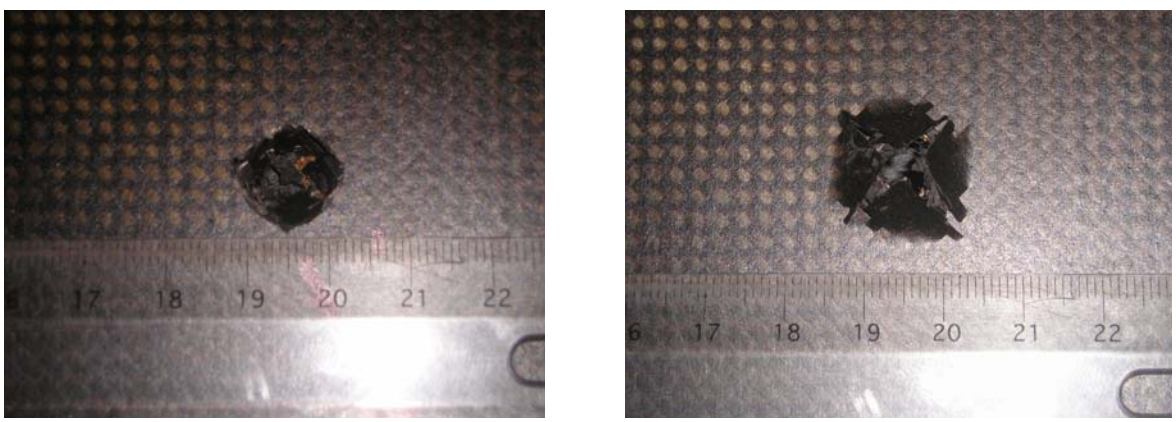

Front View   Back View

FIGURE 54. COMPOSITE PANEL TARGET WITH AN INITIAL VELOCITY OF 166 ft/s, ABOVE THE BALLISTIC LIMIT
(Note the 45° fracture lines again and the elastic recovery of the petals after perforation of the projectile.)

Front View Back View

FIGURE 55. COMPOSITE PANEL TARGET WITH AN INITIAL VELOCITY OF 315 ft/s
(Note that two of the petals have delaminated from the rear laminate.)

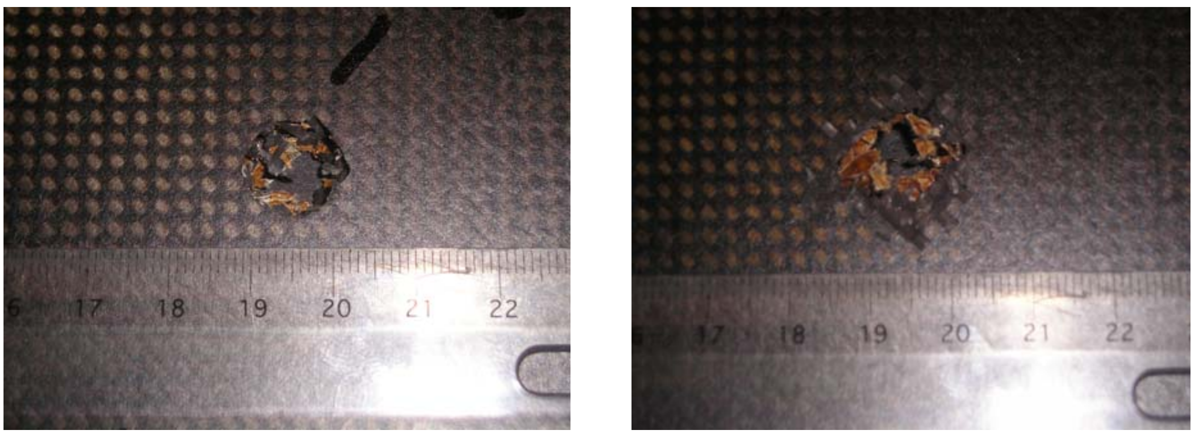

Front View Back View

FIGURE 56. COMPOSITE PANEL TARGET WITH AN INITIAL VELOCITY OF 883 ft/s
(Note that no petals remain on the rear laminate and the jagged hole formed by
the perforating projectile.)

4. ANALYSIS.

4.1 STATISTICS.

To understand more about the consistency of the data, a statistical analysis was done on the amount of energy stripped from the projectile for a fully perforated target, or the amount of energy the target absorbed. The absorbed energy for each target was calculated by subtracting the kinetic energy of the projectile after impact from the kinetic energy of the projectile before impact. For each set of targets tested, the mean of the absorbed energy was calculated along with the second, third, and fourth moments about the mean or the standard deviation, skewness, and kurtosis. The standard deviation gives a measure of the amount of dispersion within the data. The skewness is the degree of asymmetry of the distribution of the data. The kurtosis is the degree of peakedness of the distribution of the data. When the second, third, and fourth moments about the mean are all equal to zero, one has a perfect normal distribution, or the standard bell curve. The mean absorbed energy for each target is plotted with the absorbed energy graphs in figure 57, showing the amount of scatter present in each set of data. The results of the statistical analysis is shown in table 9.

The fourth column of table 9 (absorbed energy per areal density) is intended to compare energy absorption of the aluminum, polycarbonate, and composites tested. The results showed the following trends:

- The thicker the aluminum plate, the more energy it absorbed per areal density.
- The 0.25-inch-thick polycarbonate results show, approximately, an equal absorbed energy per areal density as the 0.25-inch-thick aluminum. However, looking at how much energy the polycarbonate absorbed compared to an equal weight aluminum target, it was about two times the energy absorbed.

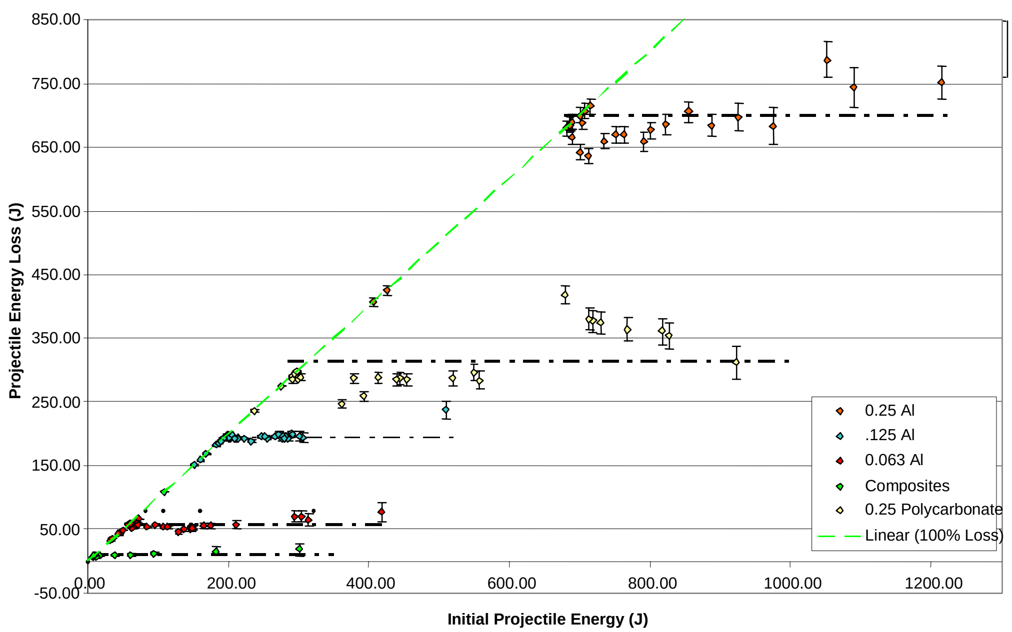

FIGURE 57. AMOUNT OF ABSORBED ENERGY OF EACH SET OF TARGETS PLOTTED AGAINST THE INITIAL PROJECTILE ENERGY ALONG WITH THE MEAN ABSORBED ENERGY

TABLE 9. MOMENTS ABOUT THE MEAN FOR THE ABSORBED ENERGY OF THE DIFFERENT TARGETS

Target	Absorbed Energy Mean (Joules)	Weight of Target Area (kg)	Absorbed Energy per Areal Density* ($J\ m^2/kg$)	Standard Deviation	Skewness	Kurtosis
0.063-in. Al	57.2	0.29	12.9	5.51	0.77	0.98
0.125-in. Al	194.6	0.57	22.1	2.77	0.64	0.05
0.25-in. Al	698.5	1.14	39.7	49.68	0.94	-0.22
Polycarbonate	314.6	0.49	41.6	47.48	0.75	-0.63
Composites	10.6	N/A	N/A	4.06	1.42	1.04

*Areal density is equal to the density of the target multiplied by the thickness.

Note that the values in table 9 were calculated excluding all the data points which the projectile did not fully perforate the target. These values would skew the mean as the amount of energy the target absorbed in these cases is less than the total possible amount of energy the target is capable of absorbing.

4.2 ENERGY ANALYSIS.

The statistical analysis in section 4.1 shows that it is a fair assumption that the amount of energy each set of targets is capable of absorbing is approximately constant above the ballistic limit. This assumption allows the formation of a simple model to relate the residual projectile velocity to the initial projectile velocity, by a conservation of energy argument. The argument is as follows:

$$\tfrac{1}{2} m_p v_i^2 = AKE + \tfrac{1}{2} m_p v_r^2 \qquad (1)$$

where m_p is the mass of the projectile, v_i is the initial projectile velocity, AKE is the absorbed kinetic energy of the target, and v_r is the residual projectile velocity assuming perforation. After rearranging equation 1, it was found that

$$v_r = \sqrt{(v_i^2 + (2/m_p)AKE)} \qquad (2)$$

From equation 2, the ballistic limit, v_{50}, can be solved by simply setting $v_r = 0$ and solving for v_i.

$$v_{50} = \sqrt{(2/m_p)AKE} \qquad (3)$$

Using this simple model and setting AKE equal to the mean absorbed energy values found for each set of data, a theoretical ballistic limit and ballistic curve could be calculated for each set of targets. Because the value of the AKE was obtained directly from the test data, it is expected that these values should match quite well. These values were then compared to the experimental values, as shown in table 10.

TABLE 10. COMPARISON OF EXPERIMENTAL AND MODEL BALLISTIC LIMITS USING THE CONSTANT *AKE* ASSUMPTION

Target	Experimental Ballistic Limit	Model Ballistic Limit	Percent Error
0.063-in. Al	391 ft/s	385 ft/s	1.5
0.125-in. Al	717 ft/s	711 ft/s	0.8
0.25-in. Al	1327 ft/s	1346 ft/s	1.4
Polycarbonate	861 ft/s	855 ft/s	0.7
Composites	141 ft/s	166 ft/s	17.7

The following graphs in figures 58 through 62 compare the experimental ballistic curves with the ballistic curves obtained using the constant *AKE* model. The constant *AKE* curves fit closely with the experimental curves, supporting the assumption of a constant absorbed energy. The 0.25-inch aluminum curve contains the most scatter, which is a result of the high projectile velocities needed for perforation. The high projectile velocities result in a greater amount of error in the residual velocity calculations. This is discussed in more detail in the error analysis in appendix A. As mentioned before, the polycarbonate curve (figure 61) seems to contain a transition from one constant absorbed energy curve to another around 1200 ft/s. Again, it is possible that this transition is a result of a change in failure mechanism that absorbs slightly more energy. One suggestion for this change is the onset of melting within the material.

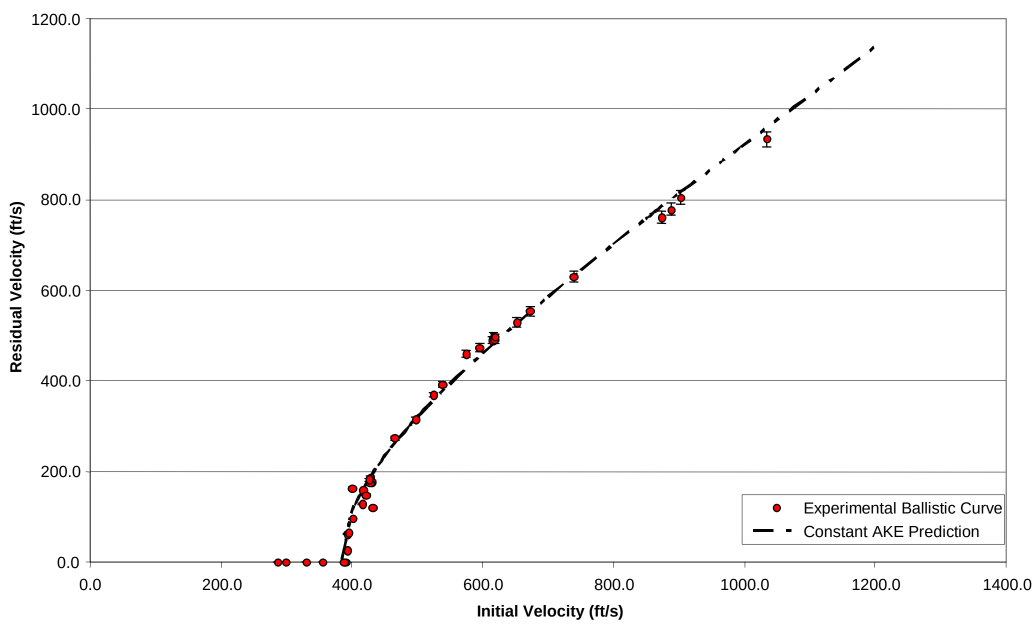

FIGURE 58. EXPERIMENTAL AND PREDICTED BALLISTIC CURVES FOR 0.063-INCH ALUMINUM

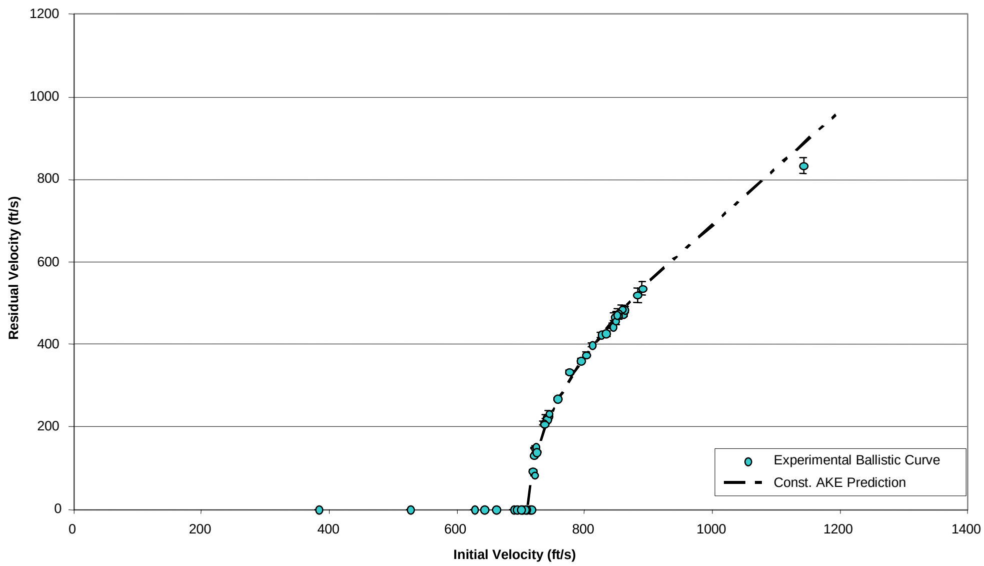

FIGURE 59. ACTUAL AND THEORETICAL BALLISTIC CURVES FOR 0.125-INCH ALUMINUM

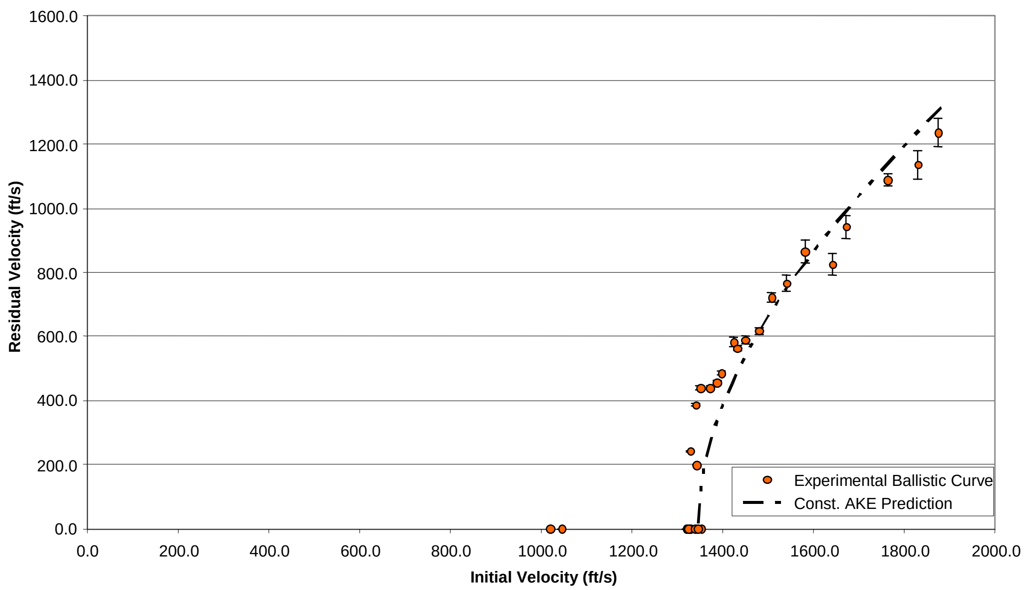

FIGURE 60. ACTUAL AND THEORETICAL BALLISTIC CURVES FOR 0.25-INCH ALUMINUM

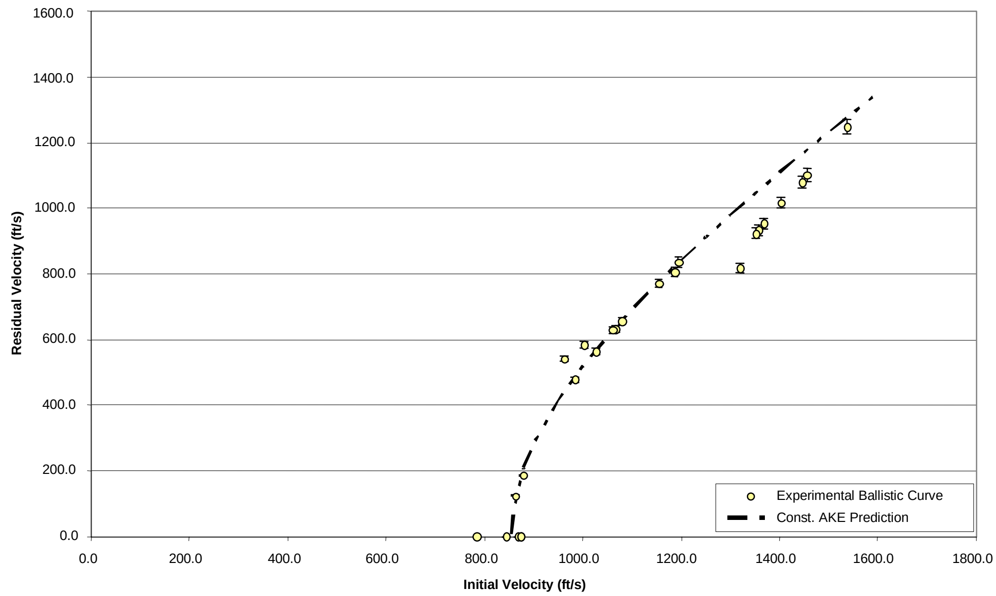

FIGURE 61. ACTUAL AND THEORETICAL BALLISTIC CURVES FOR 0.25-INCH MAKROLON POLYCARBONATE

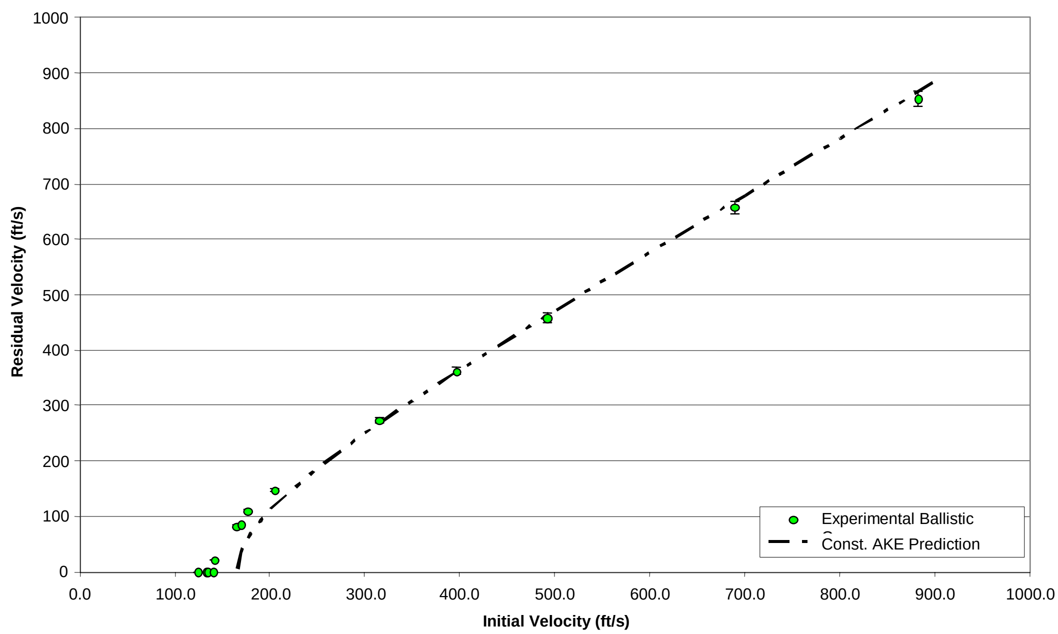

FIGURE 62. ACTUAL AND THEORETICAL BALLISTIC CURVES FOR THE SANDWICH COMPOSITE PANELS

The assumption of constant absorbed energy of the target allows a model for the ballistic behavior of a material to be developed through the use of formulas that calculate energy values for failure mechanisms a certain material undergoes based on obtainable material properties. Obviously this is a difficult task, as there are multiple mechanisms of failure for each material, which are also dependent on the thickness of the material. For example, one would need to characterize the amount of energy involved in dishing, petaling, plugging, melting, elastic and plastic wave propagation, and relate these phenomena to thickness to be able to approach a complete model for aluminum. A more reasonable approach is to develop a model that only characterizes several mechanisms that seem to absorb the most energy within a material. Obviously, the result will be lower than the actual value using this approach, as not all of the energy will be accounted for.

One model, known colloquially as the FAA energy equation [10], equates the absorbed energy to the amount of work done by shearing out a plug of a given circumference.

$$AKE = (L\, G_d\, t^2)/\cos^2\theta \tag{4}$$

Where L is the presented area perimeter in meters, G_d is the dynamic shear modulus in Pascals, t is the target thickness in meters, and θ is the obliquity of impact in degrees (0° is a normal impact). The dynamic shear modulus is not a common material property. A value of G_d[1] for aluminum was found empirically to be approximately 210 MPa from a completely unrelated set of tests [10]. This model only takes the amount of energy absorbed by pure plugging into account. As was shown, plugging was only one of the energy absorbing mechanisms that occurred in aluminum, and therefore, the values for the ballistic limit and residual velocities obtained using this model are expected to be significantly lower than the actual values. Using this model, the ballistic limits for the aluminum targets are compared with the experimental results as shown in table 11.

TABLE 11. A COMPARISON OF THE ACTUAL BALLISTIC LIMIT WITH THE CALCULATED BALLISTIC LIMIT FROM THE FAA EQUATION, ASSUMING PURE PLUGGING

Target	Actual Ballistic Limit	Ballistic Limit From FAA Equation	Percent Error
0.063-in. aluminum	391 ft/s	235.9 ft/s	39.7
0.125-in. aluminum	717 ft/s	468.0 ft/s	34.7
0.25-in. aluminum	1327 ft/s	930.5 ft/s	29.9

The percent error decreases with increasing thickness as expected, since plugging begins to dominate more as the thickness of aluminum increases. However, the model clearly underestimates the ballistic limits for the aluminum targets. This model was not useful for the polycarbonate or composite targets, as neither exhibited plugging. No useful models for polycarbonate or composite laminates could be found in the literature.

5. SUMMARY.

Fuselage fragment barrier systems are being examined for commercial airplanes to provide protection from an engine rotor burst failure. Part of this development is to understand how the

[1] G_d (in the FAA equation) is empirically derived for fan blades impacting aircraft structure. It is not calibrated for spherical projectiles.

existing aircraft materials behave under ballistic impact, and then to model those results to aid the aircraft industry in design of barriers and evaluation of existing aircraft structures for fragments from rotor burst events. The objective of this program was to acquire additional data on aluminum and titanium and preliminary data on composites and polycarbonate to support the development of barriers. This data was then used to improve material models in DYNA computer codes. This work yielded excellent test data on aluminum but more data is needed on titanium, composites, and polycarbonate, which is subject of a current collaboration between the FAA, UCB, Boeing, and LLNL.

In this test program, ballistic experiments were run on three different thicknesses of 2024 aluminum, and one thickness each of polycarbonate and composite panels. The experiments were run using the gas gun and powder gun setups in the UCB Ballistics Laboratory. The object of the experiments was to develop ballistic curves and determine the ballistic limit of 1/2-inch steel spherical projectiles centrally impacting the five different sets of targets and the failure modes and characteristics of each target. The amount of energy absorbed by each target was also determined. A detailed error analysis was done for each data point, showing the amount of error expected for each value.

Table 12 summarizes the ballistic limit for each target tested.

TABLE 12. THE BALLISTIC LIMIT FOR EACH TARGET TESTED

Target	Experimental Ballistic Limit
0.063-in. 2024-T3 aluminum	391 ft/s
0.125-in. 2024-T3 aluminum	717 ft/s
0.25-in. 2024-T351 aluminum	1327 ft/s
0.25-in. Makrolon polycarbonate	861 ft/s
0.25-in. honeycomb core composite panels	141 ft/s

For the 2024 aluminum plates, six main types of failure behavior were identified: dishing, petaling, shear plugging, denting, shattering, and melting. Petaling was the main mode of failure for the 0.063-inch plates, followed by dishing. However, as v_i increased the main mode of failure became shear plugging. For the 0.125-inch plates, shear plugging was the main mode of failure, with slight petaling and dishing. For the 0.25-inch plates, the main mode of failure remained shear plugging, with little to no petaling and dishing. The shear plugging was also accompanied by shattering and melting of the target plates.

There were four main types of failure behavior characterized for the polycarbonate targets. They were elastic bending, denting, petaling, and possible melting. The main mode of failure was denting, followed by petaling. Upon initial impact, the target underwent bending or dishing, followed by denting of the immediate impact site. The bulge formed by denting fractured and formed petals. The petaling allowed perforation of the projectile that relieved the constraint in the central region of the plate, allowing elastic recovery of the target back to a flat profile outside the immediate impact site. The petals also recovered elastically, closing the hole through which the projectile passed, became entangled, and remained bent out of the plane of the plate. It is hypothesized that melting occurred after about 1200 ft/s, resulting in a jump of absorbed energy of the target.

The main type of failure for the composite panels was petaling and delamination. The composite laminates fractured in the ±45° directions from the point of impact, forming four petals in a pyramid shape. At lower speeds, these petals would elastically recover, closing the hole that the projectile passed through. As the speed increased, the petals delaminated from the plate, leaving a jagged hole in the rear laminate.

For each set of targets, a statistical analysis was performed on the amount of the projectile's kinetic energy the target was able to absorb. It was proposed that the amount of energy that the target could absorb (at or above the ballistic limit) was a constant, independent of the velocity of the projectile.

Further work in this program might be done in the development of a more detailed model for the residual velocity and ballistic limit of a target based on the assumption of a constant absorbed kinetic energy. Also, one might explore the apparent jump in the absorbed energy of the polycarbonate more closely to better understand if there was a jump, and what caused the jump. In addition, further testing with thicker polycarbonate targets would give a better weight comparison to the 0.25-inch-thick aluminum targets.

6. REFERENCES.

1. Eyewitness Report: United Flight 232. (n.d.) Retrieved March 18, 2004, from http://www.airdisaster.com/eyewitness/ua232.shtml

2. Kay, G., "Failure Modeling of Titanium 6Al-4V and Aluminum 2024-T3 with the Johnson-Cook Material Model," FAA report DOT/FAA/AR-03/57, September 2003.

3. Lesuer, D., "Experimental Investigation of Material Models for Ti 6Al-4V and Al 2024-T3," FAA report DOT/FAA/AR-00/25, September 2000.

4. Gogolewski, R.P. and Morgan, B.R. "Ballistics Experiments With Titanium and Aluminum Targets," FAA report DOT/FAA/AR-01/21, April 2001.

5. Wright, S.C., Fleck, N.A., and Stronge, W.J., "Ballistic Impact of Polycarbonate – An Experimental Investigation," *Int. J. Impact Engng*, Vol. 13, 1993, pp. 1-20.

6. Meyers, M.A., *Dynamic Behavior of Materials*, John Wiley and Sons, New York, 1994.

7. O'Conner, E.J., Yatteau, J.D., Dzwilewski, P.T., Ford, S.R., and Black, J.W., "Size Scaling in Ballistic Limit Velocities for Small Fragments Perforating Thin Plates," *International Symposium of Ballistics*, May 11, 2001.

8. Walley, S.M., Field, J.E., Blair, P.W., and Milford, A.J., "The Effect of Temperature on the Impact Behavior of Glass/Polycarbonate Laminates," *Int. J. of Impact Engng*, Vol. 30, 2004, pp. 31-53.

9. Li, K. and Goldsmith, W., "Perforation of Steel and Polycarbonate Plates by Tumbling Projectiles," *Int. J. of Solids Structures*, Vol. 34, 1997, pp. 4581-4596.

10. Lundin, S.J., and Mueller, R.B., "Advanced Aircraft Materials, Engine Debris Penetration Testing," FAA report DOT/FAA/AR-03/37, December 2005.

11. Tanabe, Y. and Aoki, M., "Stress and Strain Measurements in Carbon-Related Materials Impacted by a High-Velocity Steel Sphere," *Int. J. Impact Engng*, Vol. 28, 2003, pp. 1045-1059.

12. Ross, C.A., Cristescu, N., and Sierakowski, R.L., "Experimental Studies on Failure Mechanisms of Impacted Composite Plates," *Fibre Science and Technology*, Vol. 9, 1976, pp. 177-188.

13. Villanueva G.R. and Cantwell W.J., "The High Velocity Impact Response of Composite and FML-Reinforced Sandwich Structures," *Composites Science and Technology*, Vol. 64, 2004, pp. 35-54.

7. GLOSSARY.

Distal Face—The surface opposite the impact surface on the target plate.

Dishing—The flexural and stretching deformation of an annular region of the plate surrounding the projectile impact point where the dished region is displaced normal to the surface of the plate.

Denting—The localized indentation of the plate material under the common interface between the projectile and the plate, often accompanied by bulging.

Bulging—The localized deformation or displacement of the distal face of the plate normal to its surface.

Petaling—The formation of petals caused by radial cracking from the point of impact.

Shear plugging—The shearing of the target plate around the point of impact causing the formation of a plug of target material.

Shattering—The case when several fragments exit the target material upon impact.

Perforation—The breaking through of the distal face of the plate by the projectile.

Ballistic limit velocity, or v_{50}, is defined here as the velocity beyond which the projectile fully perforates a target and below which it will not.

APPENDIX A—ERROR ANALYSIS

A thorough error analysis was done for all the data obtained in this program. A certain amount of errors were expected in obtaining both the initial and residual projectile velocities. The amount of error varied considerably from point to point, depending on the method of measurement. Three main measurement techniques were used to measure the velocity: the laser/photodiode setup, the grids, and the high-speed camera. The initial velocities were all measured with the laser/photodiode setup. Because the setup on the powder gun was not the same as on the gas gun, the amount of error for the initial velocity varied, depending on which gun was used.

The residual velocities were measured either with the grids or the high-speed camera. The grids provided a more accurate measurement, but did not always capture the projectile's velocity due to plugging and other random errors. In these cases, the high-speed camera had to be used to obtain a residual velocity measurement. Due to limitations on the number of frames per second the camera could capture, the ability to measure the speed accurately also varied with the projectile's velocity. The projectile's camera image became more blurry as its speed increased, making it more difficult to obtain an accurate reading. The error for each measurement will now be discussed in detail.

A.1 INITIAL PROJECTILE VELOCITY.

The equation used to calculate the initial projectile velocity for each test was

$$v_i = d_p /(t * 12) \qquad \text{(A-1)}$$

where d_p is the distance between photodiodes (in inches), t is the time between the projectile passing through the lasers and triggering the photodiodes obtained from the counters (in seconds), and 12 is a conversion factor. The error associated with the initial velocity can be found by the following equation:

$$(\delta v_i / v_i)^2 = (\delta d_p / d_p)^2 + (\delta t / t)^2 \qquad \text{(A-2)}$$

where δd_p is the tolerance in the measurement of the distance between the photodiodes, and δt is the tolerance in the time measurement on the Hewlett Packard counters. For the gas gun, $d_p = 2.5 \pm 0.00025''$ ($\delta d_p = 0.00025''$). This tolerance is the expected amount of error for the distance between the holes for the photodiodes, obtained from the tolerance in the milling machine in the UCB machine shop. For the powder gun, $d_p = 8.0 \pm 0.0625''$ ($\delta d_p = 0.0625''$). This is a subjective amount of error associated with the distance between the lasers in the projectiles path. In the powder gun setup, the lasers are not exactly parallel. The lasers and the photodiodes are a fair distance apart, resulting in a small variation in the distance between the lasers, from the laser side to the photodiode side. Therefore, the distance had to be measured manually where the projectile passed through the lasers. This measurement could only be measured to within 0.0625″. For both the powder and gas guns the tolerance for the time measurements on the counter was 2.5×10^{-10} seconds. The smallest time obtained in all the tests were approximately 230.0×10^{-6} seconds. Therefore, it can be shown for all cases that

$(\delta d_p / d_p)^2 >> (\delta t / t)^2$, which sets $(\delta t / t)^2 = 0$ in equation A-6. Hence, the tolerance for the initial velocities are the following:

$$\delta v_i = v_i * (1 \times 10^{-4}) - \textit{Gas Gun} \quad \text{(A-3)}$$

$$\delta v_i = v_i * (0.0078125) - \textit{Powder Gun} \quad \text{(A-4)}$$

A.2 RESIDUAL PROJECTILE VELOCITIES.

For the tests which the projectile successfully penetrated both grids, its residual velocity was found by the following equation:

$$v_r = d_g /(t * 12) \quad \text{(A-5)}$$

where d_g is the distance between grids (in inches), t is the time between the projectile passing through each grid measured by the counter, and 12 is a conversion factor. The error associated with the residual velocity measured by the grids can be found by the following equation:

$$(\delta v_r / v_r)^2 = (\delta d_g / d_g)^2 + (\delta t / t)^2 \quad \text{(A-6)}$$

where δd_g is the subjective error for the distance between the grids, and δt is the same as above. For both setups, d_g = 7.25 ±0.125″ (δd_g = 0.125″). As mentioned above, the amount of error associated with the time measured by the counters, δt, is very small compared to the time measured, and therefore, one can say $(\delta d_g / d_g)^2 >> (\delta t / t)^2$. This leads to the following equation to determine δv_r when the grids were used:

$$\delta v_r = v_r * (0.01724) \quad \text{(A-7)}$$

However, the grids did not always capture the projectile's residual velocity. In almost all the aluminum tests, a plug was formed and exited the material ahead of the projectile, setting off the grids. In other cases, the projectile missed the grids all together due to a lack of speed or an angular exit. In these cases, the residual velocity of the projectile had to be measured using the high-speed camera. This was done by the method described in detail in section 2. Using this method, the residual velocity was calculated using the following equation:

$$v_r = \Delta x / (C*12*\Delta t) \quad \text{(A-8)}$$

where Δx is the change in the pixel position of the projectile in the high-speed camera image from one frame to another, C is the conversion factor from pixels to inches (found by measuring the number of pixels between a known distance, L, placed in the camera image, 12 is a conversion factor from inches to feet, and Δt is the change in time from one frame to another. Both 12 and Δt are assumed to be exact values with no error associated with them, so the error for the residual velocity using the camera can be found from the following equation:

$$(\delta v_r / v_r)^2 = (\delta \Delta x / \Delta x)^2 + (\delta C / C)^2 \quad \text{(A-9)}$$

$$\delta\Delta x^2 = 2\delta x^2 \quad \text{(A-10)}$$

$$C = \Delta x / L \quad \text{(A-11)}$$

$$\delta C = \delta\Delta x / L \quad \text{(A-12)}$$

The error for the change in pixels is found directly from the error associated with measuring the pixel position of the projectile in a given frame, δx, since $\Delta x = x_2 - x_1$, where x_2 and x_1 are the pixel positions of the projectile in two chosen frames. The error for C is proportional to $\delta\Delta x$ since it is found by simply dividing a change in pixels over a given length. However, the error for measuring the pixel position varied, depending on the projectile velocity. The image of the projectile within a given frame became less clear as the velocity increased, resulting in a larger error. The error in calculating the pixel position for finding the value of C was the smallest since the ruler used was a stationary object. The error was subjectively defined based on the residual velocity of the projectile as the maximum possible error that could be expected from the image of the projectile. Table A-1 shows the amount of error used relative to velocity.

TABLE A-1. AMOUNT OF ERROR SUBJECTIVELY ASSIGNED TO THE ABILITY TO MEASURE THE PIXEL POSITION OF THE PROJECTILE FOR VARYING VELOCITIES

Residual Projectile Velocity (ft/s)	δx	$\delta\Delta x$
0 (for calculating C)	0.1	0.141
$0 < v_r < 500$	0.2	0.283
$500 < v_r < 800$	0.3	0.424
$800 < v_r < 1100$	0.4	0.566
$1100 < v_r$	0.5	0.707

The values for Δx were unique for each test, and the values for C also varied between sets of experiments as a result of the camera being moved from one setup to another. Therefore, the error in the residual velocity is very specific to each individual test. Tables for the exact values of the error for every test can be found in appendix C.

A.3 ABSORBED KINETIC ENERGY.

The absorbed kinetic energy is calculated using both the initial and residual velocities of the projectile. Therefore, the error associated with each is perpetuated to an error in the value of the absorbed kinetic energy. The equations used to calculate this error are shown below.

$$\delta AKE^2 = \delta IKE^2 + \delta RKE^2 \quad \text{(A-13)}$$

$$IKE = ½\, m_p v_i^2 \quad \text{(A-14)}$$

$$RKE = ½\, m_p v_r^2 \quad \text{(A-15)}$$

$$(\delta IKE / IKE)^2 = (\delta m_p / m_p)^2 + (2\delta v_i / v_i)^2 \quad \text{(A-16)}$$

$$(\delta RKE / RKE)^2 = (\delta m_p / m_p)^2 + (2\delta v_r / v_r)^2 \quad \text{(A-17)}$$

where *IKE* is the initial kinetic energy of the projectile, *RKE* is the residual kinetic energy of the projectile, and δm_p is the error in the measurement of the mass of the projectile. For all tests, $\delta m_p = 0.00005$ kg, which is the tolerance of the scale used to measure the mass. The complete table of error values for the absorbed kinetic energy of each test can be seen at the end of this appendix.

APPENDIX B—DEFINITION OF NORMAL DISTANCE OF PETAL DERFORMATION

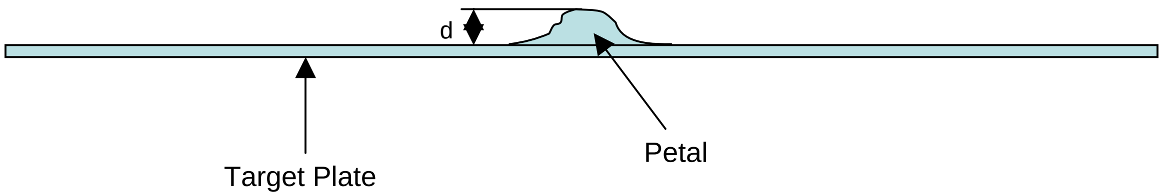

FIGURE B-1. SCHEMATIC OF DEFINITION OF NORMAL DISTANCE OF PETAL DEFORMATION

APPENDIX C—COMPLETE SET OF DATA INCLUDING ADDITIONAL GRAPHS

METALS TESTING
0.063″ Aluminum Sheets
Ballistic Limit ~ 391 ft/s

Test	V_i (ft/s)	V_r (ft/s)	m (g)	V_i (m/s)	V_r (m/s)	m (kg)	IKE (J)	AKE (J)	Percent KE Absorbed
2	389.3	0.0	8.3	118.66	0.00	0.0083	58.43	58.43	100.00%
3	431.9	120.6	8.3	131.64	36.76	0.0083	71.92	66.31	92.20%
4	355.2	0.0	8.3	108.26	0.00	0.0083	48.64	48.64	100.00%
5	416.6	159.0	8.3	126.98	48.46	0.0083	66.91	57.17	85.43%
6	465.4	274.6	8.3	141.85	83.70	0.0083	83.51	54.44	65.19%
7	497.5	316.1	8.3	151.64	96.35	0.0083	95.43	56.90	59.63%
8	524.7	369.5	8.3	159.93	112.62	0.0083	106.15	53.51	50.41%
9	538.2	391.7	8.4	164.04	119.39	0.0084	113.02	53.16	47.03%
10	574.7	459.8	8.4	175.17	140.15	0.0084	128.87	46.38	35.99%
11	594.6	473.9	8.3	181.23	144.44	0.0083	136.31	49.72	36.48%
12	617.2	498.6	8.3	188.12	151.97	0.0083	146.87	51.02	34.74%
13	651.9	529.8	8.3	198.70	161.48	0.0083	163.85	55.63	33.95%
14	672.0	554.9	8.3	204.83	169.13	0.0083	174.11	55.39	31.81%
15	739.4	629.8	8.3	225.37	191.96	0.0083	210.78	57.86	27.45%
16	873.6	761.7	8.3	266.27	232.17	0.0083	294.24	70.55	23.98%
17	392.6	26.0	8.3	119.66	7.92	0.0083	59.43	59.17	99.56%
18	415.5	128.8	8.4	126.64	39.26	0.0084	67.36	60.89	90.39%
19	330.6	0.0	8.3	100.77	0.00	0.0083	42.14	42.14	100.00%
20	286.4	0.0	8.3	87.29	0.00	0.0083	31.62	31.62	100.00%
21	299.6	0.0	8.4	91.32	0.00	0.0084	35.02	35.02	100.00%
22	390.2	0.0	8.4	118.93	0.00	0.0084	59.41	59.41	100.00%
23	428.6	186.0	8.3	130.64	56.69	0.0083	70.82	57.49	81.17%
24	430.6	177.4	8.3	131.25	54.07	0.0083	71.49	59.35	83.03%
25	428.1	174.7	8.3	130.48	53.25	0.0083	70.66	58.89	83.35%
26	421.5	148.0	8.3	128.47	45.11	0.0083	68.50	60.05	87.67%
27	426.4	182.3	8.3	129.97	55.57	0.0083	70.10	57.29	81.72%
28	615.4	490.3	8.3	187.57	149.44	0.0083	146.01	53.33	36.52%
29	614.9	490.3	8.3	187.42	149.44	0.0083	145.78	53.09	36.42%
30	617.8	491.4	8.3	188.31	149.78	0.0083	147.15	54.05	36.73%
31	618.8	497.5	8.3	188.61	151.64	0.0083	147.63	52.21	35.36%
32	400.2	163.3	8.3	121.98	49.77	0.0083	61.75	51.47	83.35%
33	392.7	61.9	8.3	119.69	18.87	0.0083	59.46	57.98	97.52%
34	387.5	0.0	8.3	118.11	0.00	0.0083	57.89	57.89	100.00%
35	388.1	0.0	8.3	118.29	0.00	0.0083	58.07	58.07	100.00%
36	401.0	96.3	8.3	122.22	29.35	0.0083	62.00	58.42	94.23%
37	394.8	65.8	8.3	120.34	20.06	0.0083	60.09	58.42	97.22%
83	903.3	805.4	8.3	275.33	245.49	0.0083	314.59	64.50	20.50%
84	888.3	778.8	8.3	270.75	237.38	0.0083	304.23	70.38	23.13%
130	1035.1	934.1	8.4	315.50	284.71	0.0084	418.07	77.61	18.56%

Stats for AKE

Mean	57.167
Std Dev	5.507
Skewness	0.766
Kurtosis	0.977

STATISTICS
0.063″ Aluminum Sheets

Test	V_0 (ft/s)	V_r (ft/s)	Mass (g)	V_0 (m/s)	V_r (m/s)	Mass (kg)	Initial Energy (J)	Absorbed Energy (J)
2	389.3	0.0	8.3	118.66	0.00	0.0083	58.43	58.43
3	431.9	120.6	8.3	131.64	36.76	0.0083	71.92	66.31
4	355.2	0.0	8.3	108.26	0.00	0.0083	48.64	48.64
5	416.6	159.0	8.3	126.98	48.46	0.0083	66.91	57.17
6	465.4	274.6	8.3	141.85	83.70	0.0083	83.51	54.44
7	497.5	316.1	8.3	151.64	96.35	0.0083	95.43	56.90
8	524.7	369.5	8.3	159.93	112.62	0.0083	106.15	53.51
9	538.2	391.7	8.4	164.04	119.39	0.0084	113.02	53.16
10	574.7	459.8	8.4	175.17	140.15	0.0084	128.87	46.38
11	594.6	473.9	8.3	181.23	144.44	0.0083	136.31	49.72
12	617.2	498.6	8.3	188.12	151.97	0.0083	146.87	51.02
13	651.9	529.8	8.3	198.70	161.48	0.0083	163.85	55.63
14	672.0	554.9	8.3	204.83	169.13	0.0083	174.11	55.39
15	739.4	629.8	8.3	225.37	191.96	0.0083	210.78	57.86
16	873.6	761.7	8.3	266.27	232.17	0.0083	294.24	70.55
17	392.6	26.0	8.3	119.66	7.92	0.0083	59.43	59.17
18	415.5	128.8	8.4	126.64	39.26	0.0084	67.36	60.89
19	330.6	0.0	8.3	100.77	0.00	0.0083	42.14	42.14
20	286.4	0.0	8.3	87.29	0.00	0.0083	31.62	31.62
21	299.6	0.0	8.4	91.32	0.00	0.0084	35.02	35.02
22	390.2	0.0	8.4	118.93	0.00	0.0084	59.41	59.41
23	428.6	186.0	8.3	130.64	56.69	0.0083	70.82	57.49
24	430.6	177.4	8.3	131.25	54.07	0.0083	71.49	59.35
25	428.1	174.7	8.3	130.48	53.25	0.0083	70.66	58.89
26	421.5	148.0	8.3	128.47	45.11	0.0083	68.50	60.05
27	426.4	182.3	8.3	129.97	55.57	0.0083	70.10	57.29
28	615.4	490.3	8.3	187.57	149.44	0.0083	146.01	53.33
29	614.9	490.3	8.3	187.42	149.44	0.0083	145.78	53.09
30	617.8	491.4	8.3	188.31	149.78	0.0083	147.15	54.05
31	618.8	497.5	8.3	188.61	151.64	0.0083	147.63	52.21
32	400.2	163.3	8.3	121.98	49.77	0.0083	61.75	51.47
33	392.7	61.9	8.3	119.69	18.87	0.0083	59.46	57.98
34	387.5	0.0	8.3	118.11	0.00	0.0083	57.89	57.89
35	388.1	0.0	8.3	118.29	0.00	0.0083	58.07	58.07
36	401.0	96.3	8.3	122.22	29.35	0.0083	62.00	58.42
37	394.8	65.8	8.3	120.34	20.06	0.0083	60.09	58.42
83	903.3	805.4	8.3	275.33	245.49	0.0083	314.59	64.50
84	888.3	778.8	8.3	270.75	237.38	0.0083	304.23	70.38

Moments on Absorbed Energy			
w/ zero values		w/o zero values	
Mean	55.428	Mean	57.167
Std Dev	7.735	Std Dev	5.507
Skewness	-1.005	Skewness	0.766
Kurtosis	2.618	Kurtosis	0.977

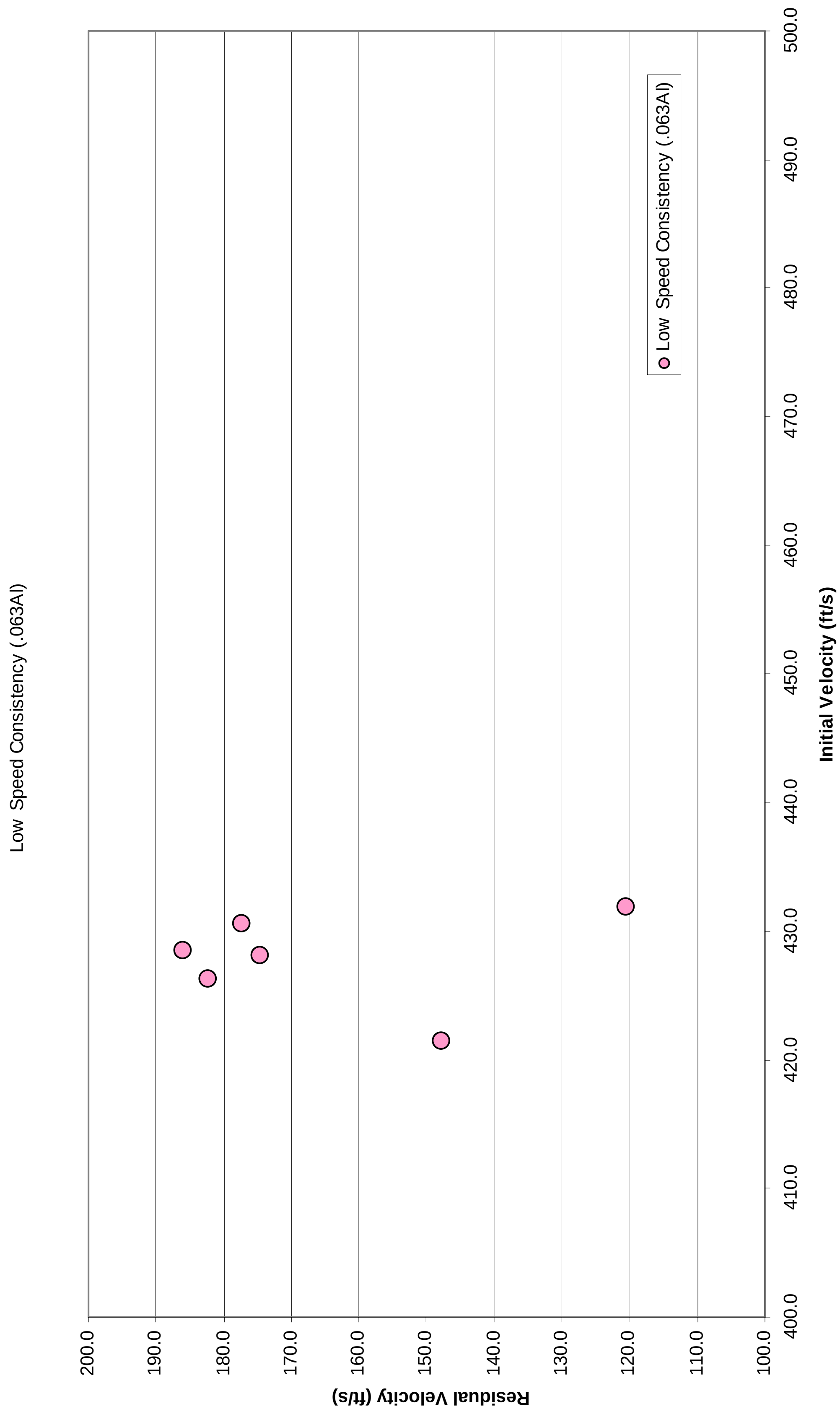
Low Speed Consistency (.063Al)
Residual Velocity (ft/s)
200.0
190.0
180.0
170.0
160.0
150.0
140.0
130.0
120.0
110.0
100.0
Initial Velocity (ft/s)
400.0
410.0
420.0
430.0
440.0
450.0
460.0
470.0
480.0
490.0
500.0
Low Speed Consistency (.063Al)

High Speed Consistency (.063Al)

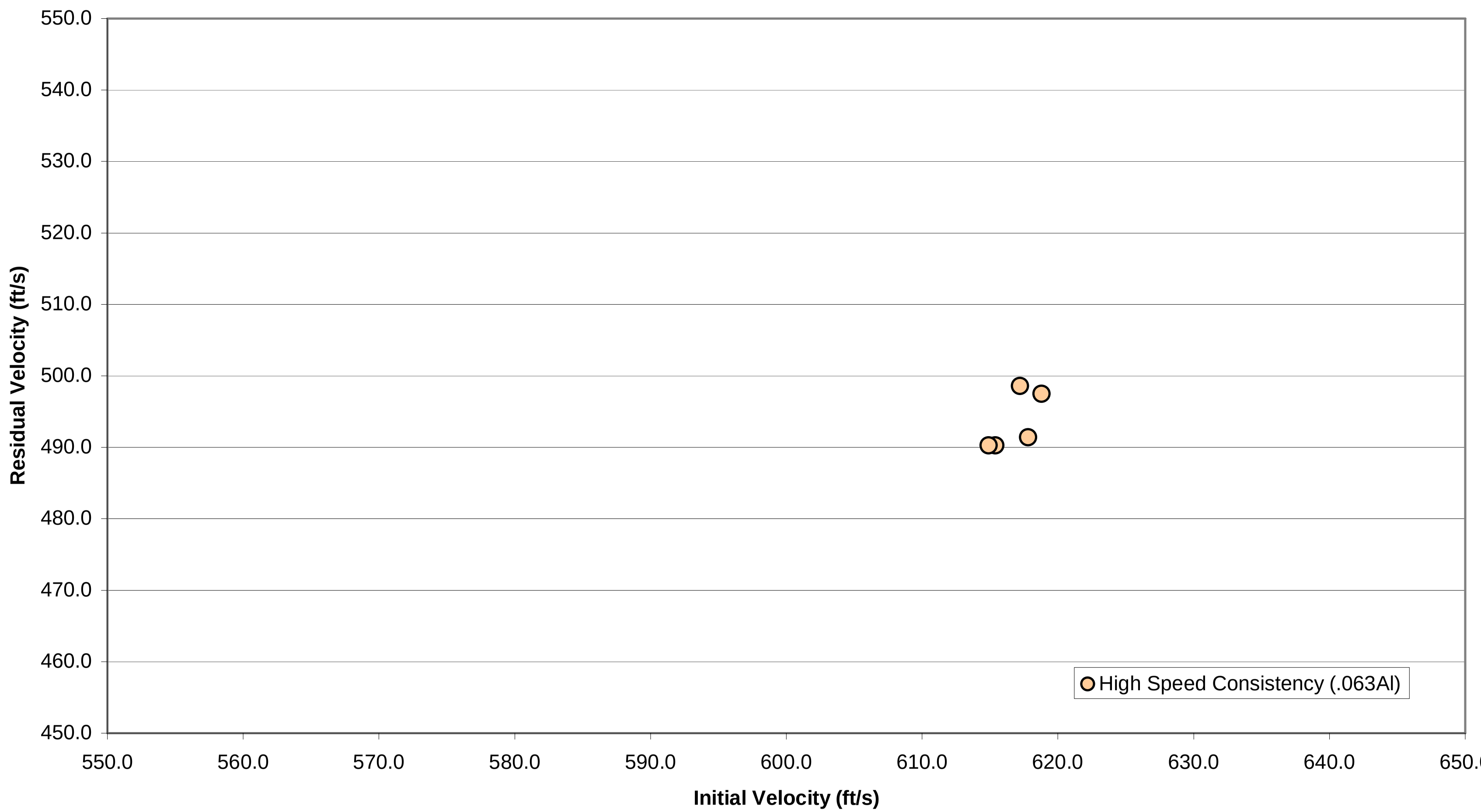

METALS TESTING
0.125″ Aluminum Sheets
Ballistic Limit ~ 717 ft/s

Test	V_i (ft/s)	V_r (ft/s)	m (g)	V_i (m/s)	V_r (m/s)	m (kg)	IKE (J)	AKE (J)	Percent KE Absorbed	m_p	V_p (ft/s)	V_p (m/s)	Plug KE (J)
38	627.4	0	8.3	191.23	0.00	0.0083	151.76	151.76	100.00%	0.0005	389.3	118.7	3.52
39	642.6	0	8.3	195.86	0.00	0.0083	159.21	159.21	100.00%	0.0005	413.5	126.0	3.97
40	660.9	0.0	8.3	201.44	0.00	0.0083	168.40	168.40	100.00%	0.0005	446.4	136.1	4.63
41	688.7	0.0	8.3	209.92	0.00	0.0083	182.87	182.87	100.00%	0.0005	492.3	150.1	5.63
42	744.2	226.3	8.3	226.83	68.98	0.0083	213.53	193.78	90.75%	0.0005	539.4	164.4	6.76
43	714.2	0.0	8.3	217.69	0.00	0.0083	196.66	196.66	100.00%	0.0005	515.0	157.0	6.16
44	721.4	149.4	8.3	219.88	45.54	0.0083	200.65	192.04	95.71%	0.0005	521.4	158.9	6.31
45	723.6	152.4	8.3	220.55	46.45	0.0083	201.87	192.92	95.56%	0.0006	510.4	155.6	7.26
46	702.3	0.0	8.3	214.06	0.00	0.0083	190.16	190.16	100.00%	0.0005	496.8	151.4	5.73
47	716.5	0.0	8.3	218.39	0.00	0.0083	197.93	197.93	100.00%	0.0006	517.7	157.8	7.47
48	693.5	0.0	8.3	211.38	0.00	0.0083	185.43	185.43	100.00%	0.0005	497.1	151.5	5.74
49	860.9	474.1	8.4	262.40	144.51	0.0084	289.19	201.49	69.67%	0.0006	680.9	207.5	12.92
50	863.2	484.9	8.4	263.10	147.80	0.0084	290.74	198.99	68.44%	0.0006	680.4	207.4	12.90
51	757.2	268.7	8.3	230.79	81.90	0.0083	221.05	193.22	87.41%	0.0006	558.5	170.2	8.69
52	794.2	360.2	8.4	242.07	109.79	0.0084	246.12	195.49	79.43%	0.0006	610.3	186.0	10.38
53	825.9	423.9	8.4	251.73	129.20	0.0084	266.15	196.04	73.66%	0.0006	647.9	197.5	11.70
54	844.4	444.0	8.3	257.37	135.33	0.0083	274.90	198.89	72.35%	0.0006	668.0	203.6	12.44
55	724	137.3	8.3	220.68	41.85	0.0083	202.09	194.83	96.40%	0.0006	524.8	160.0	7.68
56	709.4	0.0	8.3	216.23	0.00	0.0083	194.03	194.03	100.00%	0.0005	499.7	152.3	5.80
57	718.9	94.3	8.3	219.12	28.74	0.0083	199.26	195.83	98.28%	0.0006	524.0	159.7	7.65
58	721.8	83.1	8.3	220.00	25.33	0.0083	200.87	198.21	98.67%	0.0006	498.9	152.1	6.94
59	720.5	130.9	8.3	219.61	39.90	0.0083	200.15	193.54	96.70%	0.0005	516.5	157.4	6.20
61	706.9	0.0	8.3	215.46	0.00	0.0083	192.66	192.66	100.00%	0.0006	540.6	164.8	8.15
62	700.5	0.0	8.3	213.51	0.00	0.0083	189.19	189.19	100.00%	0.0006	500.9	152.7	6.99
63	775.7	333.2	8.3	236.43	101.56	0.0083	231.99	189.18	81.55%	0.0006	598.3	182.4	9.98
64	811.8	398.7	8.3	247.44	121.52	0.0083	254.08	192.80	75.88%	0.0006	649.7	198.0	11.76
65	802.1	374.8	8.4	244.48	114.24	0.0084	251.04	196.22	78.17%	0.0006	628.2	191.5	11.00
66	833.1	426.7	8.4	253.93	130.06	0.0084	270.82	199.77	73.77%	0.0006	655.6	199.8	11.98
67	384.1	0.0	8.4	117.07	0.00	0.0084	57.57	57.57	100.00%	0.0000	0.0	0.0	0.00
68	526.8	0.0	8.4	160.57	0.00	0.0084	108.29	108.29	100.00%	0.0000	0.0	0.0	0.00

METALS TESTING (Continued)

0.125″ Aluminum Sheets

Ballistic Limit ~ 717 ft/s

Test	V_i (ft/s)	V_r (ft/s)	m (g)	V_i (m/s)	V_r (m/s)	m (kg)	IKE (J)	AKE (J)	Percent KE Absorbed	m_p	V_p (ft/s)	V_p (m/s)	Plug KE (J)
69	724.7	139.5	8.4	220.89	42.52	0.0084	204.93	197.33	96.29%	0.0005	511.8	156.0	6.08
70	739.4	223.7	8.3	225.37	68.18	0.0083	210.78	191.49	90.85%	0.0005	533.2	162.5	6.60
71	740.6	218.8	8.3	225.73	66.69	0.0083	211.47	193.01	91.27%	0.0005	547.6	166.9	6.96
72	740.5	218.1	8.3	225.70	66.48	0.0083	211.41	193.07	91.33%	0.0005	537.1	163.7	6.70
73	736	209.6	8.3	224.33	63.89	0.0083	208.85	191.91	91.89%	0.0005	536.7	163.6	6.69
74	743.7	233.5	8.3	226.68	71.17	0.0083	213.24	192.22	90.14%	0.0005	536.6	163.6	6.69
75	737.2	207.5	8.3	224.70	63.25	0.0083	209.53	192.93	92.08%	0.0005	532.9	162.4	6.60
76	858.5	486.7	8.3	261.67	148.35	0.0083	284.16	192.83	67.86%	0.0006	676.6	206.2	12.76
77	846.8	467.1	8.3	258.10	142.37	0.0083	276.46	192.35	69.57%	0.0006	687.6	209.6	13.18
78	852.4	476.9	8.3	259.81	145.36	0.0083	280.13	192.45	68.70%	0.0006	675.4	205.9	12.71
79	852.6	469.5	8.3	259.87	143.10	0.0083	280.26	195.28	69.68%	0.0006	672.8	205.1	12.62
80	848.1	457.2	8.3	258.50	139.35	0.0083	277.31	196.72	70.94%	0.0005	667.1	203.3	10.34
81	850.2	472.0	8.3	259.14	143.87	0.0083	278.69	192.80	69.18%	0.0006	673.0	205.1	12.62
85	890	536.2	8.3	271.27	163.43	0.0083	305.39	194.54	63.70%	0.0006	698.1	212.8	13.58
86	882.5	520.0	8.3	268.99	158.50	0.0083	300.27	196.01	65.28%	0.0006	692.3	211.0	13.36
131	1142	833.3	8.4	348.08	253.99	0.0084	508.88	237.93	46.76%	0.0006	UNKOWN		

Stats for AKE

Mean	194.631
Std Dev	2.773
Skewness	0.642
Kurtosis	0.052

STATISTICS

0.125″ Aluminum Sheets

Test	V_0 (ft/s)	V_r (ft/s)	Mass (g)	V_0 (m/s)	V_r (m/s)	Mass (kg)	Initial Energy (J)	Absorbed Energy (J)
38	627.4	0	8.3	191.23	0.00	0.0083	151.76	151.76
39	642.6	0	8.3	195.86	0.00	0.0083	159.21	159.21
40	660.9	0.0	8.3	201.44	0.00	0.0083	168.40	168.40
41	688.7	0.0	8.3	209.92	0.00	0.0083	182.87	182.87
42	744.2	226.3	8.3	226.83	68.98	0.0083	213.53	193.78
43	714.2	0.0	8.3	217.69	0.00	0.0083	196.66	196.66
44	721.4	149.4	8.3	219.88	45.54	0.0083	200.65	192.04
45	723.6	152.4	8.3	220.55	46.45	0.0083	201.87	192.92
46	702.3	0.0	8.3	214.06	0.00	0.0083	190.16	190.16
47	716.5	0.0	8.3	218.39	0.00	0.0083	197.93	197.93
48	693.5	0.0	8.3	211.38	0.00	0.0083	185.43	185.43
49	860.9	474.1	8.4	262.40	144.51	0.0084	289.19	201.49
50	863.2	484.9	8.4	263.10	147.80	0.0084	290.74	198.99
51	757.2	268.7	8.3	230.79	81.90	0.0083	221.05	193.22
52	794.2	360.2	8.4	242.07	109.79	0.0084	246.12	195.49
53	825.9	423.9	8.4	251.73	129.20	0.0084	266.15	196.04
54	844.4	444.0	8.3	257.37	135.33	0.0083	274.90	198.89
55	724	137.3	8.3	220.68	41.85	0.0083	202.09	194.83
56	709.4	0.0	8.3	216.23	0.00	0.0083	194.03	194.03
57	718.9	94.3	8.3	219.12	28.74	0.0083	199.26	195.83
58	721.8	83.1	8.3	220.00	25.33	0.0083	200.87	198.21
59	720.5	130.9	8.3	219.61	39.90	0.0083	200.15	193.54
61	706.9	0.0	8.3	215.46	0.00	0.0083	192.66	192.66
62	700.5	0.0	8.3	213.51	0.00	0.0083	189.19	189.19
63	775.7	333.2	8.3	236.43	101.56	0.0083	231.99	189.18
64	811.8	398.7	8.3	247.44	121.52	0.0083	254.08	192.80
65	802.1	374.8	8.4	244.48	114.24	0.0084	251.04	196.22
66	833.1	426.7	8.4	253.93	130.06	0.0084	270.82	199.77

STATISTICS (Continued)

0.125″ Aluminum Sheets

Test	V_0 (ft/s)	V_r (ft/s)	Mass (g)	V_0 (m/s)	V_r (m/s)	Mass (kg)	Initial Energy (J)	Absorbed Energy (J)
67	384.1	0.0	8.4	117.07	0.00	0.0084	57.57	57.57
68	526.8	0.0	8.4	160.57	0.00	0.0084	108.29	108.29
69	724.7	139.5	8.4	220.89	42.52	0.0084	204.93	197.33
70	739.4	223.7	8.3	225.37	68.18	0.0083	210.78	191.49
71	740.6	218.8	8.3	225.73	66.69	0.0083	211.47	193.01
72	740.5	218.1	8.3	225.70	66.48	0.0083	211.41	193.07
73	736	209.6	8.3	224.33	63.89	0.0083	208.85	191.91
74	743.7	233.5	8.3	226.68	71.17	0.0083	213.24	192.22
75	737.2	207.5	8.3	224.70	63.25	0.0083	209.53	192.93
76	858.5	486.7	8.3	261.67	148.35	0.0083	284.16	192.83
77	846.8	467.1	8.3	258.10	142.37	0.0083	276.46	192.35
78	852.4	476.9	8.3	259.81	145.36	0.0083	280.13	192.45
79	852.6	469.5	8.3	259.87	143.10	0.0083	280.26	195.28
80	848.1	457.2	8.3	258.50	139.35	0.0083	277.31	196.72
81	850.2	472.0	8.3	259.14	143.87	0.0083	278.69	192.80
85	890	536.2	8.3	271.27	163.43	0.0083	305.39	194.54
86	882.5	520.0	8.3	268.99	158.50	0.0083	300.27	196.01

Moments on Absorbed Energy			
w/ zero values		w/o zero values	
Mean	186.719	Mean	194.631
Std Dev	25.107	Std Dev	2.773
Skewness	-4.030	Skewness	0.642
Kurtosis	17.665	Kurtosis	0.052

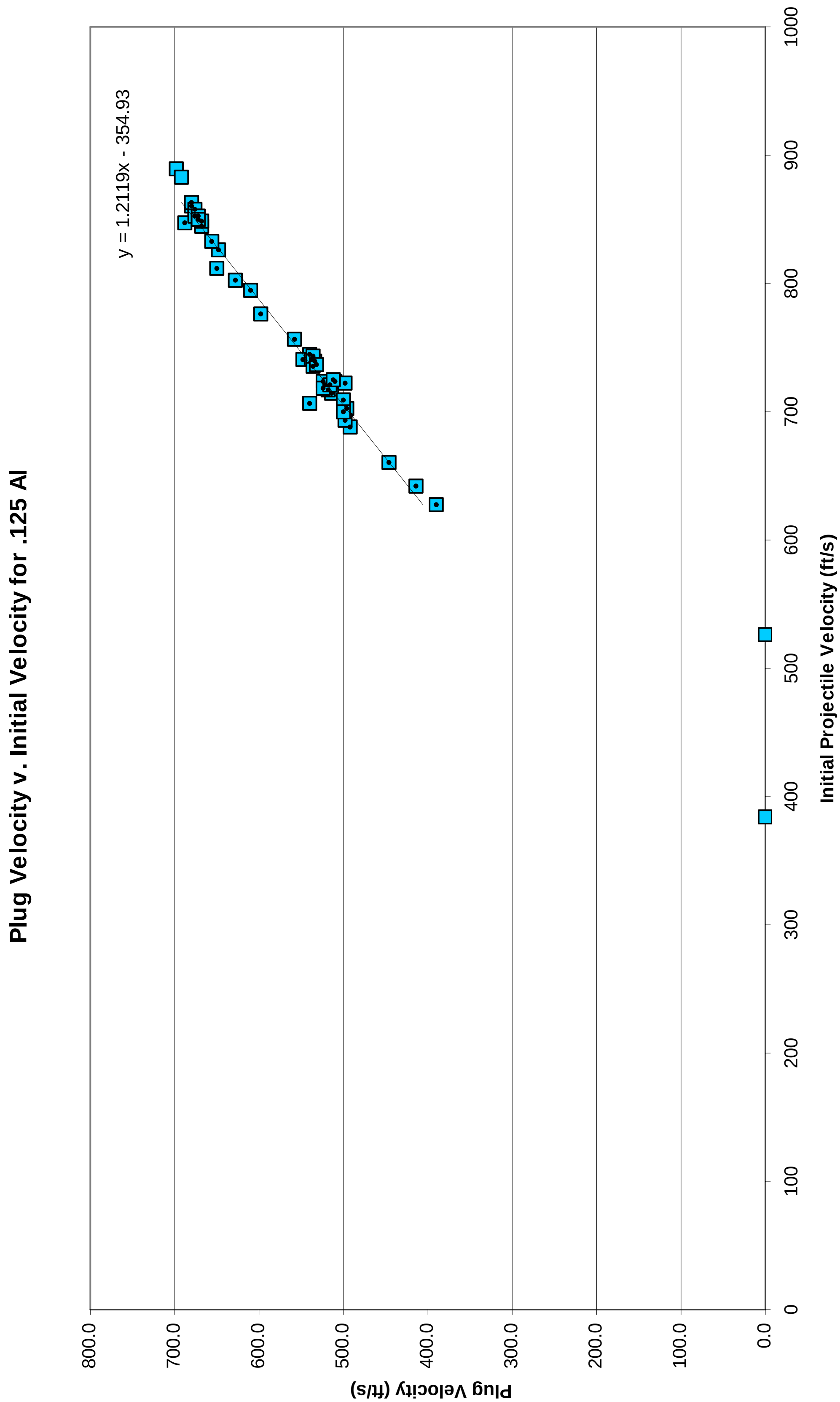
Plug Velocity v. Initial Velocity for .125 Al
y = 1.2119x - 354.93
Plug Velocity (ft/s)
Initial Projectile Velocity (ft/s)
0.0
100.0
200.0
300.0
400.0
500.0
600.0
700.0
800.0
0
100
200
300
400
500
600
700
800
900
1000

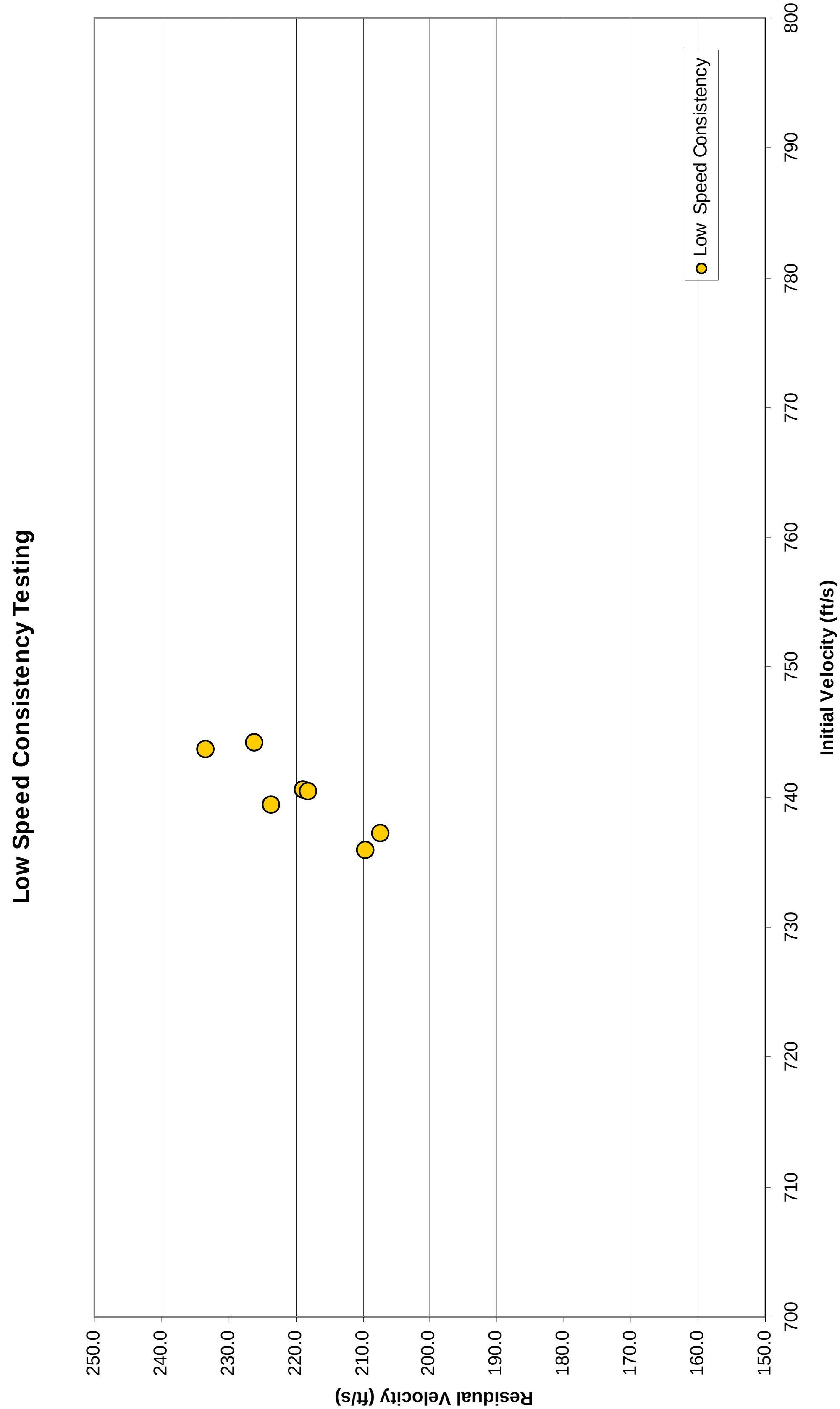
Low Speed Consistency Testing
Residual Velocity (ft/s)
250.0
240.0
230.0
220.0
210.0
200.0
190.0
180.0
170.0
160.0
150.0
Initial Velocity (ft/s)
700
710
720
730
740
750
760
770
780
790
800
Low Speed Consistency

High Speed Consistency (.125Al)

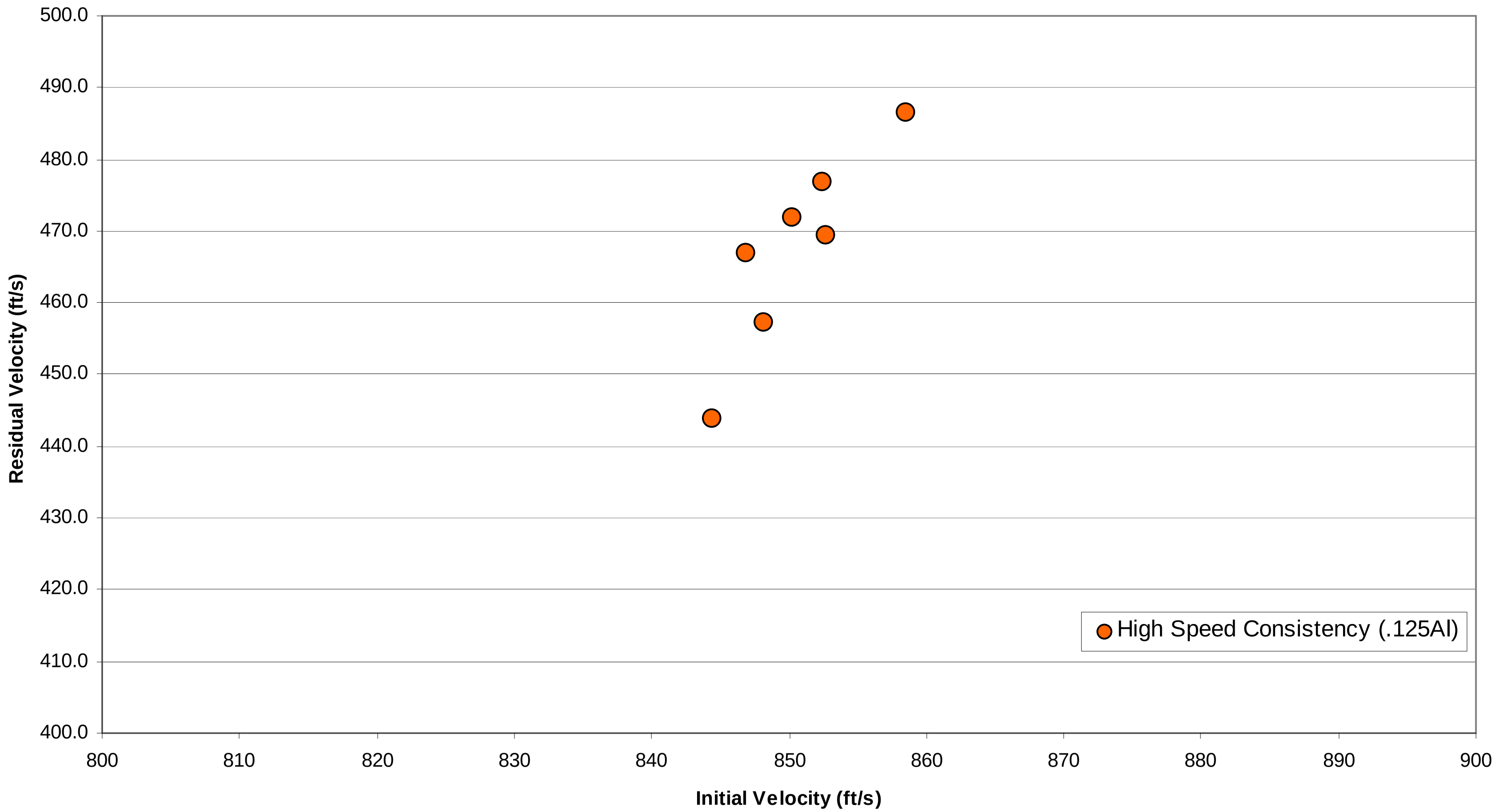

COMPOSITES TESTING
2″ x 1/32" Composite Sheets
Ballistic Limit ~ 141 ft/s

Test	V_i (ft/s)	V_r (ft/s)	m (g)	V_i (m/s)	V_r (m/s)	m (kg)	IKE (J)	AKE (J)	Percent KE Absorbed
87	491.8	458.3	8.3	149.90	139.69	0.0083	93.25	12.27	13.16%
88	315.0	273.3	8.3	96.01	83.30	0.0083	38.26	9.46	24.72%
89	205.4	147.0	8.3	62.61	44.81	0.0083	16.27	7.93	48.78%
90	133.0	0.0	8.3	40.54	0.00	0.0083	6.82	6.82	100.00%
91	165.0	82.6	8.3	50.29	25.18	0.0083	10.50	7.87	74.94%
92	170.0	86.0	8.3	51.82	26.21	0.0083	11.14	8.29	74.41%
93	124.5	0.0	8.3	37.95	0.00	0.0083	5.98	5.98	100.00%
94	176.3	109.5	8.3	53.74	33.38	0.0083	11.98	7.36	61.42%
95	134.8	0.0	8.3	41.09	0.00	0.0083	7.01	7.01	100.00%
96	142.0	21.9	8.3	43.28	6.68	0.0083	7.77	7.59	97.62%
97	140.1	0.0	8.3	42.70	0.00	0.0083	7.57	7.57	100.00%
98	882.5	853.8	8.3	268.99	260.24	0.0083	300.27	19.21	6.40%
99	689.1	658.1	8.3	210.04	200.59	0.0083	183.08	16.10	8.79%
100	396.8	362.0	8.3	120.94	110.34	0.0083	60.70	10.18	16.77%

Stats for AKE

Mean	10.627
Std Dev	4.058
Skewness	1.421
Kurtosis	1.040

Test	V_0 (ft/s)	V_r (ft/s)	Mass (g)	V_0 (m/s)	V_r (m/s)	Mass (kg)	Initial Energy (J)	Absorbed Energy (J)
87	491.8	458.3	8.3	149.90	139.69	0.0083	93.25	12.27
88	315.0	273.3	8.3	96.01	83.30	0.0083	38.26	9.46
89	205.4	147.0	8.3	62.61	44.81	0.0083	16.27	7.93
90	133.0	0.0	8.3	40.54	0.00	0.0083	6.82	6.82
91	165.0	82.6	8.3	50.29	25.18	0.0083	10.50	7.87
92	170.0	86.0	8.3	51.82	26.21	0.0083	11.14	8.29
93	124.5	0.0	8.3	37.95	0.00	0.0083	5.98	5.98
94	176.3	109.5	8.3	53.74	33.38	0.0083	11.98	7.36
95	134.8	0.0	8.3	41.09	0.00	0.0083	7.01	7.01
96	142.0	21.9	8.3	43.28	6.68	0.0083	7.77	7.59
97	140.1	0.0	8.3	42.70	0.00	0.0083	7.57	7.57
98	882.5	853.8	8.3	268.99	260.24	0.0083	300.27	19.21
99	689.1	658.1	8.3	210.04	200.59	0.0083	183.08	16.10
100	396.8	362.0	8.3	120.94	110.34	0.0083	60.70	10.18

Moments on Absorbed Energy			
w/ zero values		w/o zero values	
Mean	9.545	Mean	10.627
Std Dev	3.827	Std Dev	4.058
Skewness	1.741	Skewness	1.421
Kurtosis	2.415	Kurtosis	1.040

METALS TESTING
0.250″ Aluminum Sheets
Ballistic Limit ~ 1327

Test	V_i (ft/s)	V_r (ft/s)	m (g)	V_i (m/s)	V_r (m/s)	m (kg)	IKE (J)	AKE (J)	Percent KE Absorbed	m_p	V_p (ft/s)	V_p (m/s)	Plug KE (J)
101	1044.9	0.0	8.4	318.49	0.00	0.0084	426.02	426.02	100.00%	N/A	159.8	48.7	
102	1327.1	0.0	8.4	404.50	0.00	0.0084	687.21	687.21	100.00%	0.001	809.9	246.9	30.47
103	1423.8	583.0	8.4	433.97	177.70	0.0084	791.00	658.38	83.23%	0.001	930.5	283.6	40.22
104	1372.2	438.8	8.4	418.25	133.75	0.0084	734.71	659.58	89.77%	0.001	820.2	250.0	31.25
105	1397.7	485.8	8.4	426.02	148.07	0.0084	762.27	670.18	87.92%	N/A	883.4	269.3	
106	1353.4	0.0	8.4	412.52	0.00	0.0084	714.71	714.71	100.00%	0.0008	794.3	242.1	23.45
107	1339.9	386.3	8.4	408.40	117.74	0.0084	700.53	642.30	91.69%	0.001	738.9	225.2	25.36
108	1328.4	241.5	8.4	404.90	73.61	0.0084	688.55	665.80	96.69%	N/A	745.0	227.1	
109	1350.7	439.3	8.4	411.69	133.90	0.0084	711.86	636.56	89.42%	0.0009	829.7	252.9	28.78
110	1320.2	0.0	8.4	402.40	0.00	0.0084	680.08	680.08	100.00%	0.001	638.4	194.6	18.93
111	1450.5	588.9	8.4	442.11	179.50	0.0084	820.95	685.63	83.52%	0.0009	930.6	283.6	36.20
112	1671.5	942.3	8.4	509.47	287.21	0.0084	1090.16	743.70	68.22%	N/A	UNKNOWN		
113	1642.2	824.5	8.4	500.54	251.31	0.0084	1052.28	787.03	74.79%	0.0006	1128.9	344.1	35.52
114	1540.4	765.6	8.4	469.51	233.35	0.0084	925.86	697.15	75.30%	0.0006	1001.2	305.2	27.94
115	1432.0	563.4	8.4	436.47	171.72	0.0084	800.14	676.28	84.52%	0.0009	913.7	278.5	34.90
116	1343.0	199.3	8.4	409.35	60.75	0.0084	703.77	688.27	97.80%	0.0008	882.0	268.8	28.91
117	1020.8	0.0	8.4	311.14	0.00	0.0084	406.59	406.59	100.00%	No Plug!	0.0	0.0	
118	1508.2	721.4	8.4	459.70	219.88	0.0084	887.56	684.50	77.12%	N/A	UNKNOWN		
119	1479.8	618.4	8.4	451.04	188.49	0.0084	854.45	705.23	82.54%	0.001	UNKNOWN		
120	1581.0	865.7	8.4	481.89	263.87	0.0084	975.31	682.89	70.02%	0.0009	1058.5	322.6	46.84
121	1830.5	1136.6	8.4	557.94	346.44	0.0084	1307.43	803.36	61.45%	0.0006	1362.3	415.2	51.72
122	1764.0	1089.5	8.4	537.67	332.08	0.0084	1214.16	751.00	61.85%	0.0007	1268.5	386.6	52.32
123	1875.4	1236.7	8.4	571.62	376.95	0.0084	1372.36	775.59	56.51%	0.0006	UNKNOWN		
124	1328.8	0.0	8.4	405.02	0.00	0.0084	688.97	688.97	100.00%	0.001	748.8	228.2	26.05
125	1324.9	0.0	8.4	403.83	0.00	0.0084	684.93	684.93	100.00%	N/A	715.5	218.1	
126	1386.8	456.4	8.4	422.70	139.11	0.0084	750.42	669.15	89.17%	N/A	UNKNOWN		
127	1339.1	0.0	8.4	408.16	0.00	0.0084	699.69	699.69	100.00%	N/A	706.7	215.4	
128	1345.3	0.0	8.4	410.05	0.00	0.0084	706.18	706.18	100.00%	0.0011	691.8	210.9	24.45

Stats for AKE

Mean	698.515
Std Dev	49.680
Skewness	0.941
Kurtosis	-0.215

STATISTICS
0.25″ Aluminum Sheets

Test	V_0 (ft/s)	V_r (ft/s)	Mass (g)	V_0 (m/s)	V_r (m/s)	Mass (kg)	Initial Energy (J)	Absorbed Energy (J)
101	1044.9	0.0	8.4	318.49	0.00	0.0084	426.02	426.02
102	1327.1	0.0	8.4	404.50	0.00	0.0084	687.21	687.21
103	1423.8	583.0	8.4	433.97	177.70	0.0084	791.00	658.38
104	1372.2	438.8	8.4	418.25	133.75	0.0084	734.71	659.58
105	1397.7	485.8	8.4	426.02	148.07	0.0084	762.27	670.18
106	1353.4	0.0	8.4	412.52	0.00	0.0084	714.71	714.71
107	1339.9	386.3	8.4	408.40	117.74	0.0084	700.53	642.30
108	1328.4	241.5	8.4	404.90	73.61	0.0084	688.55	665.80
109	1350.7	439.3	8.4	411.69	133.90	0.0084	711.86	636.56
110	1320.2	0.0	8.4	402.40	0.00	0.0084	680.08	680.08
111	1450.5	588.9	8.4	442.11	179.50	0.0084	820.95	685.63
112	1671.5	942.3	8.4	509.47	287.21	0.0084	1090.16	743.70
113	1642.2	824.5	8.4	500.54	251.31	0.0084	1052.28	787.03
114	1540.4	765.6	8.4	469.51	233.35	0.0084	925.86	697.15
115	1432.0	563.4	8.4	436.47	171.72	0.0084	800.14	676.28
116	1343.0	199.3	8.4	409.35	60.75	0.0084	703.77	688.27
117	1020.8	0.0	8.4	311.14	0.00	0.0084	406.59	406.59
118	1508.2	721.4	8.4	459.70	219.88	0.0084	887.56	684.50
119	1479.8	618.4	8.4	451.04	188.49	0.0084	854.45	705.23
120	1581.0	865.7	8.4	481.89	263.87	0.0084	975.31	682.89
121	1830.5	1136.6	8.4	557.94	346.44	0.0084	1307.43	803.36
122	1764.0	1089.5	8.4	537.67	332.08	0.0084	1214.16	751.00
123	1875.4	1236.7	8.4	571.62	376.95	0.0084	1372.36	775.59
124	1328.8	0.0	8.4	405.02	0.00	0.0084	688.97	688.97

Moments on Absorbed Energy			
w/ zero values		w/o zero values	
Mean	675.708	Mean	698.515
Std Dev	91.038	Std Dev	49.680
Skewness	-1.877	Skewness	0.941
Kurtosis	4.548	Kurtosis	-0.215

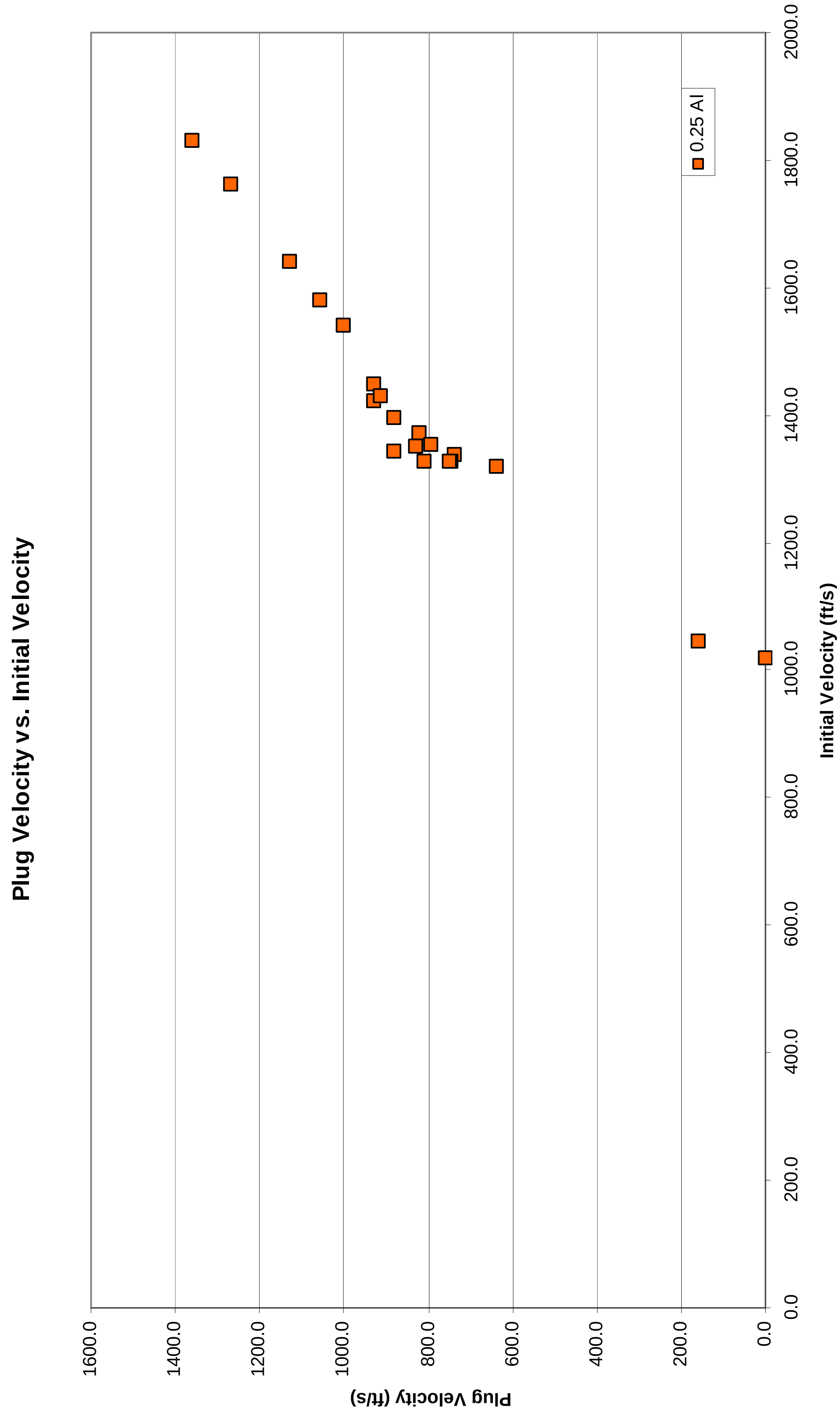

Plug Velocity vs. Initial Velocity
Plug Velocity (ft/s)
Initial Velocity (ft/s)
0.25 Al
0.0
200.0
400.0
600.0
800.0
1000.0
1200.0
1400.0
1600.0
1800.0
2000.0

POLYCARBONATE TESTING
0.25″ Polycarbonate (Makrolon) Sheets
Ballistic Limit ~ 861 ft/s

Test	V_i (ft/s)	V_r (ft/s)	m (g)	V_i (m/s)	V_r (m/s)	m (kg)	IKE (J)	AKE (J)	Percent KE Absorbed
134	783.2	0.0	8.3	238.72	0.00	0.0083	236.50	236.50	100.00%
135	844.8	0.0	8.3	257.50	0.00	0.0083	275.16	275.16	100.00%
136	867.6	0.0	8.3	264.44	0.00	0.0083	290.21	290.21	100.00%
137	874.3	0.0	8.3	266.49	0.00	0.0083	294.71	294.71	100.00%
138	873.7	0.0	8.4	266.30	0.00	0.0084	297.85	297.85	100.00%
139	1065.5	631.6	8.4	324.76	192.51	0.0084	442.98	287.33	64.86%
140	983.3	479.1	8.4	299.71	146.03	0.0084	377.27	287.71	76.26%
141	1002.5	584.4	8.4	305.56	178.13	0.0084	392.15	258.89	66.02%
142	879.8	186.8	8.4	268.16	56.94	0.0084	302.03	288.41	95.49%
143	1078.8	657.6	8.4	328.82	200.44	0.0084	454.11	285.38	62.84%
144	1154.0	771.5	8.4	351.74	235.15	0.0084	519.63	287.38	55.30%
145	1194.6	835.8	8.4	364.11	254.75	0.0084	556.83	284.26	51.05%
146	1446.3	1079.8	8.4	440.83	329.12	0.0084	816.20	361.25	44.26%
147	1356.6	934.2	8.4	413.49	284.74	0.0084	718.10	377.56	52.58%
148	1367.3	954.6	8.4	416.75	290.96	0.0084	729.47	373.90	51.26%
149	1402.8	1016.9	8.4	427.57	309.95	0.0084	767.84	364.35	47.45%
150	1351.9	922.8	8.4	412.06	281.27	0.0084	713.13	380.86	53.41%
151	1319.6	817.1	8.4	402.21	249.05	0.0084	679.46	418.95	61.66%
152	1186.0	805.9	8.4	361.49	245.64	0.0084	548.84	295.42	53.83%
153	1061.0	629.5	8.4	323.39	191.87	0.0084	439.25	284.63	64.80%
154	1455.7	1101.1	8.4	443.70	335.62	0.0084	826.84	353.76	42.79%
155	1536.5	1249.1	8.4	468.33	380.73	0.0084	921.18	312.38	33.91%
156	1027.2	563.0	8.4	313.09	171.60	0.0084	411.71	288.03	69.96%
157	863.4	124.0	8.4	263.16	37.80	0.0084	290.87	284.87	97.94%
158	962.5	542.5	8.4	293.37	165.35	0.0084	361.48	246.64	68.23%

Stats for AKE

Mean	314.609
Std Dev	47.477
Skewness	0.747
Kurtosis	-0.628

STATISTICS

0.25″ Polycarbonate (Markolon) Sheets

Test	V_0 (ft/s)	V_r (ft/s)	Mass (g)	V_0 (m/s)	V_r (m/s)	Mass (kg)	Initial Energy (J)	Absorbed Energy (J)
133	881.7	196.5	8.3	268.74	59.89	0.0083	299.72	284.84
134	783.2	0.0	8.3	238.72	0.00	0.0083	236.50	236.50
135	844.8	0.0	8.3	257.50	0.00	0.0083	275.16	275.16
136	867.6	0.0	8.3	264.44	0.00	0.0083	290.21	290.21
137	874.3	0.0	8.3	266.49	0.00	0.0083	294.71	294.71
138	873.7	0.0	8.4	266.30	0.00	0.0084	297.85	297.85
139	1065.5	631.6	8.4	324.76	192.51	0.0084	442.98	287.33
140	983.3	479.1	8.4	299.71	146.03	0.0084	377.27	287.71
141	1002.5	584.4	8.4	305.56	178.13	0.0084	392.15	258.89
142	879.8	186.8	8.4	268.16	56.94	0.0084	302.03	288.41
143	1078.8	657.6	8.4	328.82	200.44	0.0084	454.11	285.38
144	1154.0	771.5	8.4	351.74	235.15	0.0084	519.63	287.38
145	1194.6	835.8	8.4	364.11	254.75	0.0084	556.83	284.26
146	1446.3	1079.8	8.4	440.83	329.12	0.0084	816.20	361.25
147	1356.6	934.2	8.4	413.49	284.74	0.0084	718.10	377.56
148	1367.3	954.6	8.4	416.75	290.96	0.0084	729.47	373.90
149	1402.8	1016.9	8.4	427.57	309.95	0.0084	767.84	364.35
150	1351.9	922.8	8.4	412.06	281.27	0.0084	713.13	380.86
151	1319.6	817.1	8.4	402.21	249.05	0.0084	679.46	418.95
152	1186.0	805.9	8.4	361.49	245.64	0.0084	548.84	295.42
153	1061.0	629.5	8.4	323.39	191.87	0.0084	439.25	284.63
154	1455.7	1101.1	8.4	443.70	335.62	0.0084	826.84	353.76
155	1536.5	1249.1	8.4	468.33	380.73	0.0084	921.18	312.38
156	1027.2	563.0	8.4	313.09	171.60	0.0084	411.71	288.03
157	863.4	124.0	8.4	263.16	37.80	0.0084	290.87	284.87
158	962.5	542.5	8.4	293.37	165.35	0.0084	361.48	246.64

Moments on Absorbed Energy			
w/ zero values		w/o zero values	
Mean	307.739	Mean	314.609
Std Dev	45.950	Std Dev	47.477
Skewness	0.883	Skewness	0.747
Kurtosis	-0.016	Kurtosis	-0.628

Data Suggests Transition ~ 1200 ft/s:			
Values Before 1200 ft/s		Values After 1200 ft/s	
Mean	281.829	Mean	367.876
Std Dev	13.452	Std Dev	29.862
Skewness	-2.101	Skewness	-0.268
Kurtosis	3.868	Kurtosis	2.157

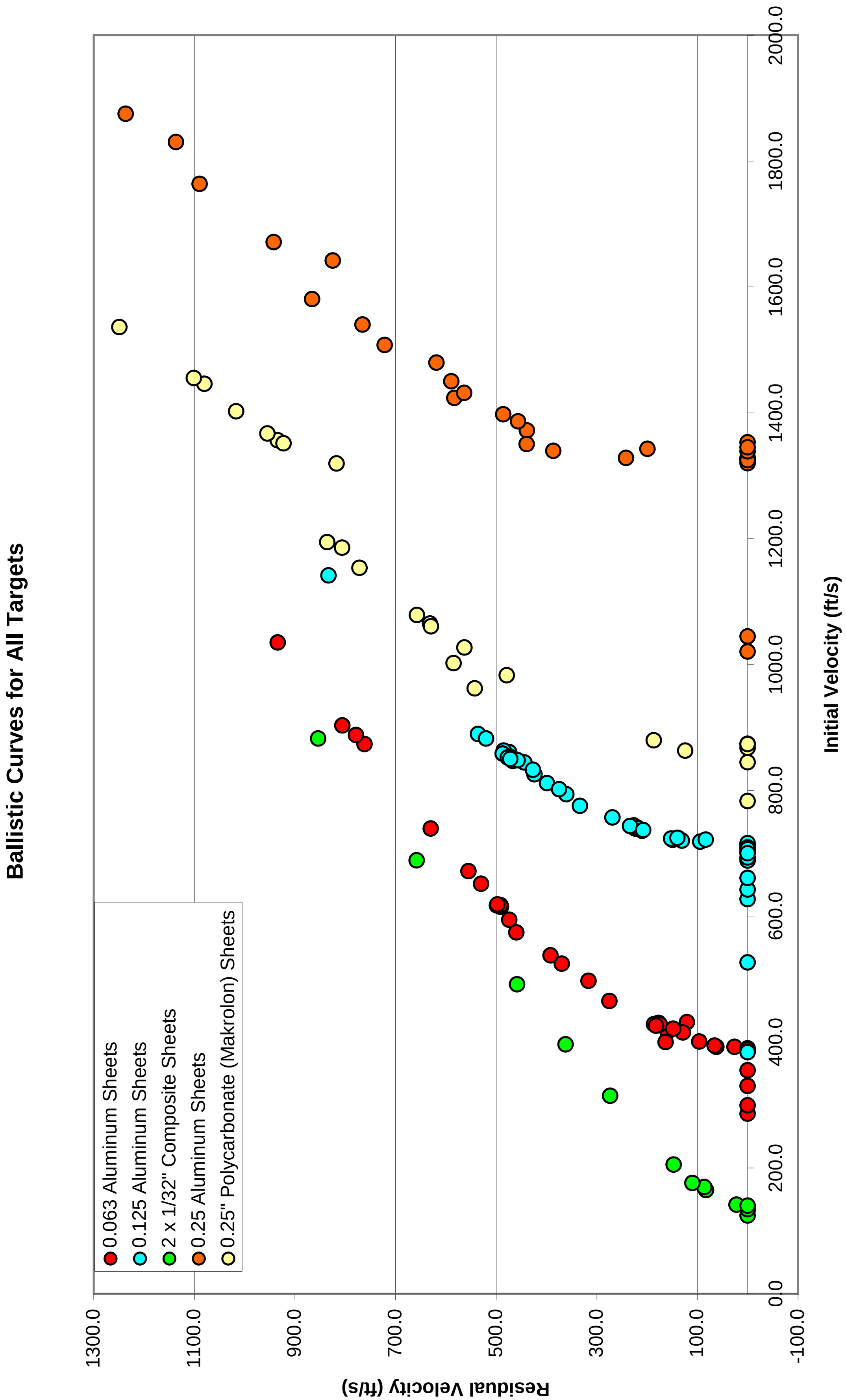
Ballistic Curves for All Targets
0.063 Aluminum Sheets
0.125 Aluminum Sheets
2 x 1/32" Composite Sheets
0.25 Aluminum Sheets
0.25" Polycarbonate (Makrolon) Sheets
Residual Velocity (ft/s)
Initial Velocity (ft/s)
1300.0
1100.0
900.0
700.0
500.0
300.0
100.0
-100.0
0.0
200.0
400.0
600.0
800.0
1000.0
1200.0
1400.0
1600.0
1800.0
2000.0

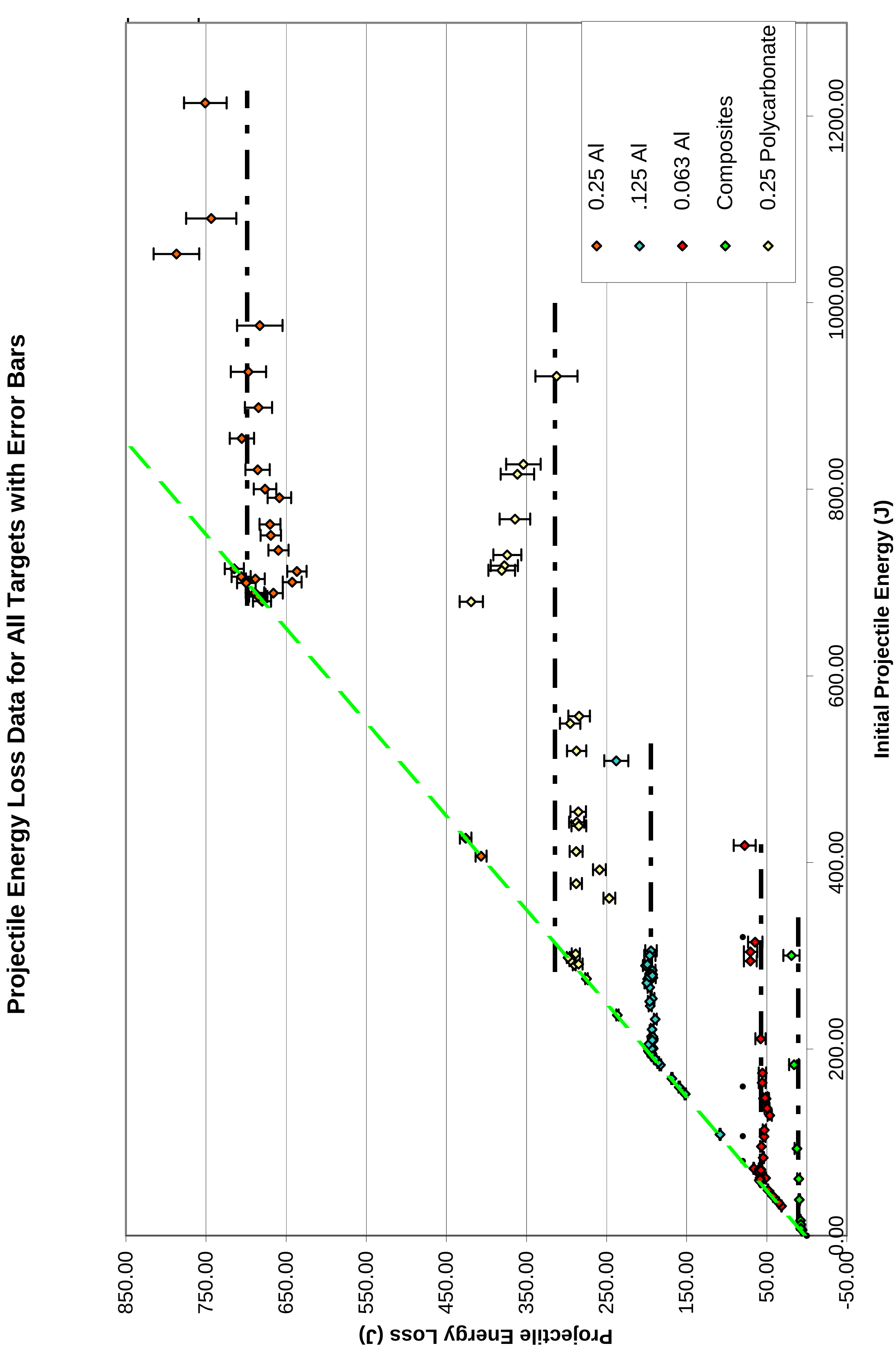
Projectile Energy Loss Data for All Targets with Error Bars
Projectile Energy Loss (J)
Initial Projectile Energy (J)
850.00
750.00
650.00
550.00
450.00
350.00
250.00
150.00
50.00
-50.00
0.00
200.00
400.00
600.00
800.00
1000.00
1200.00
0.25 Al
.125 Al
0.063 Al
Composites
0.25 Polycarbonate

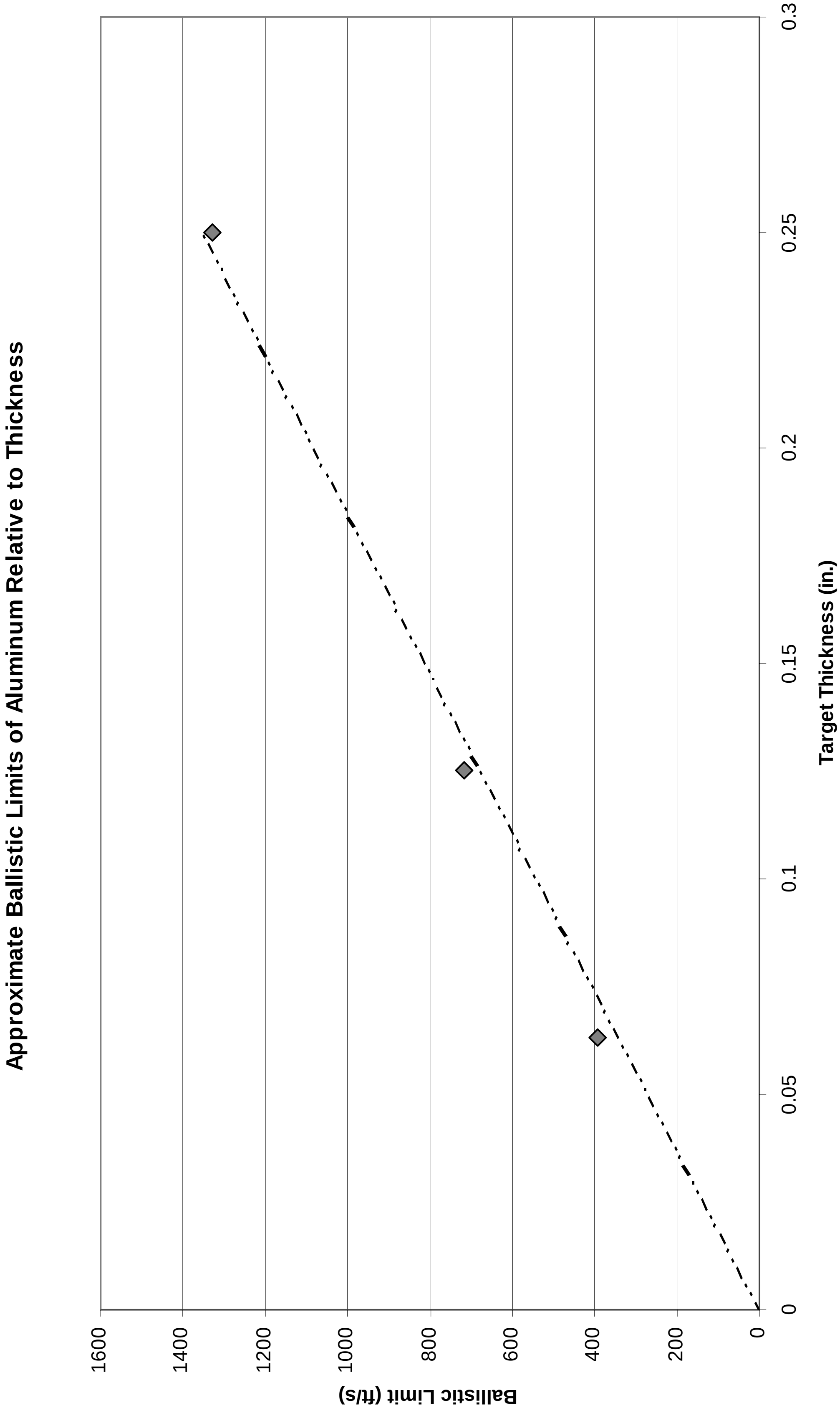

Approximate Ballistic Limits of Aluminum Relative to Thickness
Ballistic Limit (ft/s)
Target Thickness (in.)
0
200
400
600
800
1000
1200
1400
1600
0
0.05
0.1
0.15
0.2
0.25
0.3

THOR EQUATION FOR PREDICTING RESIDUAL VELOCITY

Al t (in)	Al t (cm)	Proj. Mass (g)	Presented Area (A)	Initial Velocity (m/s)	(ft/s)	a1	b1	c1	d1	e1	Residual Velocity (m/s)	(ft/s)
0.063	0.16002	8.3	1.262200701	95	311.7	1.029	-1.072	3.9356	1.251	-0.139	3.672585072	12.04916364
				110	360.9						20.51481037	67.30580839
				120	393.7						31.59057768	103.6436277
				130	426.5						42.56876358	139.6612981
				140	459.3						53.46477065	175.4093528
				160	524.9						75.05612509	246.2471299
				180	590.6						96.4354906	316.3894053
				200	656.2						117.6503843	385.9920752
				240	787.4						159.711123	523.9866249
				300	984.3						222.1632146	728.8819388
				350	1148						273.813278	898.3375277
Ballistic Limit: 301.0757466 ft/s (91.76788742 m/s)												
0.125	0.3175	8.3	1.262200701	175	574.1						5.206353549	17.08121246
				180	590.6						10.86992331	35.6624781
				190	623.4						22.13622965	72.62542547
				200	656.2						33.32880294	109.3464665
				220	721.8						55.52232006	182.159843
				240	787.4						77.49962729	254.2638694
				260	853						99.29757562	325.7794481
				280	918.6						120.9444757	396.7994615
				300	984.3						142.4625289	467.3967491
				320	1050						163.8694545	537.6294448
				360	1181						206.4047885	677.1810655
Ballistic Limit: 559.122776 ft/s (170.4206219 m/s)												

THOR EQUATION FOR PREDICTING RESIDUAL VELOCITY (Continued)

Al t (in)	Al t (cm)	Proj. Mass (g)	Presented Area (A)	Initial Velocity		a1	b1	c1	d1	e1	Residual Velocity	
				(m/s)	(ft/s)						(m/s)	(ft/s)
0.25	0.635	8.3	1.262200701	320	1050						1.398553992	4.588431739
				325	1066						7.084426889	23.24287041
				330	1083						12.75838514	41.85821903
				340	1115						24.07207136	78.97661218
				360	1181						46.57218006	152.7958666
				380	1247						68.91886874	226.1117744
				400	1312						91.12891708	298.9793872
				440	1444						135.1938906	443.5495106
				480	1575						178.8581892	586.8050835
				550	1804						254.5029322	834.9833747
				600	1969						308.0553199	1010.680185
Ballistic Limit: 1045.839218 ft/s (318.7717932 m/s)												

PREDICTED RESIDUAL VELOCITY ASSUMING A CONSTANT ABSORBED KINETIC ENERGY BY THE TARGET

0.063″ Al					
Predicted Ballistic Limit: 385.0647 ft/s (117.3677158 m/s)					
Proj. Mass (kg)	Approx. AKE	V_o (ft/s)	V_o (m/s)	V_r (m/s)	V_r (ft/s)
0.0083	57.167	385.1	117.3785	1.5896051	5.2152397
		400	121.92	33.004631	108.28291
		420	128.016	51.116685	167.70566
		440	134.112	64.891046	212.89713
		460	140.208	76.701386	251.64497
		480	146.304	87.348038	286.57493
		500	152.4	97.21409	318.94387
		550	167.64	119.69958	392.71515
		600	182.88	140.24947	460.13606
		650	198.12	159.61314	523.66515
		700	213.36	178.17775	584.57266
		750	228.6	196.17028	643.60329
		800	243.84	213.73527	701.2312
		850	259.08	230.97027	757.77648
		900	274.32	247.94411	813.46493
		1200	365.76	346.41766	1136.5409
0.125″ Al					
Predicted Ballistic Limit: 710.5048 ft/s (216.5618529 m/s)					
Proj. Mass (kg)	Approx. AKE	V_o (ft/s)	V_o (m/s)	V_r (m/s)	V_r (ft/s)
0.0083	194.631	710.6	216.5909	3.5458644	11.633414
		720	219.456	35.523229	116.54603
		740	225.552	63.044973	206.84046
		760	231.648	82.22992	269.7832
		780	237.744	98.097775	321.84309
		800	243.84	112.06654	367.67238
		820	249.936	124.77567	409.369
		840	256.032	136.57726	448.08814
		860	262.128	147.68904	484.54409
		880	268.224	158.25637	519.21381
		900	274.32	168.38179	552.43369
		1200	365.76	294.75641	967.04859

PREDICTED RESIDUAL VELOCITY ASSUMING A CONSTANT ABSORBED KINETIC ENERGY BY THE TARGET (Continued)

0.25″ Al					
Predicted Ballistic Limit: 1346.012 ft/s (410.2643873 m/s)					
Proj. Mass (kg)	Approx. AKE	V_o (ft/s)	V_o (m/s)	V_r (m/s)	V_r (ft/s)
0.0083	698.515	1346.1	410.2913	4.6975498	15.411909
		1350	411.48	31.605742	103.69338
		1360	414.528	59.300888	194.55672
		1380	420.624	92.777594	304.38843
		1400	426.72	117.35881	385.03548
		1420	432.816	137.88699	452.38514
		1440	438.912	155.97075	511.71507
		1460	445.008	172.38113	565.55488
		1500	457.2	201.77951	662.00628
		1550	472.44	234.27054	768.60414
		1600	487.68	263.65681	865.01579
		1650	502.92	290.88083	954.33344
		1700	518.16	316.50106	1038.3893
		1800	548.64	364.26499	1195.0951
		1900	579.12	408.73354	1340.9893
Composites					
Predicted Ballistic Limit: 166.0223 ft/s (50.60358576 m/s)					
Proj. Mass (kg)	Approx. AKE	V_o (ft/s)	V_o (m/s)	V_r (m/s)	V_r (ft/s)
0.0083	10.627	166.1	50.62728	1.5487378	5.0811606
		170	51.816	11.143382	36.559653
		175	53.34	16.865133	55.331801
		180	54.864	21.197538	69.545727
		190	57.912	28.16162	92.393767
		200	60.96	33.991156	111.51954
		250	76.2	56.971195	186.91337
		300	91.44	76.161347	249.87318
		350	106.68	93.91432	308.11785
		400	121.92	110.92233	363.91841
		500	152.4	143.75339	471.63186
		600	182.88	175.7395	576.57316
		700	213.36	207.2722	680.02692
		800	243.84	238.53139	782.58329
		900	274.32	269.6122	884.55447

PREDICTED RESIDUAL VELOCITY ASSUMING A CONSTANT ABSORBED KINETIC ENERGY BY THE TARGET (Continued)

0.25″ Polycarbonate							
Predicted Ballistic Limit: 854.9758 ft/s (260.5966278 m/s)				With Transition Present		Without Transition	
Proj. Mass (kg)	Approx. AKE	V_o (ft/s)	V_o (m/s)	V_r (m/s)	V_r (ft/s)	V_r (m/s)	V_r (ft/s)
0.0083	281.829	855	260.604	1.9602057	6.4311211	1.9602057	6.4311211
		860	262.128	28.292861	92.824347	28.292861	92.824347
		880	268.224	63.509934	208.36593	63.509934	208.36593
		900	274.32	85.678819	281.09849	85.678819	281.09849
		950	289.56	126.2315	414.14534	126.2315	414.14534
		1000	304.8	158.08997	518.66787	158.08997	518.66787
		1050	320.04	185.78213	609.52142	185.78213	609.52142
		1100	335.28	210.95515	692.11008	210.95515	692.11008
		1150	350.52	234.42199	769.10101	234.42199	769.10101
		1200	365.76	256.65108	842.03109	256.65108	842.03109
		1250	381	277.93956	911.87519	277.93956	911.87519
0.0083	367.876	1300	396.24	261.45997	857.80832	298.48875	979.29381
		1350	411.48	284.02636	931.845	318.44181	1044.7566
		1400	426.72	305.68798	1002.9133	337.90436	1108.6101
		1500	457.2	346.96833	1138.3475	375.66107	1232.4838
		1600	487.68	386.24728	1267.2155	412.21497	1352.4113

ERROR ANALYSIS ON INITIAL AND RESIDUAL VELOCITY VALUES

Test	V_i (ft/s)	V_r (ft/s)	Camera	Powder Gun	ΔT	Δx	C	δC	δΔx	δV_r (ft/s)	δV_i (ft/s)
0.063″ Al											
2	389.3	0.0								0.000	0.039
3	431.9	120.6								2.079	0.043
4	355.2	0.0								0.000	0.036
5	416.6	159.0								2.741	0.042
6	465.4	274.6	x		0.0008	29.0	11.00	0.141	0.283	4.431	0.047
7	497.5	316.1								5.450	0.050
8	524.7	369.5	x		0.0007	36.0	11.60	0.141	0.283	5.360	0.052
9	538.2	391.7	x		0.0006	32.0	11.35	0.141	0.283	5.985	0.054
10	574.7	459.8	x		0.0005	32.0	11.60	0.141	0.283	6.924	0.057
11	594.6	473.9	x		0.0004	26.5	11.65	0.141	0.283	7.660	0.059
12	617.2	498.6	x		0.0003	21.0	11.70	0.141	0.283	9.023	0.062
13	651.9	529.8	x		0.0004	29.5	11.60	0.141	0.424	9.989	0.065
14	672.0	554.9	x		0.0004	30.9	11.60	0.141	0.424	10.188	0.067
15	739.4	629.8	x		0.0003	26.3	11.60	0.141	0.424	12.735	0.074
16	873.6	761.7								13.133	0.087
17	392.6	26.0	x		0.0040	14.5	11.62	0.141	0.283	0.598	0.039
18	415.5	128.8								2.221	0.042
19	330.6	0.0								0.000	0.033
20	286.4	0.0								0.000	0.029
21	299.6	0.0								0.000	0.030
22	390.2	0.0								0.000	0.039
23	428.6	186.0								3.207	0.043
24	430.6	177.4	x		0.0010	24.7	11.60	0.141	0.283	2.967	0.043
25	428.1	174.7								3.012	0.043
26	421.5	148.0								2.552	0.042
27	426.4	182.3								3.143	0.043
28	615.4	490.3	x		0.0004	27.3	11.60	0.141	0.283	7.844	0.062
29	614.9	490.3	x		0.0004	27.3	11.60	0.141	0.283	7.844	0.061
30	617.8	491.4	x		0.0005	34.2	11.60	0.141	0.283	7.239	0.062
31	618.8	497.5	x		0.0004	27.7	11.60	0.141	0.283	7.912	0.062

ERROR ANALYSIS ON INITIAL AND RESIDUAL VELOCITY VALUES (Continued)

Test	V_i (ft/s)	V_r (ft/s)	Camera	Powder Gun	ΔT	Δx	C	δC	δΔx	δV_r (ft/s)	δV_i (ft/s)
0.063″ Al											
32	400.2	163.3								2.816	0.040
33	392.7	61.9	x		0.0027	22.6	11.27	0.141	0.283	1.097	0.039
34	387.5	0.0								0.000	0.039
35	388.1	0.0								0.000	0.039
36	401.0	96.3								1.660	0.040
37	394.8	65.8								1.134	0.039
83	903.3	805.4								13.886	0.090
84	888.3	778.8								13.428	0.089
130	1035.1	934.1		x						16.105	8.087
0.125″ Al											
38	627.4	0.0								0.000	0.063
39	642.6	0.0								0.000	0.064
40	660.9	0.0								0.000	0.066
41	688.7	0.0								0.000	0.069
42	744.2	226.3	x		0.0010	31.5	11.60	0.141	0.283	3.427	0.074
43	714.2	0.0								0.000	0.071
44	721.4	149.4	x		0.0015	31.2	11.60	0.141	0.283	2.270	0.072
45	723.6	152.4	x		0.0014	29.7	11.60	0.141	0.283	2.358	0.072
46	702.3	0.0								0.000	0.070
47	716.5	0.0								0.000	0.072
48	693.5	0.0								0.000	0.069
49	860.9	474.1	x		0.0005	33.0	11.60	0.141	0.283	7.065	0.086
50	863.2	484.9	x		0.0004	27.0	11.60	0.141	0.283	7.794	0.086
51	757.2	268.7	x		0.0010	37.4	11.60	0.141	0.283	3.855	0.076
52	794.2	360.2	x		0.0007	35.1	11.60	0.141	0.283	5.264	0.079
53	825.9	423.9	x		0.0006	35.4	11.60	0.141	0.283	6.179	0.083
54	844.4	444.0	x		0.0005	30.9	11.60	0.141	0.283	6.769	0.084
55	724.0	137.3	x		0.0018	34.4	11.60	0.141	0.283	2.019	0.072
56	709.4	0.0								0.000	0.071
57	718.9	94.3	x		0.0023	32.8	12.60	0.141	0.283	1.335	0.072
58	721.8	83.1	x		0.003	34.7	11.60	0.141	0.283	1.219	0.072

ERROR ANALYSIS ON INITIAL AND RESIDUAL VELOCITY VALUES (Continued)

Test	V_i (ft/s)	V_r (ft/s)	Camera	Powder Gun	ΔT	Δx	C	δC	δΔx	δV_r (ft/s)	δV_i (ft/s)
0.125″ Al (Continued)											
59	720.5	130.9	x		0.0018	32.8	11.60	0.141	0.283	1.955	0.072
61	706.9	0.0								0.000	0.071
62	700.5	0.0								0.000	0.070
63	775.7	333.2	x		0.0008	37.1	11.60	0.141	0.283	4.792	0.078
64	811.8	398.7	x		0.0006	33.3	11.60	0.141	0.283	5.924	0.081
65	802.1	374.8	x		0.0006	31.3	11.60	0.141	0.283	5.688	0.080
66	833.1	426.7	x		0.0005	29.7	11.60	0.141	0.283	6.601	0.083
67	384.1	0.0								0.000	0.038
68	526.8	0.0								0.000	0.053
69	724.7	139.5	x		0.0017	33.0	11.60	0.141	0.283	2.079	0.072
70	739.4	223.7	x		0.0006	18.2	11.30	0.141	0.283	4.464	0.074
71	740.6	218.8	x		0.0006	17.8	11.30	0.141	0.283	4.426	0.074
72	740.5	218.1	x		0.0007	20.7	11.30	0.141	0.283	4.041	0.074
73	736.0	209.6	x		0.0007	19.9	11.30	0.141	0.283	3.969	0.074
74	743.7	233.5	x		0.0006	19.0	11.30	0.141	0.283	4.541	0.074
75	737.2	207.5	x		0.0007	19.7	11.30	0.141	0.283	3.952	0.074
76	858.5	486.7	x		0.0003	19.8	11.30	0.141	0.283	9.243	0.086
77	846.8	467.1	x		0.0003	19.0	11.30	0.141	0.283	9.085	0.085
78	852.4	476.9	x		0.0003	19.4	11.30	0.141	0.283	9.163	0.085
79	852.6	469.5	x		0.0003	19.1	11.30	0.141	0.283	9.103	0.085
80	848.1	457.2	x		0.0003	18.6	11.30	0.141	0.283	9.004	0.085
81	850.2	472.0	x		0.0003	19.2	11.30	0.141	0.283	9.124	0.085
85	890.0	536.2	x		0.0002	14.8	11.50	0.141	0.424	16.725	0.089
86	882.5	520.0	x		0.0002	14.1	11.30	0.141	0.424	16.946	0.088
131	1142.0	833.3	x	x	0.0002	28.3	14.15	0.141	0.566	18.623	8.922

ERROR ANALYSIS ON INITIAL AND RESIDUAL VELOCITY VALUES (Continued)

Test	V_i (ft/s)	V_r (ft/s)	Camera	Powder Gun	ΔT	Δx	C	δC	δΔx	δV_r (ft/s)	δV_i (ft/s)
0.25″ Al											
101	1044.9	0.0		x						0.000	8.163
102	1327.1	0.0		x						0.000	10.368
103	1423.8	583.0	x	x	0.0002	19.8	14.15	0.141	0.424	13.784	11.123
104	1372.2	438.8	x	x	0.0004	29.8	14.15	0.141	0.283	6.048	10.720
105	1397.7	485.8	x	x	0.0004	33.0	14.15	0.141	0.283	6.396	10.920
106	1353.4	0.0		x						0.000	10.573
107	1339.9	386.3	x	x	0.0005	32.8	14.15	0.141	0.283	5.099	10.468
108	1328.4	241.5	x	x	0.0008	32.8	14.15	0.141	0.283	3.188	10.378
109	1350.7	439.3	x	x	0.0005	37.3	14.15	0.141	0.283	5.511	10.552
110	1320.2	0.0		x						0.000	10.314
111	1450.5	588.9	x	x	0.0002	20.0	12.30	0.141	0.424	14.208	11.332
112	1671.5	942.3	x	x	0.0001	16.0	14.15	0.141	0.566	34.621	13.059
113	1642.2	824.5	x	x	0.0001	14.0	14.15	0.141	0.566	34.319	12.830
114	1540.4	765.6	x	x	0.0001	13.0	14.15	0.141	0.424	26.131	12.034
115	1432.0	563.4	x	x	0.0003	28.7	14.15	0.141	0.424	10.053	11.188
116	1343.0	199.3	x	x	0.0013	44.0	14.15	0.141	0.283	2.368	10.492
117	1020.8	0.0		x						0.000	7.975
118	1508.2	721.4	x	x	0.0002	24.5	14.15	0.141	0.424	14.424	11.783
119	1479.8	618.4	x	x	0.0003	31.5	14.15	0.141	0.424	10.372	11.561
120	1581.0	865.7	x	x	0.0001	14.7	14.15	0.141	0.566	34.419	12.352
121	1830.5	1136.6	x	x	0.0001	19.3	14.15	0.141	0.707	43.164	14.301
122	1764.0	1089.5	x	x	0.0002	37.0	14.15	0.141	0.566	19.900	13.781
123	1875.4	1236.7	x	x	0.0001	21.0	14.15	0.141	0.707	43.437	14.652
124	1328.8	0.0		x						0.000	10.381
125	1324.9	0.0		x						0.000	10.351
126	1386.8	456.4	x	x	0.0004	31.0	14.15	0.141	0.283	6.176	10.834
127	1339.1	0.0		x						0.000	10.462
128	1345.3	0.0		x						0.000	10.510

ERROR ANALYSIS ON INITIAL AND RESIDUAL VELOCITY VALUES (Continued)

Test	V_i (ft/s)	V_r (ft/s)	Camera	Powder Gun	ΔT	Δx	C	δC	δΔx	δV_r (ft/s)	δV_i (ft/s)
Polycarbonate											
133	881.7	196.5								3.388	0.088
134	783.2	0.0								0.000	0.078
135	844.8	0.0								0.000	0.084
136	867.6	0.0								0.000	0.087
137	874.3	0.0								0.000	0.087
138	873.7	0.0								0.000	0.087
139	1065.5	631.6		x						10.890	8.324
140	983.3	479.1		x						8.260	7.682
141	1002.5	584.4		x						10.076	7.832
142	879.8	186.8	x	x	0.0015	45.4	13.50	0.141	0.283	2.276	6.873
143	1078.8	657.6		x						11.338	8.428
144	1154.0	771.5		x						13.302	9.016
145	1194.6	835.8		x						14.410	9.333
146	1446.3	1079.8		x						18.617	11.299
147	1356.6	934.2		x						16.107	10.598
148	1367.3	954.6		x						16.459	10.682
149	1402.8	1016.9		x						17.533	10.959
150	1351.9	922.8		x						15.910	10.562
151	1319.6	817.1		x						14.088	10.309
152	1186.0	805.9		x						13.895	9.266
153	1061.0	629.5		x						10.853	8.289
154	1455.7	1101.1		x						18.984	11.373
155	1536.5	1249.1		x						21.536	12.004
156	1027.2	563.0		x						9.707	8.025
157	863.4	124.0	x	x	0.0023	46.2	13.50	0.141	0.283	1.505	6.745
158	962.5	542.5		x						9.353	7.520

ERROR ANALYSIS ON INITIAL AND RESIDUAL VELOCITY VALUES (Continued)

Test	V_i (ft/s)	V_r (ft/s)	Camera	Powder Gun	ΔT	Δx	C	δC	δΔx	δV_r (ft/s)	δV_i (ft/s)
Composites											
87	491.8	458.3								7.902	0.049
88	315.0	273.3								4.712	0.032
89	205.4	147.0								2.534	0.021
90	133.0	0.0								0.000	0.013
91	165.0	82.6	x		0.0010	12.0	12.11	0.141	0.283	2.173	0.017
92	170.0	86.0								1.483	0.017
93	124.5	0.0								0.000	0.012
94	176.3	109.5	x		0.0010	15.9	12.10	0.141	0.283	2.331	0.018
95	134.8	0.0								0.000	0.013
96	142.0	21.9	x		0.0040	12.7	12.08	0.141	0.283	0.551	0.014
97	140.1	0.0								0.000	0.014
98	882.5	853.8								14.721	0.088
99	689.1	658.1								11.347	0.069
100	396.8	362.0								6.241	0.040

ERROR ANALYSIS ON ABSORBED KINTEC ENERGY VALUES

Test	V_i (m/s)	V_r (m/s)	Mass (kg)	IKE (J)	RKE (J)	AKE (J)	δV_r (m/s)	δV_i (m/s)	δm (kg)	δIKE (J)	δRKE (J)	δAKE (J)
0.063″ Al												
2	118.66	0.00	0.0083	58.43	0.00	58.43	0.000	0.012	0.00005	0.352	0.000	0.352
3	131.64	36.76	0.0083	71.92	5.61	66.31	0.634	0.013	0.00005	0.433	0.196	0.476
4	108.26	0.00	0.0083	48.64	0.00	48.64	0.000	0.011	0.00005	0.293	0.000	0.293
5	126.98	48.46	0.0083	66.91	9.75	57.17	0.836	0.013	0.00005	0.403	0.341	0.528
6	141.85	83.70	0.0083	83.51	29.07	54.44	1.351	0.014	0.00005	0.503	0.954	1.079
7	151.64	96.35	0.0083	95.43	38.52	56.90	1.661	0.015	0.00005	0.575	1.349	1.466
8	159.93	112.62	0.0083	106.15	52.64	53.51	1.634	0.016	0.00005	0.640	1.560	1.686
9	164.04	119.39	0.0084	113.02	59.87	53.16	1.824	0.016	0.00005	0.673	1.864	1.982
10	175.17	140.15	0.0084	128.87	82.49	46.38	2.110	0.018	0.00005	0.768	2.533	2.646
11	181.23	144.44	0.0083	136.31	86.59	49.72	2.335	0.018	0.00005	0.822	2.847	2.964
12	188.12	151.97	0.0083	146.87	95.85	51.02	2.750	0.019	0.00005	0.885	3.517	3.627
13	198.70	161.48	0.0083	163.85	108.22	55.63	3.045	0.020	0.00005	0.988	4.132	4.249
14	204.83	169.13	0.0083	174.11	118.72	55.39	3.105	0.020	0.00005	1.049	4.418	4.541
15	225.37	191.96	0.0083	210.78	152.93	57.86	3.882	0.023	0.00005	1.270	6.253	6.381
16	266.27	232.17	0.0083	294.24	223.69	70.55	4.003	0.027	0.00005	1.774	7.830	8.029
17	119.66	7.92	0.0083	59.43	0.26	59.17	0.182	0.012	0.00005	0.358	0.012	0.358
18	126.64	39.26	0.0084	67.36	6.47	60.89	0.677	0.013	0.00005	0.401	0.227	0.461
19	100.77	0.00	0.0083	42.14	0.00	42.14	0.000	0.010	0.00005	0.254	0.000	0.254
20	87.29	0.00	0.0083	31.62	0.00	31.62	0.000	0.009	0.00005	0.191	0.000	0.191
21	91.32	0.00	0.0084	35.02	0.00	35.02	0.000	0.009	0.00005	0.209	0.000	0.209
22	118.93	0.00	0.0084	59.41	0.00	59.41	0.000	0.012	0.00005	0.354	0.000	0.354
23	130.64	56.69	0.0083	70.82	13.34	57.49	0.977	0.013	0.00005	0.427	0.467	0.633
24	131.25	54.07	0.0083	71.49	12.13	59.35	0.904	0.013	0.00005	0.431	0.412	0.596
25	130.48	53.25	0.0083	70.66	11.77	58.89	0.918	0.013	0.00005	0.426	0.412	0.592
26	128.47	45.11	0.0083	68.50	8.45	60.05	0.778	0.013	0.00005	0.413	0.296	0.508
27	129.97	55.57	0.0083	70.10	12.81	57.29	0.958	0.013	0.00005	0.423	0.449	0.616
28	187.57	149.44	0.0083	146.01	92.68	53.33	2.391	0.019	0.00005	0.880	3.018	3.144
29	187.42	149.44	0.0083	145.78	92.68	53.09	2.391	0.019	0.00005	0.879	3.018	3.143
30	188.31	149.78	0.0083	147.15	93.10	54.05	2.207	0.019	0.00005	0.887	2.800	2.937
31	188.61	151.64	0.0083	147.63	95.43	52.21	2.411	0.019	0.00005	0.890	3.089	3.215

ERROR ANALYSIS ON ABSORBED KINTEC ENERGY VALUES (Continued)

Test	V_i (m/s)	V_r (m/s)	Mass (kg)	IKE (J)	RKE (J)	AKE (J)	δV_r (m/s)	δV_i (m/s)	δm (kg)	δIKE (J)	δRKE (J)	δAKE (J)
0.063″ Al (Continued)												
32	121.98	49.77	0.0083	61.75	10.28	51.47	0.858	0.012	0.00005	0.372	0.360	0.518
33	119.69	18.87	0.0083	59.46	1.48	57.98	0.334	0.012	0.00005	0.358	0.053	0.362
34	118.11	0.00	0.0083	57.89	0.00	57.89	0.000	0.012	0.00005	0.349	0.000	0.349
35	118.29	0.00	0.0083	58.07	0.00	58.07	0.000	0.012	0.00005	0.350	0.000	0.350
36	122.22	29.35	0.0083	62.00	3.58	58.42	0.506	0.012	0.00005	0.374	0.125	0.394
37	120.34	20.06	0.0083	60.09	1.67	58.42	0.346	0.012	0.00005	0.362	0.058	0.367
83	275.33	245.49	0.0083	314.59	250.09	64.50	4.233	0.028	0.00005	1.896	8.755	8.957
84	270.75	237.38	0.0083	304.23	233.85	70.38	4.093	0.027	0.00005	1.834	8.186	8.389
130	315.50	284.71	0.0084	418.07	340.46	77.61	4.909	2.465	0.00005	6.990	11.914	13.813
0.125″ Al												
38	191.23	0.00	0.0083	151.76	0.00	151.76	0.000	0.019	0.00005	0.915	0.000	0.915
39	195.86	0.00	0.0083	159.21	0.00	159.21	0.000	0.020	0.00005	0.960	0.000	0.960
40	201.44	0.00	0.0083	168.40	0.00	168.40	0.000	0.020	0.00005	1.015	0.000	1.015
41	209.92	0.00	0.0083	182.87	0.00	182.87	0.000	0.021	0.00005	1.102	0.000	1.102
42	226.83	68.98	0.0083	213.53	19.74	193.78	1.044	0.023	0.00005	1.287	0.610	1.424
43	217.69	0.00	0.0083	196.66	0.00	196.66	0.000	0.022	0.00005	1.185	0.000	1.185
44	219.88	45.54	0.0083	200.65	8.61	192.04	0.692	0.022	0.00005	1.209	0.267	1.238
45	220.55	46.45	0.0083	201.87	8.95	192.92	0.719	0.022	0.00005	1.217	0.282	1.249
46	214.06	0.00	0.0083	190.16	0.00	190.16	0.000	0.021	0.00005	1.146	0.000	1.146
47	218.39	0.00	0.0083	197.93	0.00	197.93	0.000	0.022	0.00005	1.193	0.000	1.193
48	211.38	0.00	0.0083	185.43	0.00	185.43	0.000	0.021	0.00005	1.118	0.000	1.118
49	262.40	144.51	0.0084	289.19	87.70	201.49	2.153	0.026	0.00005	1.722	2.666	3.174
50	263.10	147.80	0.0084	290.74	91.75	198.99	2.376	0.026	0.00005	1.732	3.000	3.463
51	230.79	81.90	0.0083	221.05	27.84	193.22	1.175	0.023	0.00005	1.332	0.816	1.562
52	242.07	109.79	0.0084	246.12	50.63	195.49	1.604	0.024	0.00005	1.466	1.510	2.104
53	251.73	129.20	0.0084	266.15	70.11	196.04	1.883	0.025	0.00005	1.585	2.086	2.620
54	257.37	135.33	0.0083	274.90	76.01	198.89	2.063	0.026	0.00005	1.657	2.362	2.886
55	220.68	41.85	0.0083	202.09	7.27	194.83	0.615	0.022	0.00005	1.218	0.218	1.237
56	216.23	0.00	0.0083	194.03	0.00	194.03	0.000	0.022	0.00005	1.169	0.000	1.169
57	219.12	28.74	0.0083	199.26	3.43	195.83	0.407	0.022	0.00005	1.201	0.099	1.205
58	220.00	25.33	0.0083	200.87	2.66	198.21	0.371	0.022	0.00005	1.211	0.080	1.213

ERROR ANALYSIS ON ABSORBED KINTEC ENERGY VALUES (Continued)

Test	V_i (m/s)	V_r (m/s)	Mass (kg)	IKE (J)	RKE (J)	AKE (J)	δV_r (m/s)	δV_i (m/s)	δm (kg)	δIKE (J)	δRKE (J)	δAKE (J)
0.125″ Al (Continued)												
59	219.61	39.90	0.0083	200.15	6.61	193.54	0.596	0.022	0.00005	1.206	0.201	1.223
61	215.46	0.00	0.0083	192.66	0.00	192.66	0.000	0.022	0.00005	1.161	0.000	1.161
62	213.51	0.00	0.0083	189.19	0.00	189.19	0.000	0.021	0.00005	1.140	0.000	1.140
63	236.43	101.56	0.0083	231.99	42.80	189.18	1.460	0.024	0.00005	1.398	1.258	1.881
64	247.44	121.52	0.0083	254.08	61.29	192.80	1.806	0.025	0.00005	1.531	1.858	2.408
65	244.48	114.24	0.0084	251.04	54.81	196.22	1.734	0.024	0.00005	1.495	1.695	2.260
66	253.93	130.06	0.0084	270.82	71.04	199.77	2.012	0.025	0.00005	1.613	2.238	2.759
67	117.07	0.00	0.0084	57.57	0.00	57.57	0.000	0.012	0.00005	0.343	0.000	0.343
68	160.57	0.00	0.0084	108.29	0.00	108.29	0.000	0.016	0.00005	0.645	0.000	0.645
69	220.89	42.52	0.0084	204.93	7.59	197.33	0.634	0.022	0.00005	1.220	0.231	1.242
70	225.37	68.18	0.0083	210.78	19.29	191.49	1.361	0.023	0.00005	1.270	0.779	1.490
71	225.73	66.69	0.0083	211.47	18.46	193.01	1.349	0.023	0.00005	1.275	0.755	1.481
72	225.70	66.48	0.0083	211.41	18.34	193.07	1.232	0.023	0.00005	1.274	0.689	1.448
73	224.33	63.89	0.0083	208.85	16.94	191.91	1.210	0.022	0.00005	1.259	0.650	1.417
74	226.68	71.17	0.0083	213.24	21.02	192.22	1.384	0.023	0.00005	1.285	0.827	1.529
75	224.70	63.25	0.0083	209.53	16.60	192.93	1.205	0.022	0.00005	1.263	0.640	1.416
76	261.67	148.35	0.0083	284.16	91.33	192.83	2.817	0.026	0.00005	1.713	3.512	3.908
77	258.10	142.37	0.0083	276.46	84.12	192.35	2.769	0.026	0.00005	1.666	3.311	3.707
78	259.81	145.36	0.0083	280.13	87.69	192.45	2.793	0.026	0.00005	1.688	3.411	3.806
79	259.87	143.10	0.0083	280.26	84.99	195.28	2.775	0.026	0.00005	1.689	3.335	3.738
80	258.50	139.35	0.0083	277.31	80.59	196.72	2.744	0.026	0.00005	1.671	3.211	3.620
81	259.14	143.87	0.0083	278.69	85.89	192.80	2.781	0.026	0.00005	1.680	3.361	3.757
85	271.27	163.43	0.0083	305.39	110.85	194.54	5.098	0.027	0.00005	1.841	6.948	7.187
86	268.99	158.50	0.0083	300.27	104.25	196.01	5.165	0.027	0.00005	1.810	6.824	7.060
131	348.08	253.99	0.0084	508.88	270.95	237.93	5.676	2.719	0.00005	8.509	12.217	14.888

ERROR ANALYSIS ON ABSORBED KINTEC ENERGY VALUES (Continued)

Test	V_i (m/s)	V_r (m/s)	Mass (kg)	IKE (J)	RKE (J)	AKE (J)	δV_r (m/s)	δV_i (m/s)	δm (kg)	δIKE (J)	δRKE (J)	δAKE (J)
0.25″ Al												
101	318.49	0.00	0.0084	426.02	0.00	426.02	0.000	2.488	0.00005	7.123	0.000	7.123
102	404.50	0.00	0.0084	687.21	0.00	687.21	0.000	3.160	0.00005	11.490	0.000	11.490
103	433.97	177.70	0.0084	791.00	132.62	658.38	4.201	3.390	0.00005	13.226	6.321	14.659
104	418.25	133.75	0.0084	734.71	75.13	659.58	1.844	3.268	0.00005	12.285	2.119	12.466
105	426.02	148.07	0.0084	762.27	92.09	670.18	1.949	3.328	0.00005	12.745	2.486	12.986
106	412.52	0.00	0.0084	714.71	0.00	714.71	0.000	3.223	0.00005	11.950	0.000	11.950
107	408.40	117.74	0.0084	700.53	58.23	642.30	1.554	3.191	0.00005	11.713	1.576	11.819
108	404.90	73.61	0.0084	688.55	22.76	665.80	0.972	3.163	0.00005	11.513	0.616	11.529
109	411.69	133.90	0.0084	711.86	75.30	636.56	1.680	3.216	0.00005	11.903	1.942	12.060
110	402.40	0.00	0.0084	680.08	0.00	680.08	0.000	3.144	0.00005	11.371	0.000	11.371
111	442.11	179.50	0.0084	820.95	135.32	685.63	4.331	3.454	0.00005	13.727	6.579	15.222
112	509.47	287.21	0.0084	1090.16	346.46	743.70	10.552	3.980	0.00005	18.228	25.542	31.379
113	500.54	251.31	0.0084	1052.28	265.25	787.03	10.460	3.910	0.00005	17.595	22.138	28.278
114	469.51	233.35	0.0084	925.86	228.71	697.15	7.965	3.668	0.00005	15.481	15.672	22.029
115	436.47	171.72	0.0084	800.14	123.85	676.28	3.064	3.410	0.00005	13.379	4.481	14.109
116	409.35	60.75	0.0084	703.77	15.50	688.27	0.722	3.198	0.00005	11.767	0.380	11.773
117	311.14	0.00	0.0084	406.59	0.00	406.59	0.000	2.431	0.00005	6.798	0.000	6.798
118	459.70	219.88	0.0084	887.56	203.06	684.50	4.396	3.591	0.00005	14.840	8.210	16.960
119	451.04	188.49	0.0084	854.45	149.22	705.23	3.161	3.524	0.00005	14.287	5.084	15.164
120	481.89	263.87	0.0084	975.31	292.42	682.89	10.491	3.765	0.00005	16.308	23.318	28.455
121	557.94	346.44	0.0084	1307.43	504.07	803.36	13.156	4.359	0.00005	21.861	38.403	44.189
122	537.67	332.08	0.0084	1214.16	463.16	751.00	6.066	4.201	0.00005	20.301	17.143	26.571
123	571.62	376.95	0.0084	1372.36	596.77	775.59	13.240	4.466	0.00005	22.946	42.072	47.923
124	405.02	0.00	0.0084	688.97	0.00	688.97	0.000	3.164	0.00005	11.520	0.000	11.520
125	403.83	0.00	0.0084	684.93	0.00	684.93	0.000	3.155	0.00005	11.452	0.000	11.452
126	422.70	139.11	0.0084	750.42	81.28	669.15	1.883	3.302	0.00005	12.547	2.252	12.748
127	408.16	0.00	0.0084	699.69	0.00	699.69	0.000	3.189	0.00005	11.699	0.000	11.699
128	410.05	0.00	0.0084	706.18	0.00	706.18	0.000	3.203	0.00005	11.808	0.000	11.808

ERROR ANALYSIS ON ABSORBED KINTEC ENERGY VALUES (Continued)

Test	V_i (m/s)	V_r (m/s)	Mass (kg)	IKE (J)	RKE (J)	AKE (J)	δV_r (m/s)	δV_i (m/s)	δm (kg)	δIKE (J)	δRKE (J)	δAKE (J)
Polycarbonate												
133	268.74	59.89	0.0083	299.72	14.89	284.84	1.033	0.027	0.00005	1.807	0.521	1.880
134	238.72	0.00	0.0083	236.50	0.00	236.50	0.000	0.024	0.00005	1.425	0.000	1.425
135	257.50	0.00	0.0083	275.16	0.00	275.16	0.000	0.026	0.00005	1.659	0.000	1.659
136	264.44	0.00	0.0083	290.21	0.00	290.21	0.000	0.026	0.00005	1.749	0.000	1.749
137	266.49	0.00	0.0083	294.71	0.00	294.71	0.000	0.027	0.00005	1.776	0.000	1.776
138	266.30	0.00	0.0084	297.85	0.00	297.85	0.000	0.027	0.00005	1.774	0.000	1.774
139	324.76	192.51	0.0084	442.98	155.66	287.33	3.319	2.537	0.00005	7.407	5.447	9.194
140	299.71	146.03	0.0084	377.27	89.56	287.71	2.518	2.341	0.00005	6.308	3.134	7.044
141	305.56	178.13	0.0084	392.15	133.26	258.89	3.071	2.387	0.00005	6.557	4.663	8.046
142	268.16	56.94	0.0084	302.03	13.62	288.41	0.694	2.095	0.00005	5.050	0.342	5.062
143	328.82	200.44	0.0084	454.11	168.73	285.38	3.456	2.569	0.00005	7.593	5.904	9.618
144	351.74	235.15	0.0084	519.63	232.25	287.38	4.054	2.748	0.00005	8.688	8.127	11.897
145	364.11	254.75	0.0084	556.83	272.57	284.26	4.392	2.845	0.00005	9.310	9.538	13.329
146	440.83	329.12	0.0084	816.20	454.95	361.25	5.675	3.444	0.00005	13.647	15.920	20.969
147	413.49	284.74	0.0084	718.10	340.53	377.56	4.909	3.230	0.00005	12.007	11.916	16.916
148	416.75	290.96	0.0084	729.47	355.57	373.90	5.017	3.256	0.00005	12.197	12.442	17.423
149	427.57	309.95	0.0084	767.84	403.49	364.35	5.344	3.340	0.00005	12.839	14.119	19.084
150	412.06	281.27	0.0084	713.13	332.27	380.86	4.849	3.219	0.00005	11.924	11.627	16.654
151	402.21	249.05	0.0084	679.46	260.51	418.95	4.294	3.142	0.00005	11.361	9.116	14.566
152	361.49	245.64	0.0084	548.84	253.42	295.42	4.235	2.824	0.00005	9.177	8.868	12.761
153	323.39	191.87	0.0084	439.25	154.62	284.63	3.308	2.527	0.00005	7.344	5.411	9.122
154	443.70	335.62	0.0084	826.84	473.08	353.76	5.786	3.466	0.00005	13.825	16.554	21.568
155	468.33	380.73	0.0084	921.18	608.80	312.38	6.564	3.659	0.00005	15.402	21.304	26.288
156	313.09	171.60	0.0084	411.71	123.68	288.03	2.959	2.446	0.00005	6.884	4.328	8.131
157	263.16	37.80	0.0084	290.87	6.00	284.87	0.459	2.056	0.00005	4.864	0.150	4.866
158	293.37	165.35	0.0084	361.48	114.84	246.64	2.851	2.292	0.00005	6.044	4.018	7.258

ERROR ANALYSIS ON ABSORBED KINTEC ENERGY VALUES (Continued)

Test	V_i (m/s)	V_r (m/s)	Mass (kg)	IKE (J)	RKE (J)	AKE (J)	δV_r (m/s)	δV_i (m/s)	δm (kg)	δIKE (J)	δRKE (J)	δAKE (J)
Composites												
87	149.90	139.69	0.0083	93.25	80.98	12.27	2.408	0.015	0.00005	0.562	2.835	2.890
88	96.01	83.30	0.0083	38.26	28.80	9.46	1.436	0.010	0.00005	0.231	1.008	1.034
89	62.61	44.81	0.0083	16.27	8.33	7.93	0.773	0.006	0.00005	0.098	0.292	0.308
90	40.54	0.00	0.0083	6.82	0.00	6.82	0.000	0.004	0.00005	0.041	0.000	0.041
91	50.29	25.18	0.0083	10.50	2.63	7.87	0.662	0.005	0.00005	0.063	0.139	0.153
92	51.82	26.21	0.0083	11.14	2.85	8.29	0.452	0.005	0.00005	0.067	0.100	0.120
93	37.95	0.00	0.0083	5.98	0.00	5.98	0.000	0.004	0.00005	0.036	0.000	0.036
94	53.74	33.38	0.0083	11.98	4.62	7.36	0.710	0.005	0.00005	0.072	0.199	0.211
95	41.09	0.00	0.0083	7.01	0.00	7.01	0.000	0.004	0.00005	0.042	0.000	0.042
96	43.28	6.68	0.0083	7.77	0.18	7.59	0.168	0.004	0.00005	0.047	0.009	0.048
97	42.70	0.00	0.0083	7.57	0.00	7.57	0.000	0.004	0.00005	0.046	0.000	0.046
98	268.99	260.24	0.0083	300.27	281.05	19.21	4.487	0.027	0.00005	1.810	9.838	10.003
99	210.04	200.59	0.0083	183.08	166.98	16.10	3.458	0.021	0.00005	1.104	5.845	5.948
100	120.94	110.34	0.0083	60.70	50.52	10.18	1.902	0.012	0.00005	0.366	1.769	1.806

Ballistic Curves for Aluminum with Error Bars

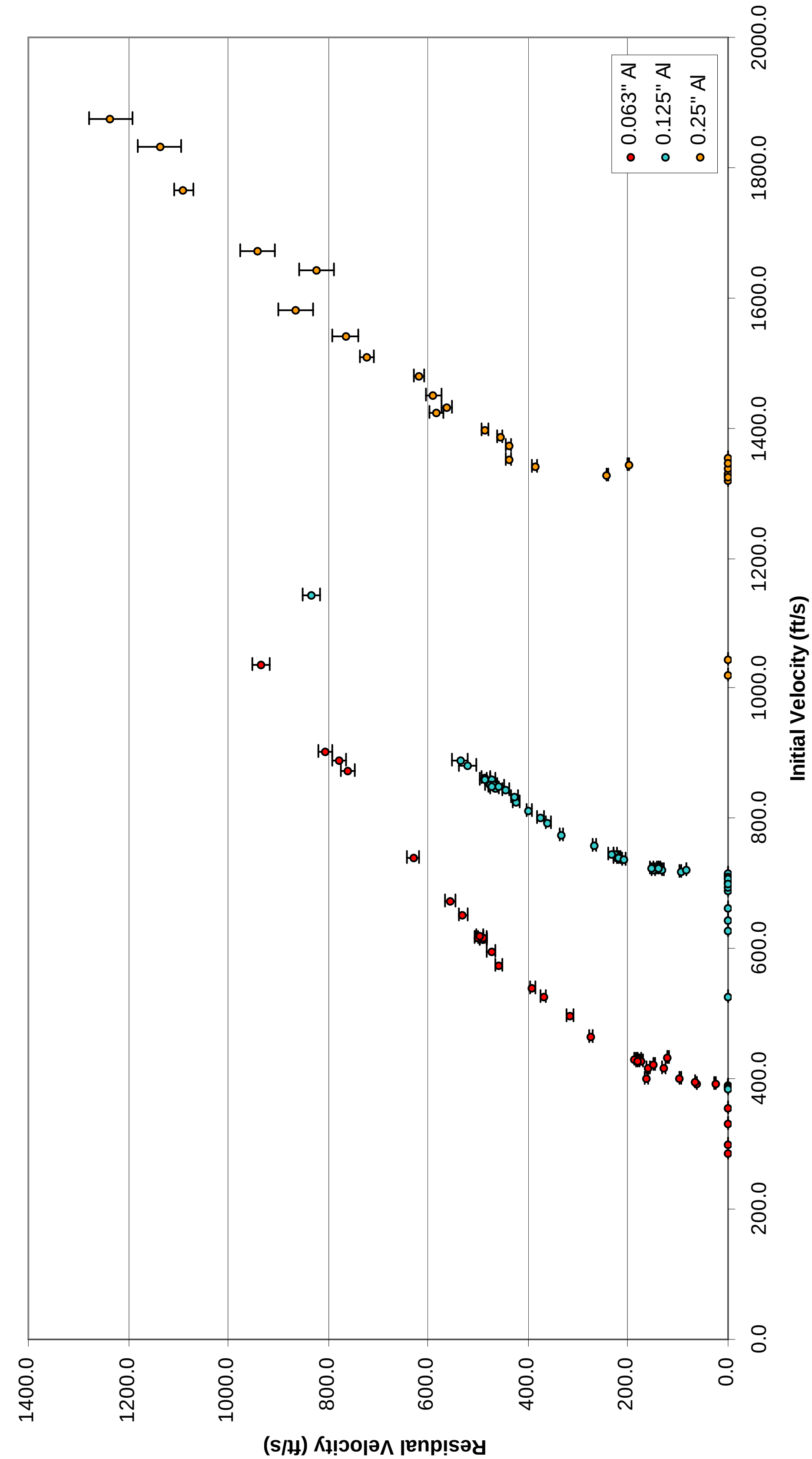

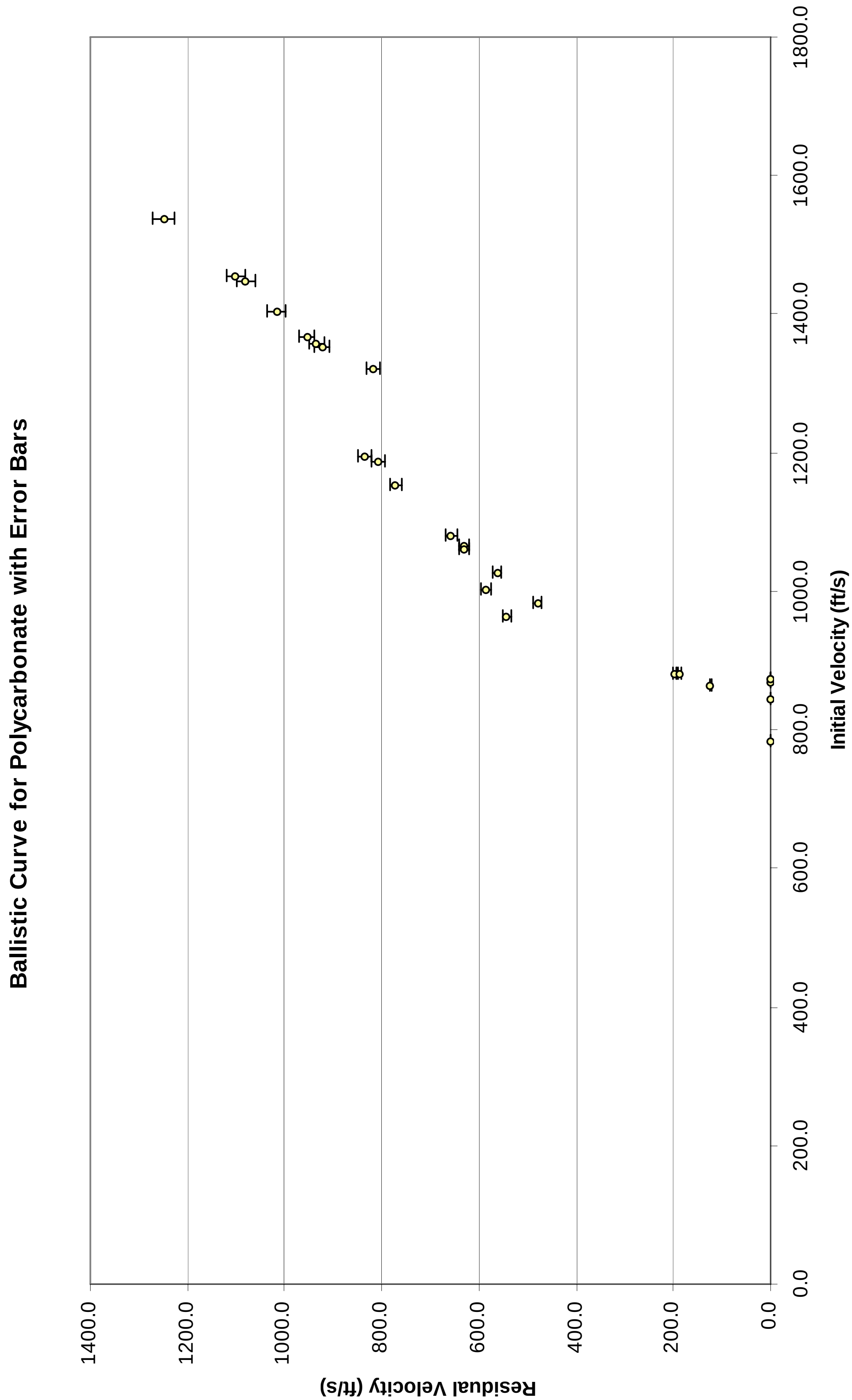
Ballistic Curve for Polycarbonate with Error Bars
Residual Velocity (ft/s)
Initial Velocity (ft/s)
0.0
200.0
400.0
600.0
800.0
1000.0
1200.0
1400.0
1600.0
1800.0

Ballistic Curve for Composite Panels with Error Bars

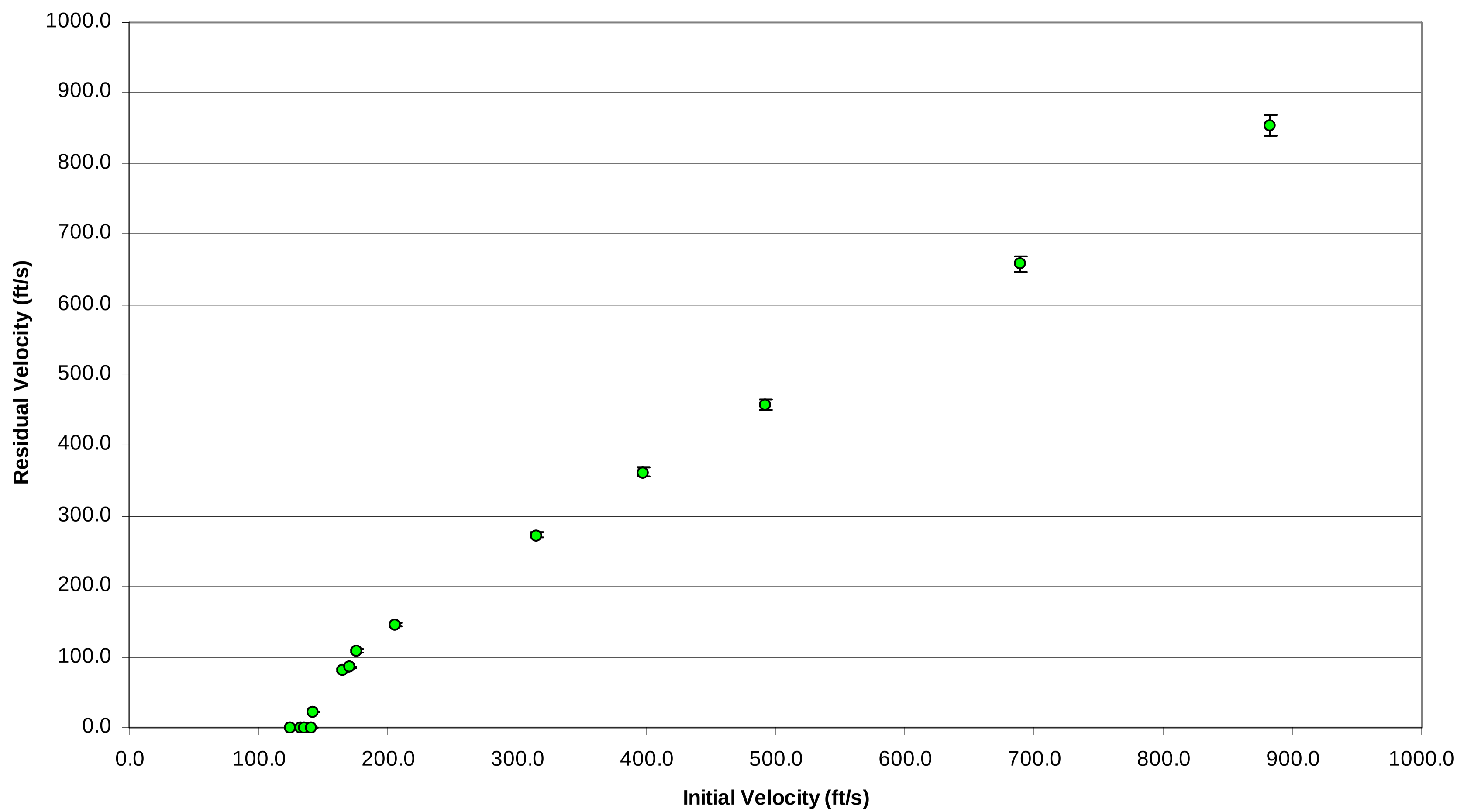

APPENDIX D—CIRCUIT DIAGRAM FOR PHOTODIODE SETUP AND DATA SHEETS

IS489

Low Voltage Operating Type High Sensitivity OPIC Light Detector

■ Features

1. Low voltage operating type (Vcc : 1.4 to 7.0V)
2. High sensitivity type (E_{VHL} : TYP. 5 lx)
3. Built-in Schmidt trigger circuit
4. Low level output under incident light

■ Outline Dimensions

(Unit : mm)

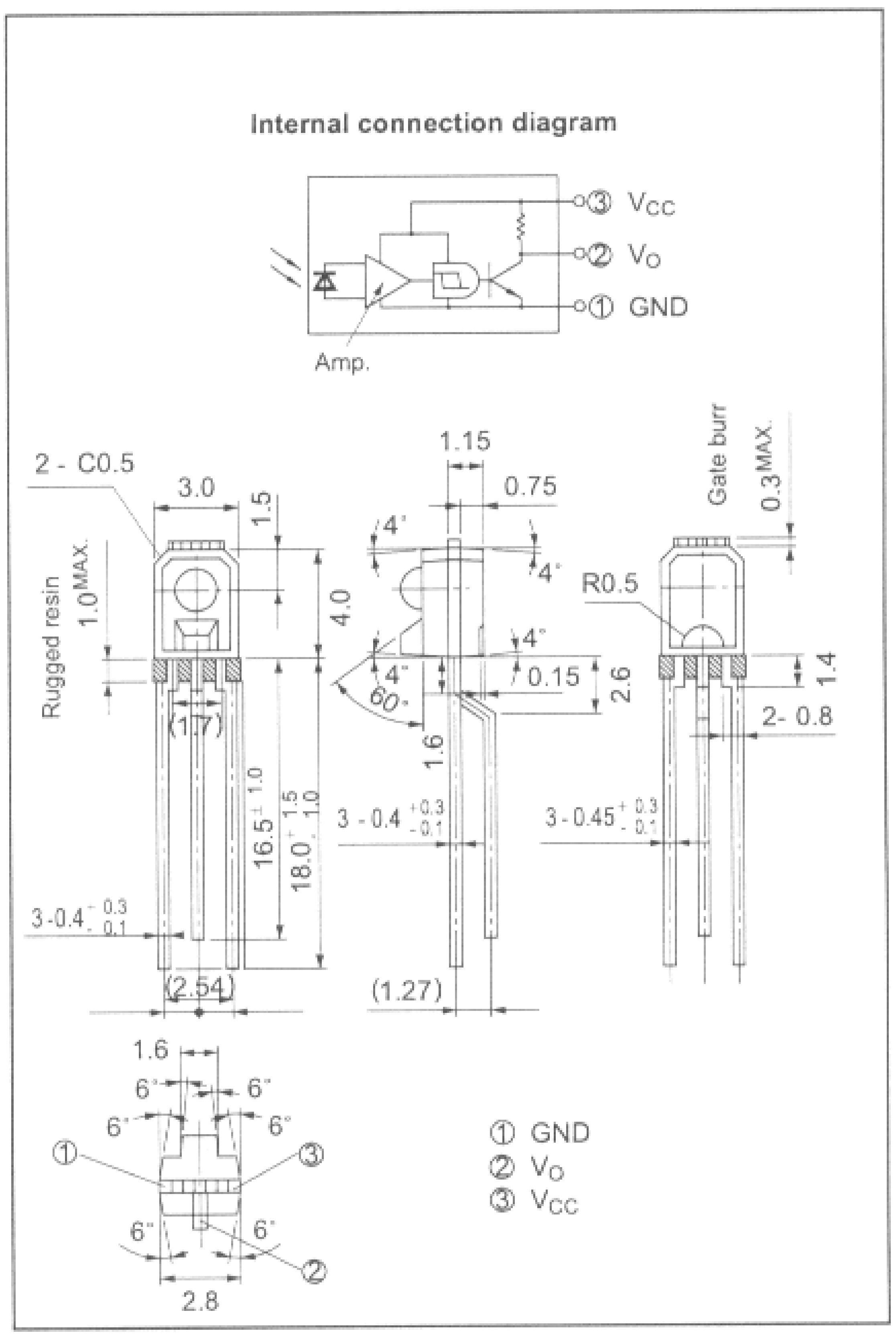

* OPIC (Optical IC) is a trademark of the SHARP Corporation. An OPIC consists of a light-detecting element and signal-processing circuit integrated onto a single chip.

■ Applications

1. Amusement equipment
2. Battery-driven portable equipment

■ Absolute Maximum Ratings

(Ta=25°C)

Parameter	Symbol	Rating	Unit
Supply voltage	V_{CC}	- 0.5 to + 8	V
*1 Output current	Io	2	mA
*2 Total power dissipation	P	80	mW
Operating temperature	T_{opr}	-25 to + 85	°C
Storage temperature	T_{stg}	- 40 to +100	°C
*3 Soldering temperature	T_{sol}	260	°C

*1 Output current vs. ambient temperature : Per Fig. 1
*2 Total power dissipation vs. ambient temperature : Per Fig. 2
*3 For 5 seconds at the position of 1.4 mm from the resin edge

■ Electro-optical Characteristics

(Ta=0 to 70˚C, V_{CC}=3V unless otherwise specified)

Parameter		Symbol	Conditions	MIN.	TYP.	MAX.	Unit
Low level output voltage		V_{OL}	I_{OL} = 1mA, E_V = 50 lx	-	0.1	0.4	V
High level output voltage		V_{OH}	E_V = 0 lx	2.9	-	-	V
Low level supply current		I_{CCL}	E_V = 50 lx	-	0.6	1.2	mA
High level supply current		I_{CCH}	E_V = 0 lx	-	0.4	0.5	mA
*1 "High →Low" threshold illuminance		E_{VHL}	Ta = 25˚C	-	4.8	15	lx
			-	-	-	22	
*2 "Low→High" threshold illuminance		E_{VLH}	Ta = 25˚C	0.6	3.7	-	lx
			-	0.4	-	-	
*3 Hysteresis		E_{VLH} /E_{VHL}	Ta = 25˚C	0.55	0.75	0.95	-
Response time	"High→Low" propagation delay time	t_{PHL}	E_V = 125 lx or equivalent, R_L = 3kΩ, Ta = 25˚C	-	1.3	15	μs
	"Low →High" propagation delay time	t_{PLH}		-	8.5	30	
	Rise time	t_r		-	0.1	3.0	
	Fall time	t_f		-	0.06	1.0	
Peak sensitivity wavelength		λ_P	-	-	900	-	nm

*1 E_{VHL} represents illuminance by CIE standard light source A (tungsten lamp) when output changes from "high" to "low".

*2 E_{VLH} represents illuminance by CIE standard light source A (tungsten lamp) when output changes from "low" to "high".

*3 Hysteresis standards for E_{VLH}/E_{VHL}.

■ Recommended Operating Conditions

(Ta=25˚C)

Parameter	Symbol	MIN.	MAX.	Unit
Supply voltage	V_{CC}	1.4	7.0	V
Output current	I_{OL}	-	1.0	mA

Fig. 1 Output Current vs. Ambient Temperature

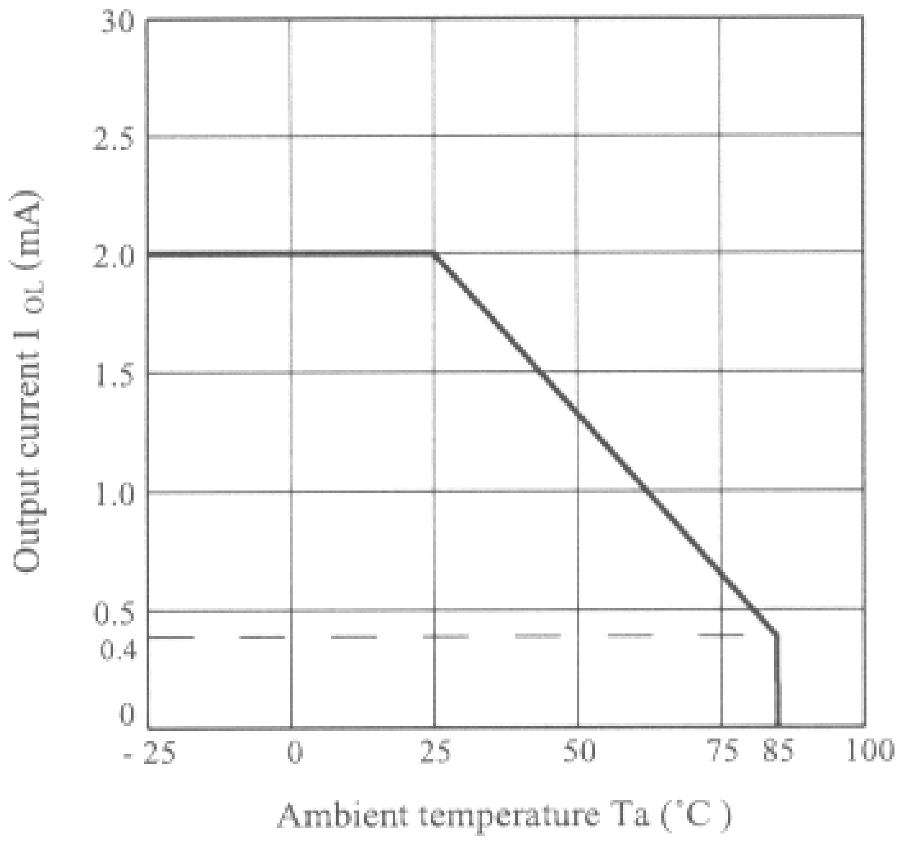

Fig. 2 Output Power Dissipation vs. Ambient Temperature

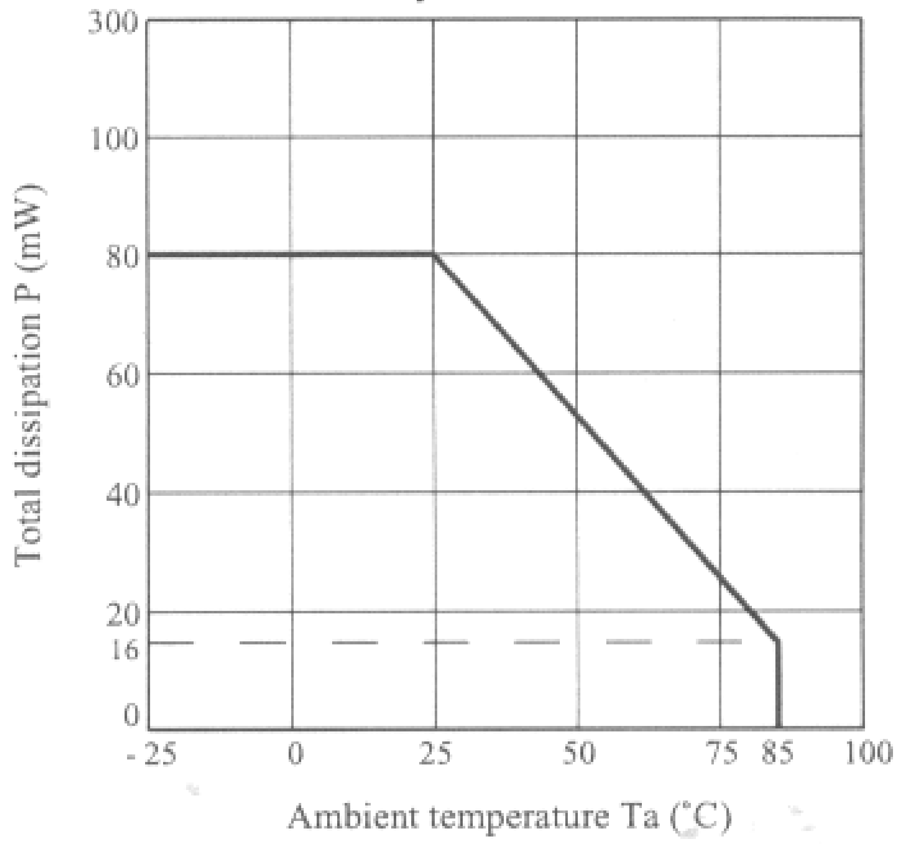

Fig. 3 Low Level Output Voltage vs. Low Level Output Current

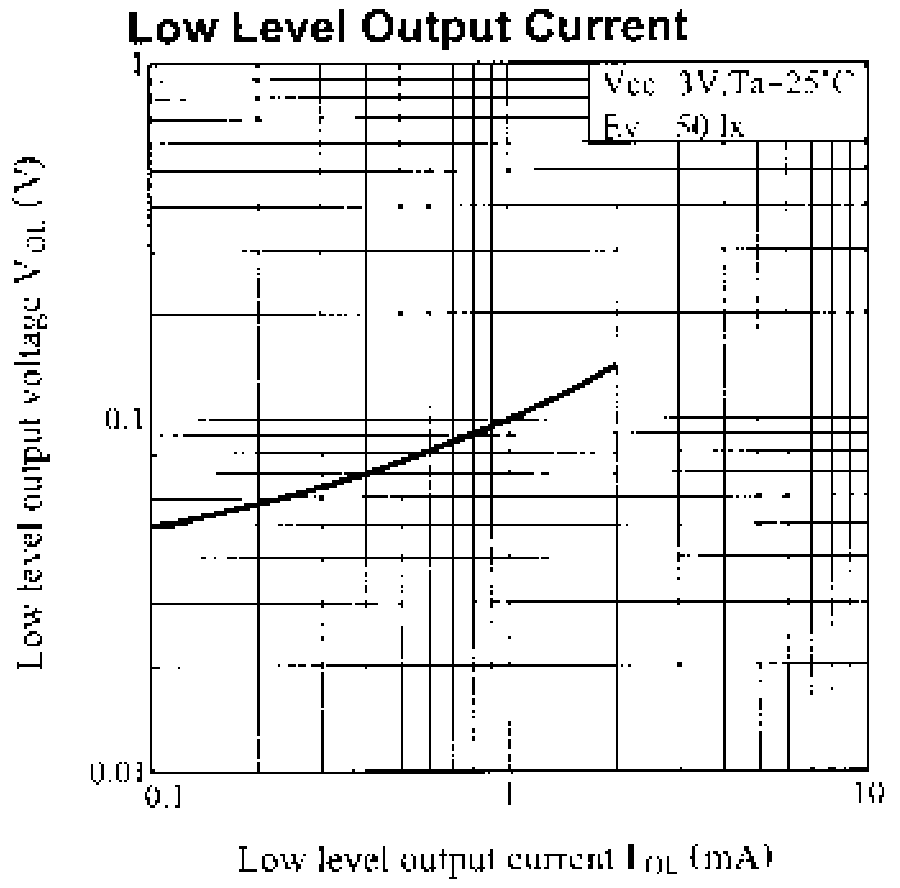

Fig. 4 Supply Current vs. Ambient Temperature

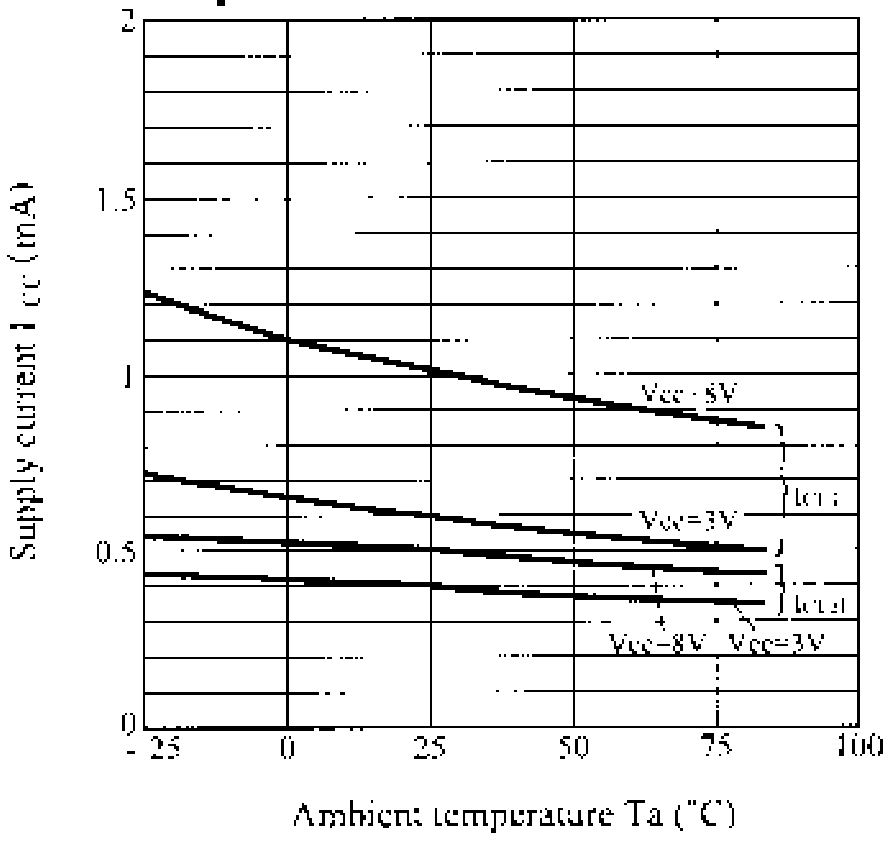

Fig. 5 Rise, Fall Time vs. Load Resistance

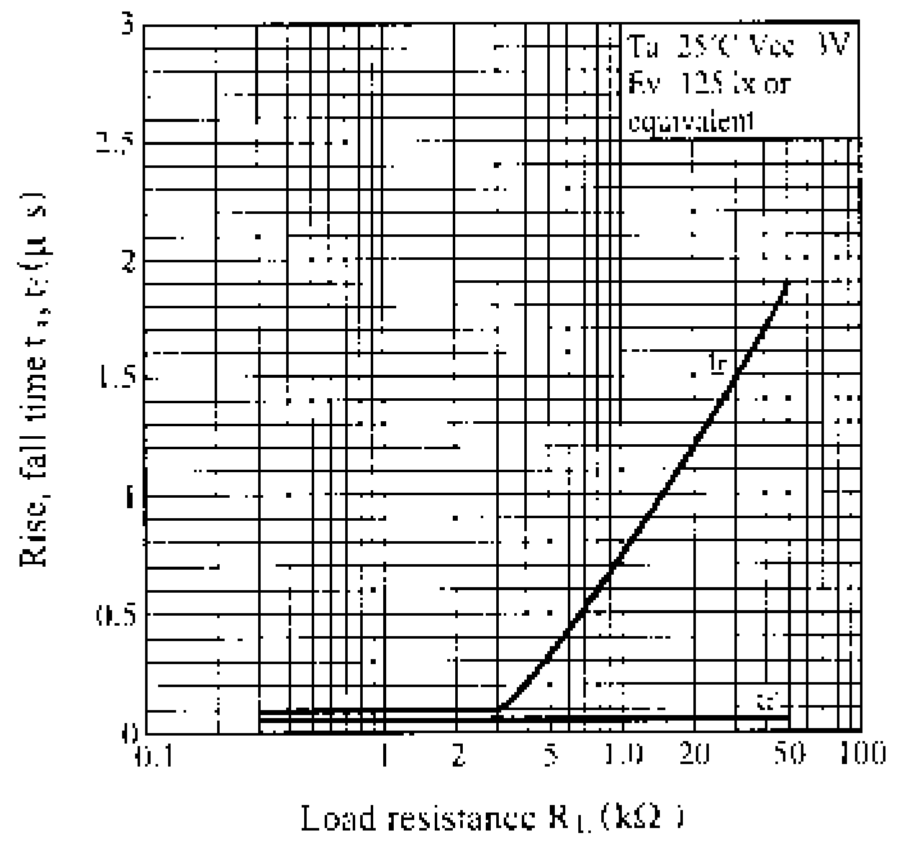

Test Circuit for Response Time

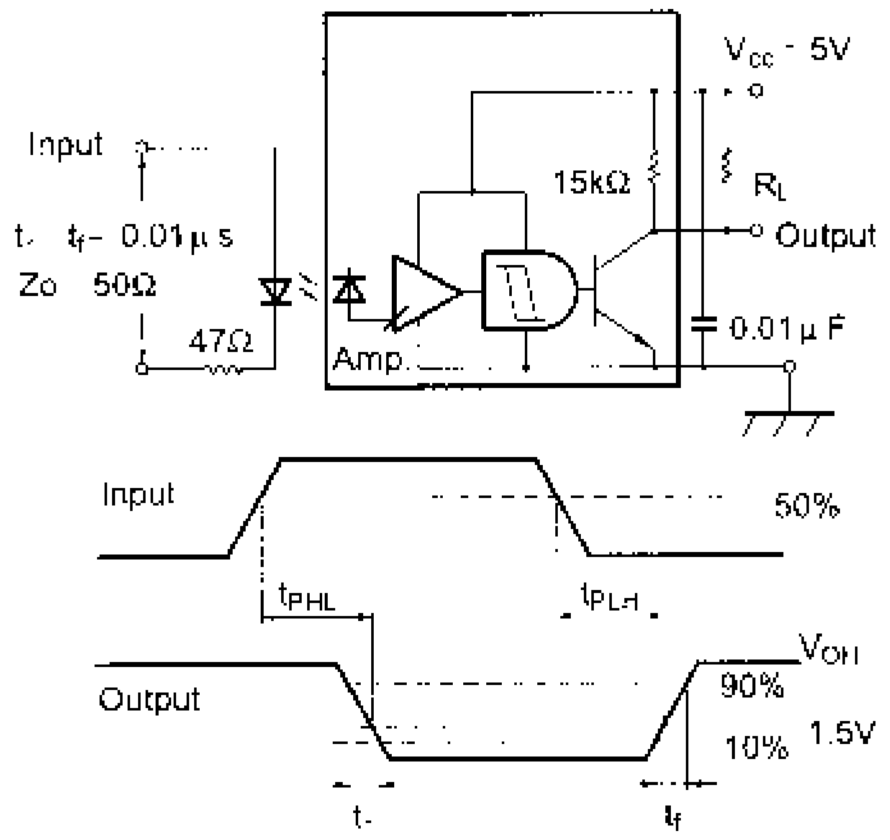

Fig. 6 Radiation Diagram (Ta=25 °C)

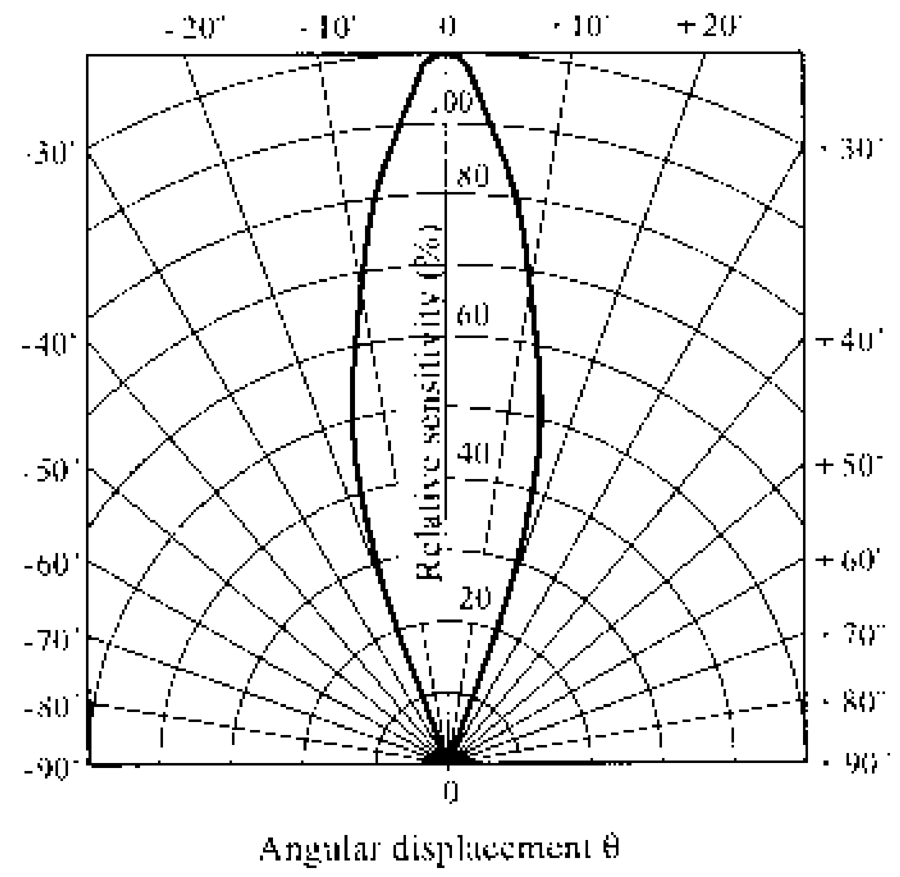

Fig. 7 Spectral Sensitivity

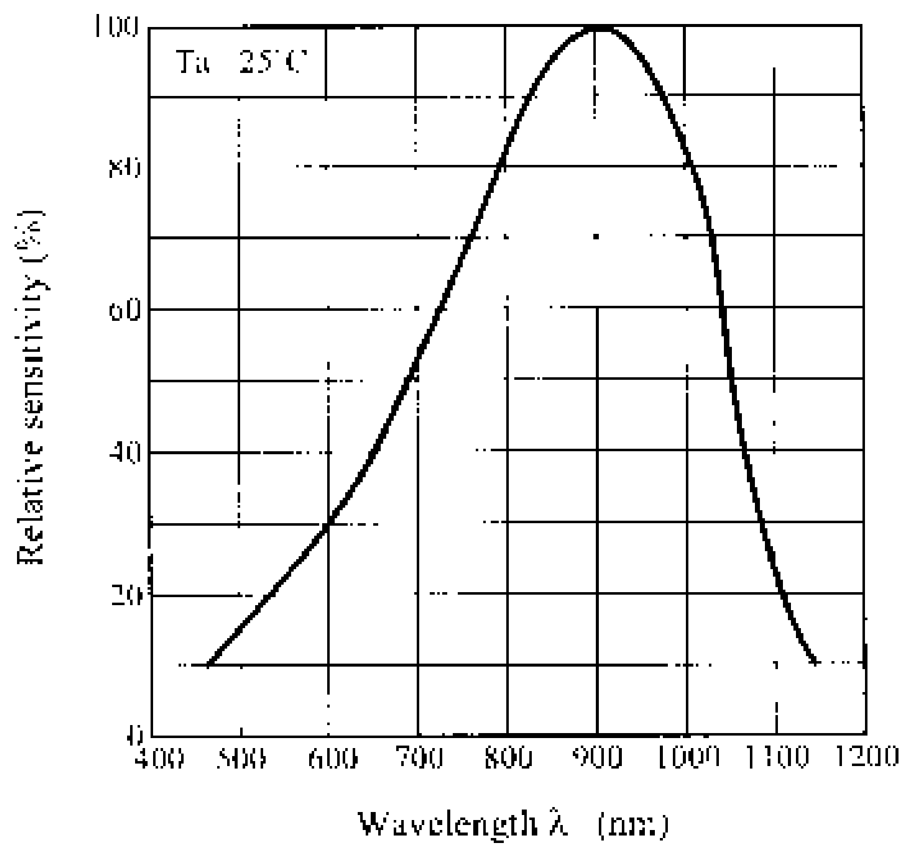

● Please refer to the chapter "Precautions for Use". (Page 78 to 93)

NOTICE

- The circuit application examples in this publication are provided to explain representative applications of SHARP devices and are not intended to guarantee any circuit design or license any intellectual property rights. SHARP takes no responsibility for any problems related to any intellectual property right of a third party resulting from the use of SHARP's devices.
- Contact SHARP in order to obtain the latest device specification sheets before using any SHARP device. SHARP reserves the right to make changes in the specifications, characteristics, data, materials, structure, and other contents described herein at any time without notice in order to improve design or reliability. Manufacturing locations are also subject to change without notice.
- Observe the following points when using any devices in this publication. SHARP takes no responsibility for damage caused by improper use of the devices which does not meet the conditions and absolute maximum ratings to be used specified in the relevant specification sheet nor meet the following conditions:

  (i) The devices in this publication are designed for use in general electronic equipment designs such as:
  - Personal computers
  - Office automation equipment
  - Telecommunication equipment [terminal]
  - Test and measurement equipment
  - Industrial control
  - Audio visual equipment
  - Consumer electronics

  (ii) Measures such as fail-safe function and redundant design should be taken to ensure reliability and safety when SHARP devices are used for or in connection with equipment that requires higher reliability such as:
  - Transportation control and safety equipment (i.e., aircraft, trains, automobiles, etc.)
  - Traffic signals
  - Gas leakage sensor breakers
  - Alarm equipment
  - Various safety devices, etc.

  (iii) SHARP devices shall not be used for or in connection with equipment that requires an extremely high level of reliability and safety such as:
  - Space applications
  - Telecommunication equipment [trunk lines]
  - Nuclear power control equipment
  - Medical and other life support equipment (e.g., scuba).
- Contact a SHARP representative in advance when intending to use SHARP devices for any "specific" applications other than those recommended by SHARP or when it is unclear which category mentioned above controls the intended use.
- If the SHARP devices listed in this publication fall within the scope of strategic products described in the Foreign Exchange and Foreign Trade Control Law of Japan, it is necessary to obtain approval to export such SHARP devices.
-
- Contact and consult with a SHARP representative if there are any questions about the contents of this publication.

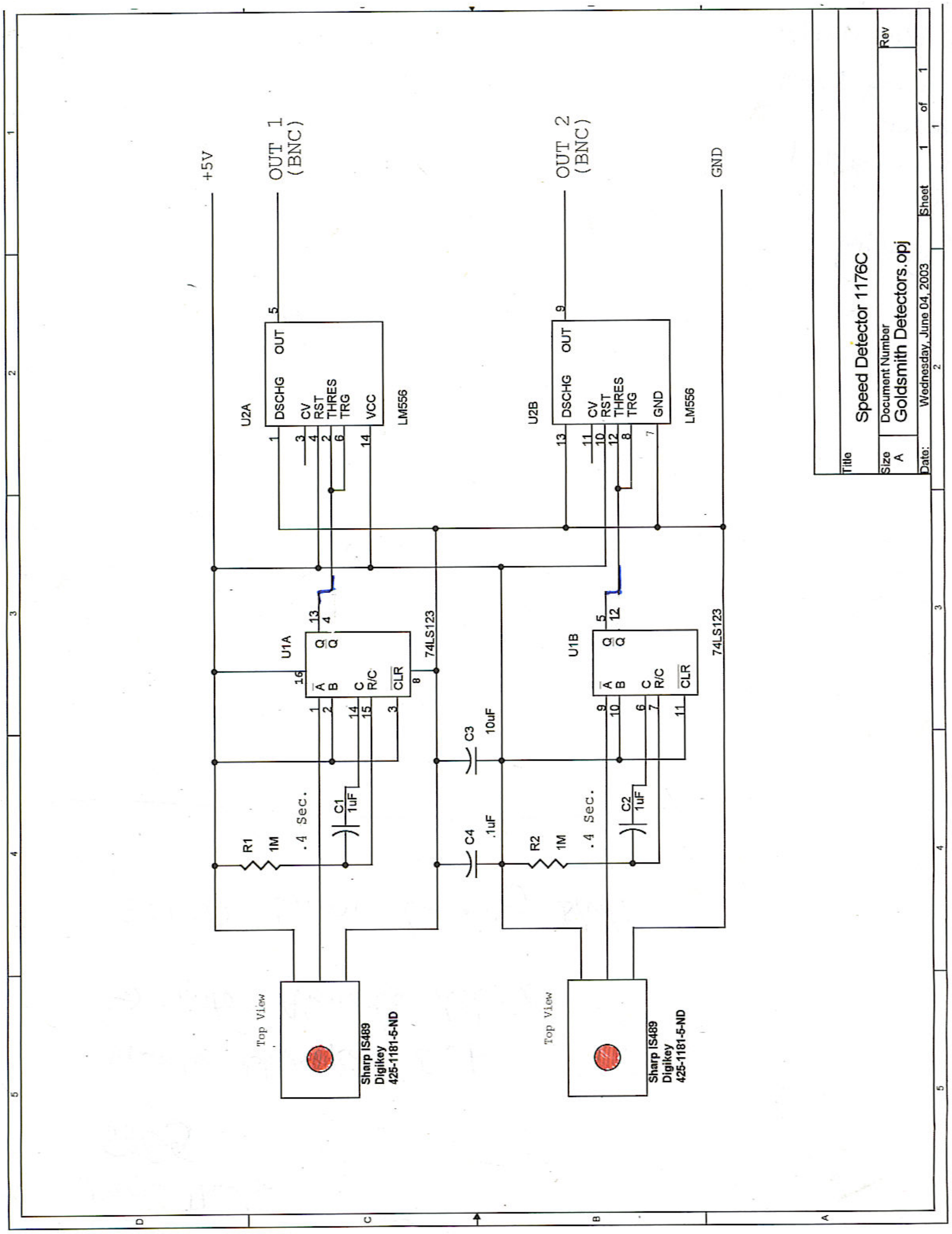
Title
Speed Detector 1176C
Size
A
Document Number
Goldsmith Detectors.opj
Rev
Date: Wednesday, June 04, 2003
Sheet 1 of 1
+5V
OUT 1 (BNC)
OUT 2 (BNC)
GND
U2A
LM556
U2B
LM556
DSCHG
CV
RST
THRES
TRG
VCC
GND
OUT
U1A
74LS123
U1B
74LS123
R/C
CLR
R1 1M
R2 1M
C1 1uF
C2 1uF
C3 10uF
C4 .1uF
.4 Sec.
.4 Sec.
Top View
Sharp IS489
Digikey
425-1181-5-ND
Top View
Sharp IS489
Digikey
425-1181-5-ND